UTRECHT UNIVERSITY, FACULTY OF GEOSCIENCES

MSC THESIS

Coupling a large-scale hydrological model to a high-resolution hydrodynamical model

A study of floods within the Niger Inner Delta as a first step towards a potential global application

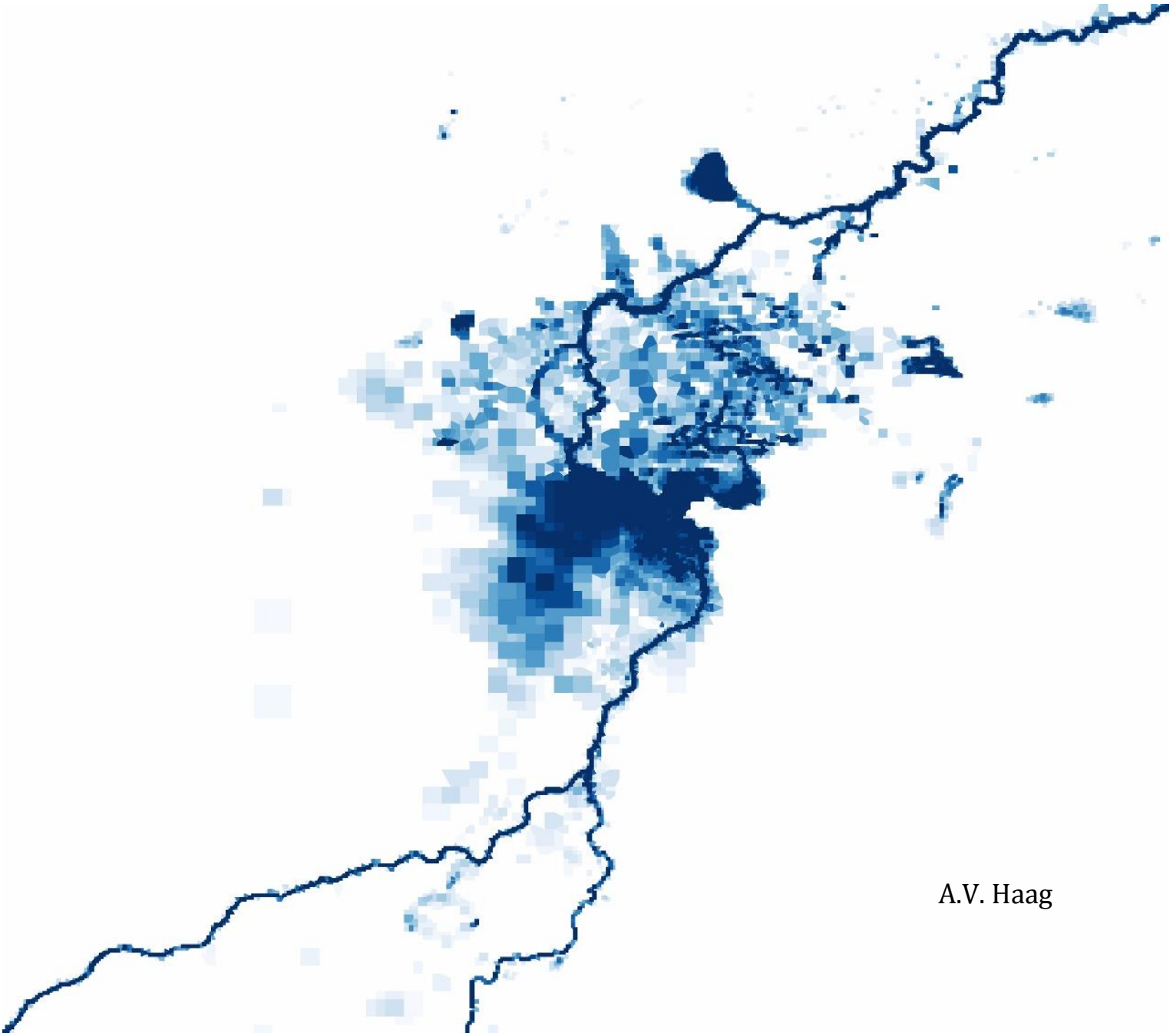

A.V. Haag

Coupling a large-scale hydrological model to a high-resolution hydrodynamical model

A study of floods within the Niger Inner Delta as a first step towards a potential global application

MSc thesis for the Master's Programme Earth Surface and Water (track Hydrology) at the Department of Physical Geography and Faculty of Geosciences of Utrecht University, combined with an internship at Deltares in Delft, the Netherlands

Author:

A.V. Haag

Completion date:

April 7th 2015

Supervisors:

Utrecht University:	Prof. Dr. Ir. M.F.P. Bierkens
Deltares:	Dr. H. Winsemius and G. Donchyts

Acknowledgements:

The author is grateful to have received discharge data of gauging stations along the Niger River from the Global Runoff Data Center, 56068 Koblenz, Germany.

Figure on front page:

View of water depths within the Niger Inner Delta (with darker colours representing higher values), as simulated by one of the two-way coupled models used in this study.

Preface

The internship that was part of this thesis started on the 7th of May 2014, which means that I have worked on it for exactly eleven months (with about one month of vacation in between). During this time, I have experienced excitement about progress in the study and frustrations about a lack thereof, as I am sure many other students have experienced during the work on their theses. However, most of the time it felt like I was trying to solve a giant puzzle and I can honestly say that I enjoyed it. I found the subject to be very interesting and challenging, and I want to thank my supervisor Marc Bierkens for giving me the opportunity to work on it (and for supporting my wish to combine the thesis work with an internship).

A very big thanks goes out to all my official and unofficial supervisors for making time in their busy schedules to assist me and answer my questions; Gennadii Donchyts has helped me a lot with software-related issues and coupling procedures (and made me a big fan of Far Manager and IPython Notebook), Hessel Winsemius has helped me a lot with hydrology-related questions and the general matters of the internship, and both Rens van Beek and Edwin Sutanudjaja have helped me a lot with questions regarding the PCR-GLOBWB model. Finally, I want to thank Herman Kernkamp and Sander van der Pijl for answering my questions about the D-Flow Flexible Mesh model.

This thesis could be seen as the final test of my abilities as a student, but it can also be seen as the final step on a (in my case, rather long) path of academic education. Such a path is wrought with the dangerous distractions of student life and I am happy to have a few of those side-track me from the main road, as they shaped me into the person that I am today. That being said, I am amazed (and very grateful) for the enormous patience that my parents displayed regarding this matter. The same holds true for my incredible girlfriend, who might not have waited as long as my parents, but who did have to endure living with a constantly broke and busy student.

While it can be said that the research for this thesis is finished, there is still a lot that needs to be done before the work presented here could be successfully applied on a global level. This is therefore more of a long-term goal and I am very happy that a PhD research has recently been started on the matter, which is being carried out by Jannis Hoch. I hope that the work presented in this thesis provides a good starting point and I am looking forward to learning more about the subject from his research.

Finally, I want to apologize to my supervisors (and anybody else crazy enough to read the full thesis) for creating a thesis of 122 pages. In my defence, it is a description of ten months of hard work on a (in my eyes) complicated subject and I did not want to leave out anything that might contain relevant information, especially given the fact that it might be useful for Jannis' PhD research. Fortunately, the 122 pages do contain a lot of figures, which should make reading it more manageable.

I hope you find it to be an interesting read.

Arjen Haag

Gouda, April 7th 2015

Abstract

The PCRaster GLOBal Water Balance model (PCR-GLOBWB) is a global hydrological model that has been used successfully as part of a framework for the global assessment of flood risk related to river floods (GLObal Flood Risk with IMAGE Scenarios [GLOFRIS]). However, its ability to accurately simulate discharge extremes, which are strongly related to the occurrence and extent of flooding, has been questioned for some river basins located in semi-arid regions, most notably the Niger River in Western Africa. Since PCR-GLOBWB operates on scales much larger than those required to accurately model floods, the GLOFRIS framework applies downscaling techniques to obtain the required data at sufficiently small scales. These downscaling techniques are applied after model simulations and can therefore not account for dynamic feedbacks to hydrological processes, which have a strong influence on the discharge regime of the Niger River. Seasonal peak flows cause large flooding within the Niger Inner Delta, an extensive wetland located within the Sahel, allowing hydrological processes such as evaporation to greatly reduce the volume of water within the river.

To make sure that the dynamic feedbacks between hydrology and inundation are taken into account, and at the same time work with the fine scales required to accurately model this inundation, PCR-GLOBWB is coupled to a high-resolution hydrodynamical model (D-Flow Flexible Mesh [D-Flow FM]). A two-way coupling procedure is created using the Basic Model Interface (BMI), which facilitates the exchange of information between models and allows complete control over model timesteps and variables. Because of the large differences in model resolution, the source code of PCR-GLOBWB is adjusted to ensure a proper representation of hydrological processes affected by inundation. The coupled model is applied to the Niger River and its Inner Delta to test its capabilities and explore the potential for a global application. With this in mind, the study focusses on methods that can be automated to be easily applied on a global scale. The flexible mesh of D-Flow FM allows the use of an unstructured grid that optimizes computational efficiency by only creating cells of high-resolution in river channels and flood-prone areas. A relatively new terrain model, the Height Above Nearest Drainage (HAND), is used in combination with the Courant-based grid refinement operator of D-Flow FM to automatically create a model grid that meets the desired requirements.

The coupled model was tested for the period 1995-2000, to allow a comparison between modelled and observed discharges values at several locations along the river. Model performance was further assessed by comparing the values of hydrological properties with those listed in other studies. Coupling had a strong influence on results, caused by the dynamic feedbacks between hydrology and inundation, improving results compared to the stand-alone PCR-GLOBWB model. However, it also revealed a number of issues which impacted results in a negative way; (1) the related processes of infiltration, groundwater recharge and baseflow were all severely overestimated compared to other studies, (2) the automatic grid creation using HAND was unable to properly represent side-channels, (3) the bathymetry of river channels and lakes was not properly included due to a relatively simplistic stream burning method and (4) the computation time was relatively large, which is problematic for a global application. These issues will need to be dealt with before the coupled model can be successfully applied within the GLOFRIS framework. The use of a 1D network for river channels could already improve results, as it would lead to a better representation of side-channels and channel bathymetry (if the required data with global coverage is of sufficient quality), and it would also reduce computation times compared to the current 2D-only approach. The issue related to the overestimation of certain fluxes probably requires a revision of their functions in PCR-GLOBWB.

Contents

1 Introduction

1.1 Background information and problem definition

Floods are one of the most frequently occurring natural disasters and responsible for roughly one third of the total economic losses inflicted by all natural hazards worldwide (Munich Re, 2010; UNISDR, 2009). These economic losses, as well as the number of people exposed to floods, have increased over the last half century and this trend is expected to continue (IPCC, 2012; UNISDR, 2011, Visser et al., 2012). This has led to increased attention for strategic (global) flood risk assessments, which are now being done more frequently as part of global integrated assessments (e.g. OECD, 2012; UNISDR, 2009, 2011).

These global risk assessments are used by international financing institutes to determine the best investment options for natural disaster risk reduction, by intra-national institutes to monitor progress in activities that reduce risk and by insurance companies to justify insurance coverage (Winsemius et al., 2013). These assessments typically look at disasters that have already taken place and analyse trends in disaster risk over a certain period. However, future changes in both the frequency and intensity of natural disasters, coupled with socio-economic conditions, have so far not been included and this has been identified as a research priority (e.g. Field et al., 2011).

To this end, Winsemius et al. (2013) developed a framework for the global assessment of flood risk related to river floods (GLObal Flood Risk with IMAGE Scenarios [GLOFRIS]), which was subsequently updated and applied at the global scale by Ward et al. (2013). This framework uses a global hydrological model and global impact assessment models in combination with downscaling methods to use and obtain hazard and exposure maps at sufficiently small scales. Recently (March 2015), an extension of this work was launched as an interactive web-based platform in the form of the Aquaduct Global Flood Analyzer[1]. This tool is designed to assess the risk of river floods across the globe and allows users to analyse the impact of river floods in terms of affected population, Gross Domestic Product (GDP) and urban damage (www.wri.org[2]).

Both Winsemius et al. (2013) and Ward et al. (2013) used the global hydrological model PCR-GLOBWB (Van Beek & Bierkens, 2008) in their studies. This model has been validated in previous studies; validation on discharge (van Beek et al., 2011) and terrestrial water storage (Wada et al., 2012) revealed fair to good model performance. Ward et al. (2013) also carried out their own validation, using observed daily discharge data from the Global Runoff Data Centre (GRDC) to compare discharge extremes, which are an important indicator of floods. They assessed the relative error and extreme value distributions of modelled and observed discharge at several locations around the globe. In most cases, the relative error was reasonable (between −25 and +25%), but clear overestimations were found in some arid regions (see Figure 1 on the next page).

Overestimations of extreme discharges were especially notable in the Niger River, where floods are known to re-infiltrate or evaporate from the large wetland that is its Inner Delta (Liersch et al., 2013). Other wetlands with a strong feedback between inundation and hydrology include the Okavango Delta (Akoko et al., 2013) and the Sudd wetland of the Nile River (Mohamed et al., 2006; Rebelo et al., 2012; Senay et al., 2014). The overestimation of discharge becomes especially apparent when observed and modelled discharge values are compared, as is shown in Figure 2 on the next page.

[1] http://floods.wri.org/

[2] http://www.wri.org/resources/maps/aqueduct-global-flood-analyzer

Other studies on global river discharge using PCR-GLOBWB have shown that the Niger River has one of the worst performances out of all large river basins (Candogan Yossef et al., 2012; Sperna Weiland et al., 2010), which highlights the challenges involved in the accurate modelling of discharge for this river. Re-infiltration and evaporation in the Niger Inner Delta are related to the inundation process, something which is not explicitly included in the current model setup (Ward et al., 2013). This reveals the strong relationship between hydrological processes and floods within this region, and shows that it is required to include all of these aspects within a model in order to generate realistic results.

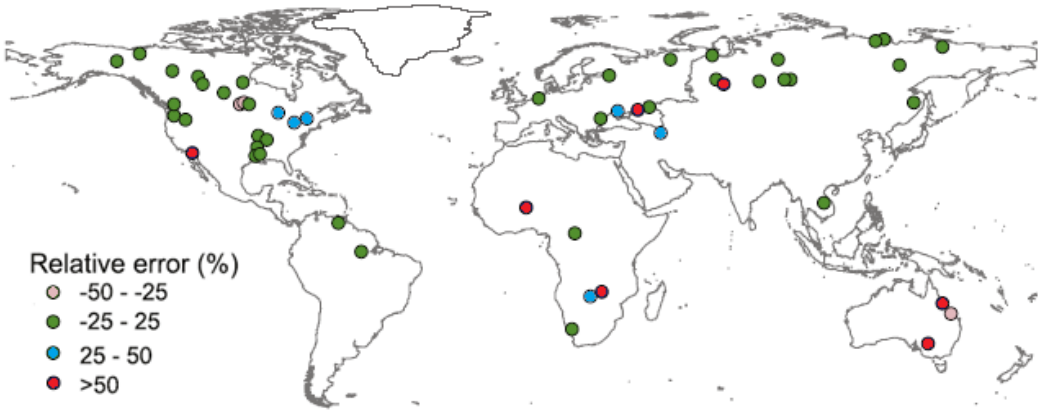

Figure 1: Relative error between modelled and observed discharge with a return-period of 10 years (Ward et al., 2013)

In their study, Winsemius et al. (2013) also stated that a more dynamic downscaling approach, as suggested by Neal et al. (2012), could potentially improve results. Neal et al. (2012) used the Niger Inner Delta to evaluate their large-scale hydraulic model and obtained good results. However, their model requires calibration of channel parameters, which is difficult to do in global assessments, and also uses observed discharge values as upstream boundary conditions, which makes it impossible to assess possible future scenarios. Therefore, another approach is required to improve flood modelling under the GLOFRIS framework.

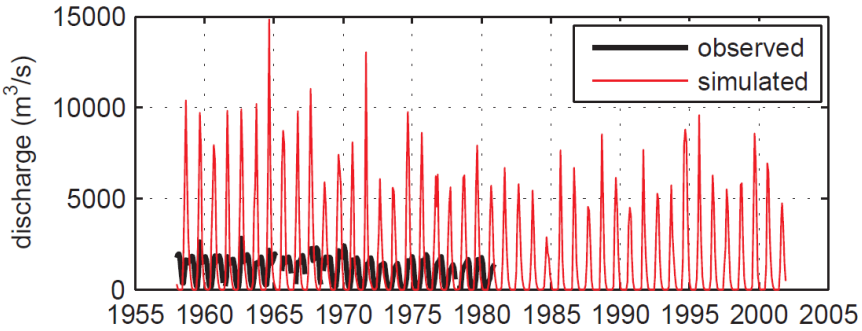

Figure 2: Discharge of the Niger River, with simulated values from PCR-GLOBWB (Candogan Yossef et al., 2012)

1.1.1 Model coupling

PCR-GLOBWB, as a well-tested hydrological model with global coverage, provides a good starting point, but it cannot accurately model floods and inundation dynamics, which typically occur at much smaller spatial scales than those at which global models operate (Winsemius et al., 2013). The downscaling method applied by Winsemius et al. (2013) and Ward et al. (2013) may reduce the scale issue, but it is a post-processing tool and therefore it cannot account for any dynamic feedback effects to hydrological processes affected by inundation. PCR-GLOBWB also does not include the full Saint-Venant equations thought to best describe the overland flow of water, which are typically found in more detailed hydrodynamical models (e.g. Finaud-Guyot et al., 2011; Kuiry et al., 2010).

These hydrodynamical models are specifically designed to accurately model river flows and inundation, but often lack a detailed description of relevant hydrological processes and are generally difficult to apply at a global scale.

In order to accurately model large wetlands in (semi-) arid regions such as the Niger Inner Delta, it is imperative that both the inundation itself and the hydrological processes influenced by this are included in the model. It is thought that exposing inundated water to the processes of evaporation and infiltration could improve results, as various studies have shown that evaporative losses are severely influenced by inundation patterns and result in a significant loss of discharge (Dadson et al., 2010; Mahé et al., 2009; Zwarts et al., 2006). This could potentially be handled by a single model, for example by expanding an existing hydrodynamical model with the required hydrological processes. However, the scales at which these kinds of models operate are too small to be used for global assessment studies, because such a model would not be able to run global simulations within an acceptable timeframe, given the current computational capabilities. Expanding an existing hydrological model with better hydrodynamical modelling tools would also lead to scale-related issues, as explained before. For these reasons, another strategy should be considered that is able to overcome the aforementioned problems: the coupling of a hydrological model to a hydrodynamical model.

Model coupling lets both models work at their own spatial scales and timesteps, which are after all designed to be best suited to that which the model attempts to simulate. There is an exchange of information from one model to the other, which could for example allow infiltration calculated within a hydrological model to affect inundation simulated by a hydrodynamical model. The strong interdependence between hydrology and hydrodynamics has been recognized in many recent studies, which has led to an increased interest in the development of coupled models (e.g. Kim et al., 2012; Lerat et al., 2012; Peyrard et al., 2008).

1.1.2 Previous coupling studies

For instance, Lerat et al. (2012) coupled an existing rainfall-runoff (RR) model to a hydrodynamical model, in which the RR model was used to provide the hydrodynamical model with lateral inflows. While this gave interesting results, upstream discharge was still modelled with a boundary condition using measured flows and the two models were used to simulate different regions of the total study area, with no overlap in model grids, which makes it difficult to include a two-way exchange of information between models. Indeed, there was only a one-directional exchange of information (with the hydrodynamical model having no influence on the RR model), which is often referred to as one-way coupling. The strong relationship between inundation and hydrology in the Niger basin requires an exchange of information in both ways, also known as two-way coupling. Finally, their hydrodynamical model did not include the full Saint-Venant equations, using an approximation (the 'diffusive wave') instead.

Kim et al. (2012) developed a model with overlapping grids by coupling an existing hydrological model (tRIBS) to an existing hydrodynamical model (OFM) that uses the full Saint-Venant equations. Their model did not require upstream or downstream boundary conditions, with the hydrodynamical model receiving all required input from the hydrological model. Compared to Lerat et al. (2012), the study of Kim et al. (2012) comes closer to what would be required to accurately model all relevant processes within the Niger Inner Delta. However, it still used one-way coupling of models, with no feedback from the hydrodynamical model to the hydrological model. The grids of both models also

had a similar resolution, which makes it unsuitable for large-scale to global applications because of the previously mentioned reasons.

Peyrard et al. (2008) did create a two-way coupled model, describing the exchange of water between a river and its adjacent floodplain. The model used the full Saint-Venant equations for river flows and coupled this to the Dupuit equations for aquifer flows in the floodplain, by linking the equations in a single matrix so that they were solved simultaneously. While this does ensure accurate two-way coupling, this also implies that the processes are coupled at the same spatial scale, which makes the method unsuitable for large-scale applications, because of the already mentioned issues. This kind of coupling, in which equations are linked together, would also not be suitable for the coupling with a hydrological model such as PCR-GLOBWB, as this describes a large number of different processes at a daily timestep, which is a too large timestep to accurate resolve the full Saint-Venant equations.

No study could be found that uses a two-way coupling between a large-scale hydrological model and a high-resolution hydrodynamical model that uses the full Saint-Venant equations, with the aim of assessing river discharge and floods for large river basins. Such a model could be used at a global scale, would potentially be able to include future scenarios and overcome the aforementioned issues of global flood modelling. This would not only make it a valuable tool for global flood risk assessments, it would also allow more detailed hydrological analyses than possible with the hydrological model alone, because inundation dynamics can be included in the coupled model. The creation of such a model will therefore be attempted in this study.

1.1.3 Existing coupling tools

The coupling itself can be handled using various methods, as can be seen from the studies mentioned above. The coupled modelling of hydrological processes and inundation dynamics require a two-way exchange of information between models at every grid cell. Furthermore, when existing models are used in the coupling, it is desirable that the coupling can be created in such a way that adjustments to the source code of the models themselves are avoided. This would allow the models to be further developed and improved individually, without having to take the other model or the coupling into account.

The increased interest in the coupling of models has also led to the development of tools specifically designed for this purpose, such as the Open Modelling Interface [OpenMI] (Gregersen et al., 2007) and the Basic Model Interface [BMI] of the Community Surface Dynamics Modeling System [CSDMS] (Peckham et al., 2013). These tools facilitate the coupling of existing models by coupling them through an interface, which can be seen as a standardized set of functions or methods, which in turn allow the exchange of information between models. While such an interface has to be specifically created for each model, because the structure of models is often unique, this does negate the need to make adjustments to the source code of the models themselves.

Out of the known coupling tools, the BMI created by Peckham et al. (2013) is thought to be best suited for this study because of its relative simplicity and general applicability. This should make sure that the creation of the coupling interface for this study is feasible. It was successfully used by Ashton et al. (2013) to couple existing models of coastline evolution and fluvial dynamics, showing its capability to couple independently developed models that were designed for different purposes.

1.2 Research objective and research questions

In light of what is written above, the research objective is formulated as follows:

To determine whether the two-way coupling of a global hydrological model to a high-resolution hydrodynamical model can improve the large-scale modelling of river discharge and floods, by testing and evaluating the coupled model for the Niger River.

This objective will be met if answers are found to the following research questions:

1. *How should the hydrological model be coupled to the hydrodynamical model?*
    a. *How can the grid cells of both models be coupled, when these are most likely not similar in size and/or shape?*
    b. *At what time step should both models operate to allow efficient coupling?*
    c. *Which variables are required to model the relevant hydrological and hydrodynamical processes in each model, and how can these best be used to exchange information between models?*
2. *Does the coupled model have the potential to improve the large-scale modelling of river discharge and floods, judging from results obtained by applying the model to the Niger River?*
    a. *What are appropriate criteria to evaluate the performance of large-scale hydrological models and hydrodynamical models?*
    b. *What is the influence of the coupling on model results?*
    c. *Which of the tested model setups has the best performance and is this performance considered good for modelling purposes?*
    d. *What are the identified issues associated with the coupled model?*
    e. *Does the coupled model have the potential to be used at a global scale and/or are there any other potential applications?*

In order to meet the objective and research questions stated above, a coupled model will first have to be created, which requires a hydrological model and a hydrodynamical model. Since PCR-GLOBWB has been the model of choice for the previous studies of the GLOFRIS framework, the model will also be used in this study. The GLOFRIS framework was partially developed at the institute of Deltares, which is why this research is combined with an internship at their department in Delft, the Netherlands. They are currently developing a new hydrodynamical model (D-Flow Flexible Mesh [D-Flow FM]), which is already in the later stages of testing and has great potential for this study. It also already has a BMI to facilitate the coupling and is therefore chosen as hydrodynamical model to be used in this study. The BMI for PCR-GLOBWB will be created as part of this study.

1.3 Thesis outline

This thesis is made up of eight other chapters, each describing a specific part of the study. Chapter 2 gives a detailed analysis of the study area, with a specific focus on the Niger Inner Delta and its impact on downstream river discharge. Chapters 3 and 4 describe the used models, PCR-GLOBWB and D-Flow FM respectively, with chapter 5 describing how the grid of D-Flow FM was created for this study. Chapter 6 gives all the details on the coupling of the models, describing the relevant BMI functions and other methods used to facilitate the coupling. Chapter 7 shows the results of several different model setups and analyses their differences. Chapter 8 describes all the issues discovered during this study and discusses their implications. The main text ends with conclusions in chapter 9. Several appendices give further information on selected subjects.

2 Study area: Niger basin

2.1 Introduction

The Niger basin is located in Western Africa. It is spread out over a total of 10 countries, with the largest sections in Mali, Niger and Nigeria, each covering about 25% of the total basin area (Olomoda, 2002; Zwarts et al., 2006), as can be seen in Figure 3 below. The river itself has a total length of about 4200 km, making it the largest river in Western Africa and third longest river on the continent after the Nile and Congo (Olomoda, 2002; Pedinotti et al., 2012; Zwarts et al., 2006). Although its sources in Guinea and Ivory Coast are located in tropical regions, a large part of the basin is situated in the semi-arid region of the Sahel, with the most northern section covering parts of the Sahara, receiving almost no rainfall (Ogilvie et al., 2010; Olomoda, 2002; Zwarts et al., 2006).

As a consequence, a relatively large section of the basin is not hydrologically active; of the approximately 2.3 million km^2 that make up the total basin area, only an area of 1.2 to 1.5 million km^2 is considered to be hydrologically active (Ogilvie et al., 2010; Olomoda, 2002). This is also highlighted in the uneven distribution of precipitation over the basin; the upstream sections in the south can receive over 2000 mm of precipitation during the rainy season (July - October), while the more northern sections only receive 200-500 mm per year (or as little as 0 mm for the Saharan parts) (Liersch et al., 2013; Zwarts et al., 2006; www.fao.org[3]). Besides this, there is also an enormous seasonal and interannual variation in rainfall as well as river flow (Pedinotti et al., 2012; Zwarts et al., 2006).

Figure 3: The Niger Basin with relevant gauging stations and approximate area of the Niger Inner Delta (created with data from HydroSHEDS[4] [basin extent], Natural Earth[5] [countries and rivers] and the GRDC[6] [gauging station locations])

[3] http://www.fao.org/docrep/w4347e/w4347e0i.htm
[4] http://www.hydrosheds.org/
[5] http://www.naturalearthdata.com/
[6] http://www.bafg.de/GRDC/EN/Home/homepage_node.html

The uneven distribution of precipitation is the reason why the relatively small sections of the basin in Guinea and Ivory Coast (together only 5.3 % of the total basin area) are responsible for most of the water flowing through the river until the confluence with the Benue River, a major tributary flowing into the Niger near Lokoja (see Figure 3). In fact, the amount of water entering Mali from these two countries (about 40 km^3/year) exceeds the amount entering Nigeria from Niger (about 36 km^3/year), even though the river has travelled roughly 1800 km further downstream, theoretically allowing a lot of additional input (Zwarts et al., 2006). This is caused by a relatively low input from precipitation and small tributaries along this stretch of the river, and by the high amounts of evaporation in the Niger Inner Delta (Dadson et al., 2010; Mahé et al., 2009; Mahe et al., 2011; Olomoda, 2002; Zwarts et al., 2006).

2.2 The Niger Inner Delta

The Niger Inner Delta is located in Mali, roughly between the towns of Ke-Macina and Tombouctou (see Figure 4 on the next page). It is a seasonally inundated floodplain, forming an extensive network of streams, swamps and lakes (Liersch et al., 2013). It is the largest floodplain of West Africa (Mahe et al., 2011) and one of the largest Ramsar sites in the world (which designates it as a critically important wetland, see also www.ramsar.org[7]). Yearly rainfall over the area varies between 356 and 682 mm, with an average of 545 mm, and the delta receives most of its water from upstream discharge (Mahé et al., 2009). The Bani River, with an upstream area of 102,000 km^2, joins the Niger River (which has an upstream area of 147,000 km^2 at this point) within the delta near the town of Mopti. There are many lakes in the delta, which are recharged by the river when it reaches flood levels. During periods with low water levels the flow in these lakes reverses and they discharge into the river. The flow path between the lakes and the river can have elevation thresholds, which dam large quantities of water that then evaporate slowly (Mahé et al., 2009).

The exact area of the delta is hard to determine and this can differ greatly between various sources. Kuper et al. (2003) place it at 36,000 km^2, Mahé et al. (2009) at 73,000 km^2 and Schuol et al. (2008) at 80,000 km^2. Similarly, there is no consensus on the maximum flooded surface area. This could potentially be as high as 45,000 km^2 (Schuol et al., 2008) or as low as 6150 km^2 (Mahe et al., 2011). This in turn leads to different estimates of water loss due to evaporation in the delta. Gourcy et al. (2000) state an evaporation rate of over 2000 mm/year, which they say would lead to a 25% reduction in water volume across the delta. Mahé et al. (2009) give an average of 800 mm/year, with a minimum and maximum of 400 and 1300 mm/year respectively. This would be an average loss of input discharge of about 40%, according to the authors. These differences are likely caused by the fact that the different studies considered different time periods and that not all studies made a distinction between a northern and southern part of the delta (Liersch et al., 2013). However, all studies indicate that the evaporative losses over the area are substantial and that these lead to large reductions in discharge downstream of the delta.

This has implications for water management in the entire region, as large areas are completely dependent on the water of the Niger River (Dadson et al., 2010; Liersch et al., 2013; Ogilvie et al., 2010; Zwarts et al., 2006). As stated by Zwarts et al. (2006), Mali is a classic case of a 'river-dependent economy', with over one million people making a living from arable farming, fisheries and livestock within the Niger Inner Delta. That is why accurate predictions of the flood extent have been identified as an important research topic (Mahe et al., 2011).

[7] https://rsis.ramsar.org/ris/1365

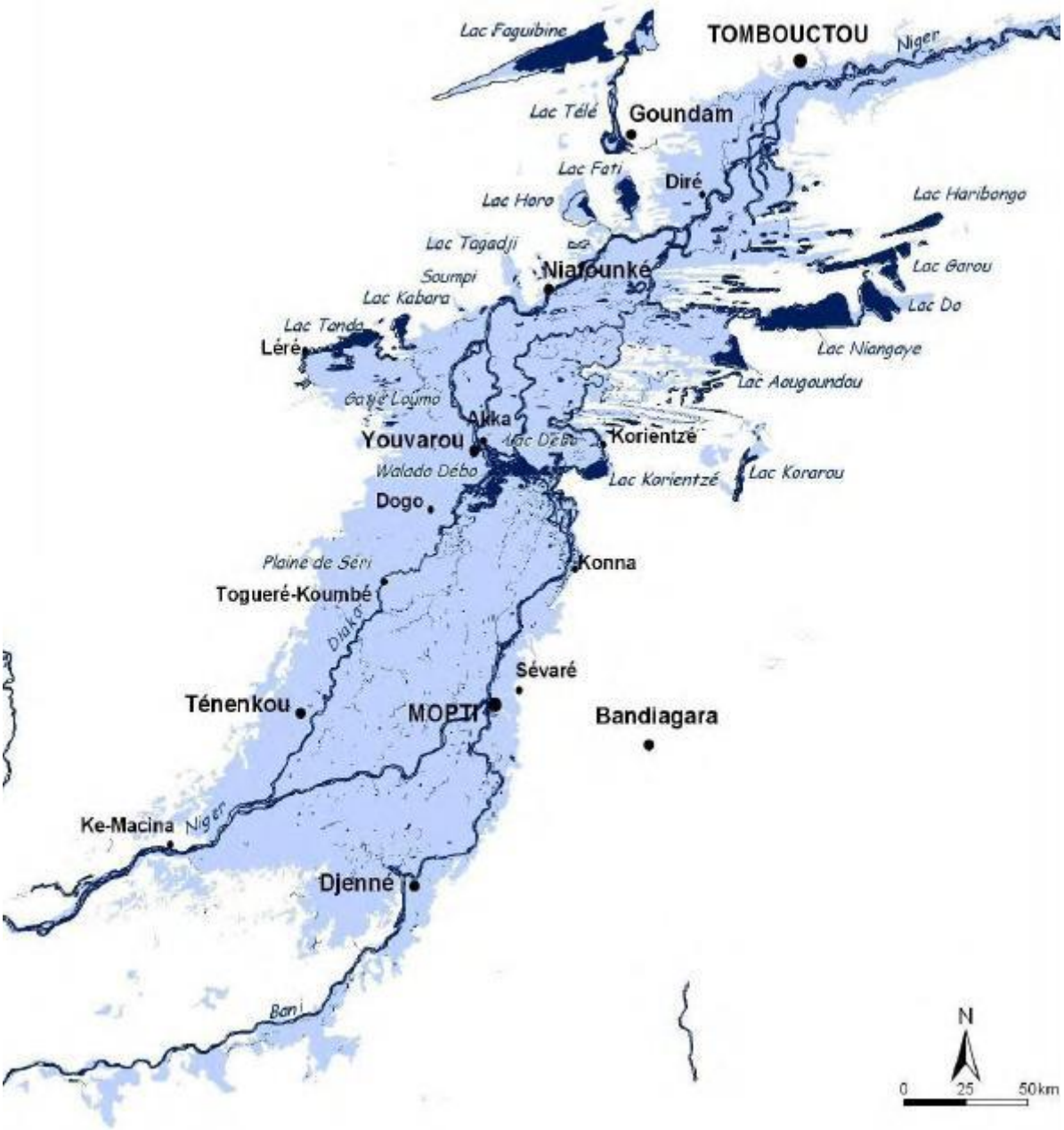

Figure 4: The Niger Inner Delta (www.wetlands.org[8])

Mahé et al. (2009) carried out an extensive research on water losses within the delta, for which they made a distinction between a northern and southern part of the delta. The southern part, which is roughly located south of the central lakes and the town of Youvarou (see Figure 4), functions mostly as a transit zone that delays a large part of the river flow as a result of inundation. The northern part traps the largest quantities of water, as flooding recharges lateral depressions and a string of lakes. In the north, both potential evapotranspiration and infiltration may also be higher than in the south, due to higher temperatures and less cloud cover, and the fact that the floodplains there consist of very sandy soils and sandhills. In the study of Mahé et al. (2009) it is stated that the most important losses seem to occur by evaporation over the entire delta during the period September-January.

[8] http://www.wetlands.org/Portals/0/publications/Other%20publication/floodplains%20of%20IND.jpg

2.3 Hydrological characteristics of the Niger River

As stated before, the Niger River receives a lot of rainfall from its headwaters in Guinea and Ivory Coast. This is still the case in south-western Mali, before it reaches the Inner Delta. The average input discharge here is approximately 1490 m^3/s (over the period 1955-1996), which is decreased while it is passing through the delta until there is approximately 900 m^3/s left as output discharge near the town of Tombouctou (Mahé et al., 2009). Inflow from the Bani tributary does not compensate this loss of discharge (Zwarts et al., 2006). After the Inner Delta the Niger River does not receive any additional inflow over a long distance, with its discharge remaining relatively stable. The lower reaches of the Niger River are located in more humid regions, where it receives input from a number of small tributaries and the Benue River (near the town of Lokoja), which is by far its largest tributary. In fact, the discharge of the Benue exceeds that of the Niger itself. Shortly afterwards, the river reaches its coastal delta and discharges into the Atlantic Ocean.

Figure 5 below shows the average discharge of the Niger River over its entire length, with discharge values obtained for the period 1920-1990. It clearly shows the decrease in discharge that occurs over the Inner Delta, as well as the large contribution of the Benue River to the total discharge of the Niger. This figure is constructed with yearly averaged values and does thus not show seasonal variations. These variations are very important regarding the flooding of the Inner Delta, as this only occurs during the peak flows of the wet season.

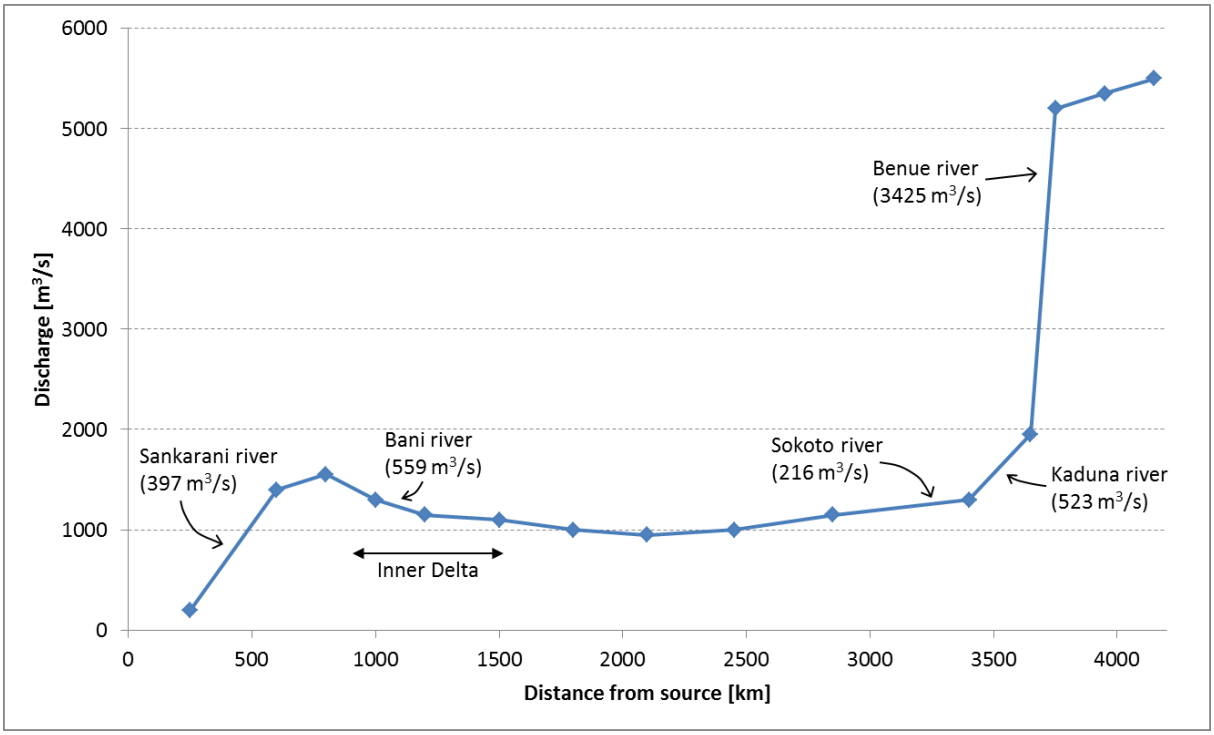

Figure 5: Average discharge of the Niger River over its entire length, including the contribution of its main tributaries (adapted from www.fao.org[3])

The seasonal variation is shown in Figure 6, which shows the average monthly discharge at four locations; upstream of the Inner Delta (Koulikoro), at the confluence of the Bani River (Mopti), towards the end of the Inner Delta (Dire) and further downstream near Niamey. This figure clearly illustrates the reduction in discharge, due to the loss of water over the Inner Delta. It also shows a delay of the peak flow of about two to three months, which was already mentioned by Zwarts et al. (2006). Using these averaged values, the annual reduction in discharge between Koulikoro and Dire

would be close to 30%, which is between the values reported in the literature of 25% (Gourcy et al., 2000) and 40% (Mahé et al., 2009). However, it should be noted that most of this loss occurs during the flood season (July-November), with the values shown in Figure 6 indicating that the discharge has its peak flow reduced by about 60%.

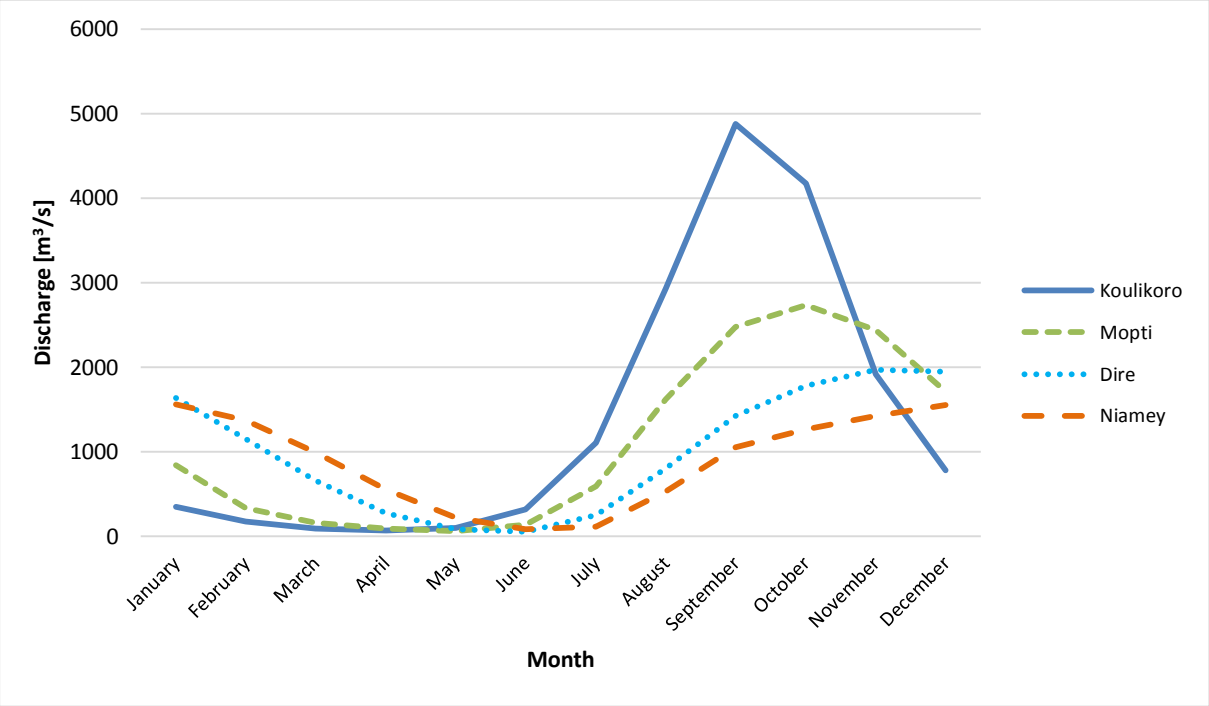

Figure 6: Average monthly discharge of the Niger River at several locations: upstream of the Inner Delta (Koulikoro), at the confluence with the Bani River (Mopti), towards the end of the Inner Delta (Dire) and further downstream (Niamey) (created with data of the GRDC for the period 1920-1990)

3 The global hydrological model PCR-GLOBWB

3.1 Introduction

PCR-GLOBWB is a large-scale hydrological model developed at Utrecht University's Department of Physical Geography. Its first version was coded in the programming language PCRaster (Wesseling et al., 1996), the latest version has been completely converted to PCRaster-Python (Karssenberg, 2010). The model name is a reference to this, as PCR-GLOBWB is an abbreviation for PCRaster GLOBal Water Balance model. The model is intended for global to regional hydrological studies and has been applied successfully in a large variety of studies.

On the global scale, PCR-GLOBWB has been used in many studies on the subjects of groundwater abstractions, irrigation practices, water stress and the effect of human actions on discharge (Van Beek et al., 2011; Wada et al., 2010, 2012). On a more regional scale, it has been used to estimate sediment, carbon and nutrient fluxes for a range of catchments including the Rhine (e.g. Loos et al., 2009) and to study the influence of local hydrology on methane emissions of boreal and arctic wetlands (Petrescu et al., 2010). A study by Bierkens & Van Beek (2009) focused on the seasonal predictability of discharge in European rivers, assessing the influence of North Atlantic Oscillation (NAO) based weather predictions, hydrological properties of river basins and the correct assessment of initial hydrological states.

Various studies have used PCR-GLOBWB to model global discharge. Sperna Weiland et al. (2010) used it to assess the usefulness of Global Climate Model (GCM) data for hydrological studies, by forcing it with climate data output from a selection of twelve GCMs and comparing simulated discharge with observations, focusing on discharge variability and extremes. Candogan Yossef et al. (2012) made an assessment of PCR-GLOBWB's potential skill in forecasting monthly flow extremes by comparing the simulated discharge of 20 large rivers with observed monthly streamflow records. These two studies were already briefly mentioned in the first chapter. Another study by Candogan Yossef et al. (2013) investigated the effect that initial conditions and meteorological forcing data had on the skill of global seasonal streamflow forecasts. For the Niger River, the relative importance of initial conditions and meteorological forcing showed the strongest seasonality of all investigated river systems. They state that initial conditions, especially related to groundwater outflow, are the most important factor for forecasts for the months of January to July, but that meteorological forcing becomes more important for the period of August-December.

PCR-GLOBWB has also been used to study the effects of climate change. For example, Sperna Weiland et al. (2012) investigated the influence of climate change on global hydrological regimes. Their results indicate that globally discharge would increase by more than ten percent, but the Niger had a decrease in both mean and extreme discharge. Of all the studied African rivers, the Niger was the only one with a decreasing runoff coefficient, indicating that the part of precipitation that evaporates increases. In fact, the Niger was the only basin globally with a decrease in runoff coefficient of more than 10 %.

More information on the model itself and its applications can be found online[9,10]. A thorough technical overview of PCR-GLOBWB can be found in its official documentation (Van Beek & Bierkens,

[9] http://www.globalhydrology.nl/

[10] http://pcraster.geo.uu.nl/projects/applications/pcrglobwb/

2008). A lot work is currently being carried out on improving the model (Sutanudjaja et al., in prep.), so it is understandably hard to keep this documentation completely up-to-date. It would also greatly improve the readability of this thesis if several key-aspects of the model were listed here. Therefore, the most relevant aspects of PCR-GLOBWB will be described below. This includes the basic model concepts, as well as more detailed information on certain processes that are important for coupling it to the hydrodynamical model.

3.2 Model concepts

PCR-GLOBWB is a grid-based model, which operates globally at a resolution of either 30 arcmin (approximately 0.5 degrees or 50x50 km) or 5 arcmin (approximately 0.08 degrees or 10x10 km). It includes all important processes of terrestrial hydrology and uses a daily timestep. In each cell, PCR-GLOBWB distinguishes between a groundwater layer, two vertically stacked soil layers and a surface layer. The model uses process-based equations to compute the storage and vertical exchange of water between the different layers of a cell, as well as the horizontal exchange of surface water between hydrologically connected cells. The model is forced with meteorological data, with precipitation and temperature being obligatory, while evapotranspiration can also be calculated from the temperature input using the Hamon method (Hamon, 1963). The different stores and fluxes of the model are shown in Figure 7 below.

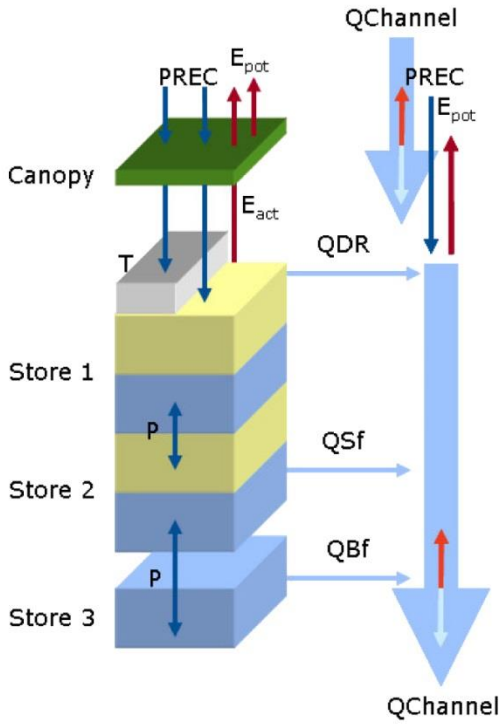

Figure 7: Model concept of PCR-GLOBWB (Van Beek & Bierkens, 2008)

The left of the figure shows the different layers and processes within a cell. Precipitation input can be intercepted by the canopy or go straight to the surface as throughfall, where it can evaporate or infiltrate into the soil. Capillary rise and percolation control the vertical fluxes within the soil. From each layer, water can flow into lakes or rivers through direct runoff (QDR), interflow (QSf) and baseflow (QBf). This ends up in channels, which form a horizontal connection within the model and can thus transport water over the model grid as discharge (QChannel). Direct gains and losses from the channel, in the form of precipitation and evaporation, are also considered. The model can also account for snow, lakes, reservoirs, irrigation and their related processes.

PCR-GLOBWB recognizes four different land cover types that each have their own distinct hydrological characteristics; two natural classes (short and tall vegetation) and two irrigation classes (paddies and non-paddies). The user has to specify whether a simulation is carried out using only the two natural classes or all four classes, with the irrigation classes being most useful for studies related to water stress, irrigation practices and groundwater abstractions. The model simulates all hydrological processes for the specified land cover types, while taking account of the fraction within a cell that each land cover type occupies.

Other cases of sub-grid variability include (Van Beek & Bierkens, 2008):

- the fraction covered with freshwater (rivers, lakes and reservoirs)
- the distribution of soil types and the effect on soil hydrological properties
- the distribution of the water-holding capacity of the soil as a result of variations in soil depth, effective porosity and elevation distributions, leading to variable saturation excess overland flow (i.e. the improved Arno scheme [Hagemann & Gates, 2003], which will be described in more detail in paragraph 3.4.1)

3.3 Initial conditions and spin-up

Since PCR-GLOBWB uses only meteorological forcing data as input variables, the initial conditions of all terrestrial stores (soil moisture, groundwater, channel storage, etc.) either have to be known beforehand and given as input data, or be determined from the meteorological input by means of a spin-up run. This spin-up starts with a 'cold state' consisting of empty stores (zero conditions) and then simulates the first year of the specified time period, after which it checks if specified convergence criteria have been met. As long as this is not the case, the simulation of the first year is repeated. When the convergence criteria have been met (or the specified maximum number of spin-up years has been reached), the spin-up stops and the normal, transient run starts.

The convergence criteria work by calculating the difference in the values of the most important stores (e.g. soil storage, groundwater storage and channel storage) at the start and end of the year. If this difference is below a user-specified percentage, the model has converged. The idea behind this is that the volume of water in the stores should not change dramatically when running the model for the same year over and over (all the time using the same input variables). If the volume of water does show large changes, this probably means more water is being added to the system, which means that the initial conditions are not properly set yet. When the changes are small, this indicates that the system has reached a relative steady-state with accurate initial conditions.

The model saves the states of all stores at the end of each year to a 'warm state' file, which means that these can be used to supply the model with information about initial conditions (if a run with similar parameter values is carried out). This negates the need for a long spin-up period, substantially reducing model calculation time.

3.4 Relevant hydrological processes

PCR-GLOBWB includes a very long list of hydrological processes; this paragraph describes those that are most relevant for this study (i.e. the processes that play an important role when the model is coupled to the hydrodynamical model). These have been identified as the calculation of infiltration, evapotranspiration, runoff and discharge. The hydrological processes at the land surface are shown in Figure 8 to the left. In this figure, which represents the top soil layer of the model, T stands for transpiration, P is precipitation, E is evaporation, I is infiltration, D is percolation, C is capillary rise and R is direct runoff. Precipitation that is not intercepted will

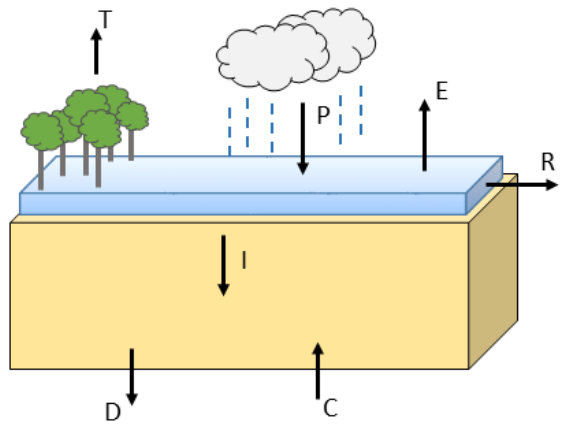

Figure 8: Schematic representation of hydrological processes within PCR-GLOBWB's land surface

end up on top of the first soil layer as surface water, where it will be partitioned into evaporation, infiltration and runoff. The water that infiltrates goes to the storage of the soil layer, runoff will end up in channel storage, while the water that evaporates is lost to the system entirely, as PCR-GLOBWB does not include an atmospheric feedback.

3.4.1 Partitioning of surface water into direct runoff, infiltration and evaporation

Surface water is first exposed to possible open water evaporation, which only occurs over irrigated paddy fields, and afterwards the improved Arno scheme (Hagemann & Gates, 2003) is used to partition the remaining water into runoff and infiltration. This is visualized in Figure 9 below, with the equation for the fraction of saturated soil depicted next to it. In this equation, w_{max} is the maximum average storage in the upper soil layer, w_{min} is the minimum average storage and w_{act} is the actual storage. The parameter b is a dimensionless shape factor that defines the distribution of soil water storage within the larger cell and is calculated based on the distribution of maximum rooting depths.

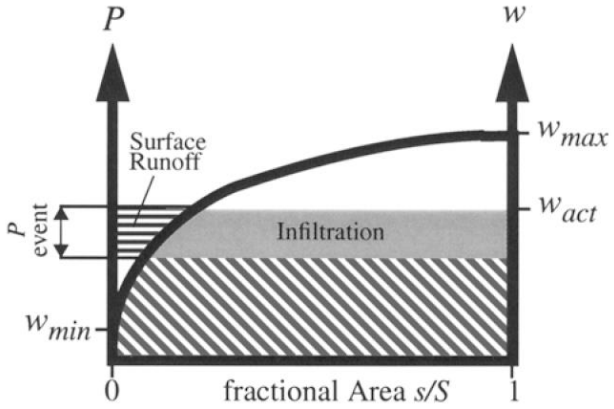

$$\frac{s}{S} = 1 - \left(\frac{w_{max} - w_{act}}{w_{max} - w_{min}}\right)^{\frac{b}{b+1}}$$

Figure 9: Surface runoff related to the fraction of saturated soil (Hagemann & Gates, 2003)

The figure shows how the calculation of runoff depends on the current storage within the cell and the fraction of saturated soil. After the calculation of runoff, all remaining surface water is free to infiltrate into the upper soil layer with a speed of up to the saturated hydraulic conductivity. After all the fluxes for the first soil layer are calculated (which also includes the vertical fluxes with the lower soil layer, i.e. capillary rise and percolation, as well as losses through bare soil evaporation and transpiration), any excess of the total storage of this layer is added to the previously calculated runoff. The total runoff of a cell consists of this saturation excess surface runoff (i.e. direct runoff) and runoff from the second soil reservoir (interflow), which are shown in Figure 7 as QDR and QSf, respectively.

3.4.2 River discharge and routing

In PCR-GLOBWB, river discharge is calculated by accumulating and routing specific runoff along the drainage network (often referred to as a Local Drainage Direction map [LDD]), while taking dynamic storage effects, evaporative losses and riverbed infiltration into account (Van Beek & Bierkens, 2008). This is visualized in Figure 10 and Figure 11 on the next page. Figure 10 show a generic schematization of the routing of a flood wave (i.e. discharge peak) over a small section of a drainage network, while Figure 11 shows the different processes, as well as the order in which they occur, that are influencing the update of channel storage in PCR-GLOBWB through its routing scheme. PCR-GLOBWB gives the option to choose between two routing methods, which both follow the routing scheme of Figure 11, but which might have different update steps and numerical equations. These methods are discussed in more detail in the next paragraph.

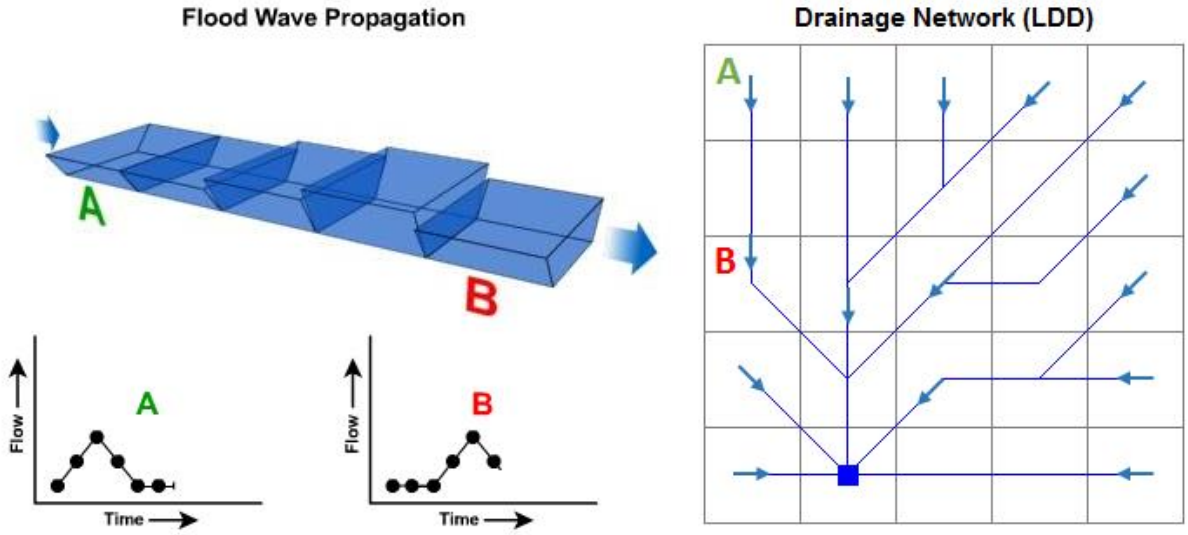

Figure 10: Schematization of routing a flood wave over a channel or drainage network (LDD), from point A to point B (adapted from www2.ucar.edu[11] [left] and pcraster.geo.uu.nl[12] [right])

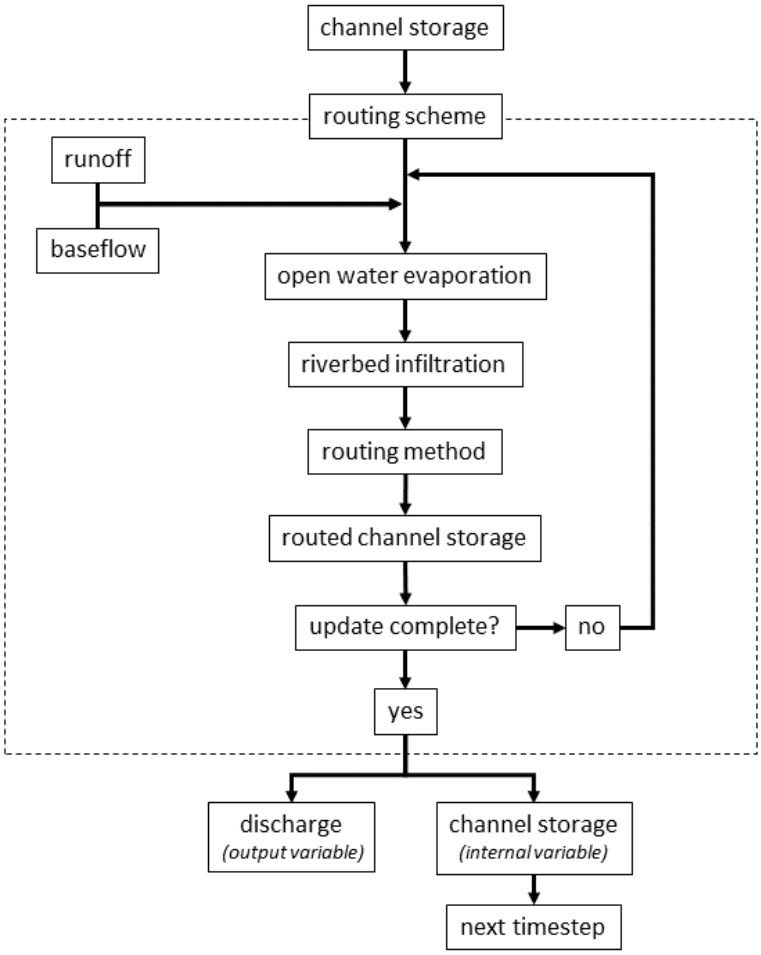

Figure 11: The calculation of discharge and update of channel storage within PCR-GLOBWB

[11] http://stream2.cma.gov.cn/pub/comet/HydrologyFlooding/StreamflowRoutingInternationalEdition/comet/hydro/basic_int /routing/media/graphics/flood_wave_prop.jpg
[12] http://pcraster.geo.uu.nl/pcraster/4.0.2/doc/manual/_images/accu_Ldd.png

3.5 Routing options

The two routing options currently available in PCR-GLOBWB are a flow velocity based scheme, named 'accuTravelTime', and a numerical solution to the kinematic wave equations, named 'kinematicWave'.

3.5.1 Flow velocity based routing (accuTravelTime)

This is a relatively simple routing method which depends only on the flow velocity. The flow velocity determines the distance that a volume of water can travel. During routing, this volume is transported downstream over the LDD using the specific flow velocity at every grid cell. In practice this is done in the following three steps:

1. Before the actual routing takes place, the time necessary to cross a cell is determined for all individual cells as:

$$t_i = \frac{dx_i}{u_i}$$

   In which dx_i is the distance between the center of cell i and the next downstream cell, u_i the flow velocity at this cell and t_i the total time required to cross this cell.
2. During the routing procedure, a volume of water is transported downstream over the LDD, while adding up the travel times (t_i) of all the cells it flows through.
3. When the sum of the travel times equals 1 day (or more), the water volume is deposited in that cell. If the sum is higher than exactly 1, this means that the volume has not reached the center of the current cell but is actually somewhere between the centers of the current cell (destination cell) and the last upstream cell. If this is the case, the volume is split over these two cells, as follows:

$$V_{i-1} = \frac{\sum t - 1}{t_i} \cdot V_0$$

$$V_i = V_0 - V_{i-1}$$

   In which V_0 is the original material within a cell before routing, $\sum t$ is the sum of previously encountered travel times, t_i is the travel time of the current cell, V_{i-1} is the material that will be deposited in the upstream cell and V_i the material that will be deposited in the destination cell.

This procedure is illustrated with an example in Figure 12 on the next page, in which the original volume of 50 m^3 before routing is transported over the channel network or LDD and ends up in two cells further downstream, as 13.3 and 36.7 m^3 respectively. The flux for each cell (i.e. the discharge in m^3/day) is shown on the far right of this figure. The method updates with the same timestep as the PCR-GLOBWB model (i.e. one day), and as such the steps of the routing scheme shown in Figure 11 are carried out once per daily update of PCR-GLOBWB.

In PCR-GLOBWB the velocity is calculated using Manning's equation (Manning, 1891):

$$v = \frac{R^{2/3} \cdot S^{1/2}}{n}$$

In which v is the velocity $[m/day]$, R the hydraulic radius $[m]$, S the bed slope $[-]$ and n is Manning's roughness coefficient $\left[day/m^{1/3}\right]$.

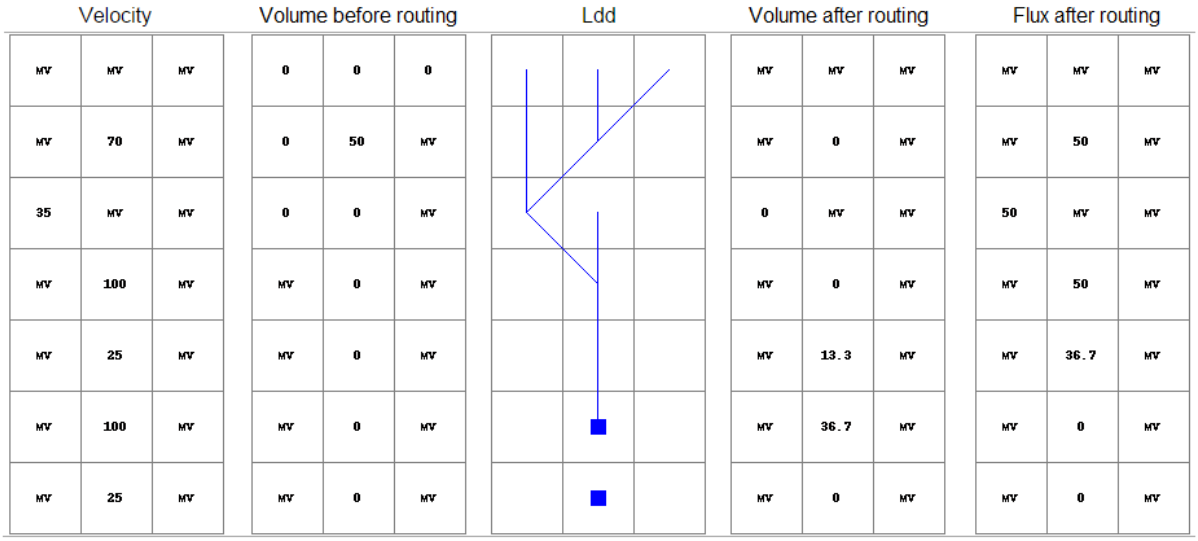

Figure 12: Example of the accuTravelTime routing method of PCRaster (adapted from pcraster.geo.uu.nl[13])

By assuming a simple rectangular shape for the channel, the hydraulic radius can be estimated from the width of the channel and the water depth:

$$R = \frac{A}{P} = \frac{w \cdot y}{w + 2 \cdot y}$$

With A being the wet area $[m^2]$, P the wet perimeter $[m]$, w the channel width $[m]$ and y the water depth $[m]$. In PCR-GLOBWB the channel width and water depth are estimated from an empirical relationship using average discharge (which itself is calculated from all discharge simulated up to the current timestep):

$$y = \eta \cdot \overline{Q}^{\nu}$$

$$w = \tau \cdot \overline{Q}^{\varphi}$$

In which η, ν, τ and φ are empirically derived parameters with set values (being 0.25, 0.40, 8.0 and 0.58 respectively) and $\overline{Q}$ is the average discharge. Since the average discharge changes with every timestep, so do the estimated channel widths and water depths.

Using this relatively simple routing scheme has the obvious advantage of fast calculation speeds. However, it may be less accurate than other, more sophisticated routing methods. Since the routing only depends on travel times per cell, each volume is water is essentially treated separately and thus upstream or downstream discharge does not affect the routing of a specific cell. This, combined with the fact that the momentum equation is omitted (which is often used in more sophisticated routing schemes, see also the description of the D-Flow FM hydrodynamical model in the next chapter), means that the method cannot simulate so-called “backwater effects” Backwater effects occur in areas where a downstream phenomenon has an influence on upstream flow conditions, as would be the case with tidal fluctuations or an obstruction to the flow. Also, since the method uses average discharge to calculate flow velocities, it might be unable to simulate suddenly occurring peak flows, during which the calculated channel widths and water depths will be underestimated.

[13] http://pcraster.geo.uu.nl/pcraster/4.0.1/doc/manual/op_accutraveltime.html

3.5.2 Kinematic Wave approximation (kinematicWave)

PCR-GLOBWB also has the option to use a kinematic wave routing method. This is a more complex routing method than the one described in the previous paragraph, based on a numerical solution to the kinematic wave equations. The kinematic wave equations are an approximation of the physics-based Saint-Venant equations to describe shallow water flow in open channels (Chow et al., 1988). This is done by combining the continuity equation:

$$\frac{\partial Q}{\partial x} + \frac{\partial A}{\partial t} = q$$

with a general form of the Chezy or Manning equation:

$$\alpha \cdot Q^{\beta} = A$$

to form the following equation:

$$\frac{\partial Q}{\partial x} + \alpha \cdot \beta \cdot Q^{\beta - 1} \cdot \left(\frac{\partial Q}{\partial t}\right) = q$$

In which Q is the discharge $[m^3/s]$, A is the wetted area $[m^2]$, ∂x is the channel length through the cell $[m]$, ∂t is the timestep $[s]$ and q is the lateral inflow into the channel $[m^3/s]$. α and β are coefficients which can be obtained from the original Chezy or Manning equation, e.g. for Manning:

$$Q = \frac{R^{2/3} \cdot \sqrt{S}}{n} \cdot A$$

In which R is the hydraulic radius $[m]$, S the bed slope $[-]$ and n is Manning's roughness coefficient $\left[s/m^{1/3}\right]$. The assumption of broad sheet flow and a rectangular channel gives $\beta = 0.6$ for the Manning equation (Van Beek, 2014) and allows α to be calculated as:

$$\alpha = \left(n \cdot P^{2/3} \cdot S^{-1/2}\right)^{\beta}$$

Given the required input, the kinematic wave function in PCRaster calculates for each cell the accumulated volume (volume in the cell itself plus the volume from upstream cells) that flows out of the cell into its neighbouring downstream cell. This routing method updates with timesteps smaller than that of PCR-GLOBWB, and as such the steps of the routing scheme shown in Figure 11 are looped over multiple times per daily update of PCR-GLOBWB. The number of sub-timesteps is determined before the update of the routing scheme, so that a correct fraction of the total runoff and baseflow are added to the channel storage at every update. Because of this, this method has an advantage over the method described in the previous paragraph, since it can be used in situations where the average travel time through a grid cell is within the magnitude of the model timestep. The method is still not that computationally intensive, especially when compared to the full Saint-Venant equations.

However, this method still has its drawbacks. Unlike the full Saint-Venant equations, which describe unsteady and non-uniform flow, the kinematic wave equation assumes steady and uniform flow. This implies that the kinematic wave equation cannot account for the effects of a downstream boundary condition on discharge. As stated by Beven (2001), "essentially the effects of any disturbance to the flow will generate a kinematic wave, but the equation can only predict the downslope or downstream movement of these waves. Thus a kinematic wave description cannot predict the effects of a drawdown of a water table due to an incised channel at the base of a hillslope, or the backwater effects of an obstruction to the flow for a surface flow". Another possible issue is the

problem associated with kinematic shocks. Since it is assumed that the speed with which a wave moves downstream increases with its depth, this could lead to a built up of a large steepening wave, which would lead to a sudden jump in discharge when such a front reaches the base of a slope (Singh, 1996). This is a side-effect of the mathematics of the kinematic wave. It is not expected to be problem for this study, as it does not focus on hillslopes and kinematic shocks rarely occur within channels (Ponce, 1991).

4 The hydrodynamical model D-Flow FM

4.1 Introduction

The accurate modelling of the inundation patterns within the Niger Inner Delta require a model that can operate at a higher resolution than PCR-GLOBWB and that is also specifically designed for the simulation of hydrodynamic processes. Hydrodynamical models are particularly concerned with the movement of fluids (i.e. water) and thus use more sophisticated equations and numerical schemes to simulate this than those used in the routing module of PCR-GLOBWB (or other hydrological models).

Currently, D-Flow Flexible Mesh (D-Flow FM), a new software engine for hydrodynamical simulations, is being developed by Deltares in Delft, the Netherlands and is set to become part of the successful Delft3D suite[14,15]. D-Flow FM is a shallow-water solver based on the finite-volume method applied on unstructured grids. It solves the full Saint-Venant equations and thus guarantees both mass and momentum conservation, while also accurately representing the drying and flooding of grid cells (Kernkamp et al., 2011; Verwey et al., 2011). Because the model is still in active development, not all features that it is set to receive are currently implemented. However, the features required for this study (e.g. 2D hydrodynamic flow modelling, discharge and water level boundary conditions and the automatic generation of a grid) were implemented in the model at the start of this research and could thus be used in the study.

It has been successfully applied on a number of test-cases, such as water level simulations at the Zandvliet-Berendrecht lock complex in Belgium (Maximova et al., 2013) and tropical cyclone storm surge simulations on the east coast of Queensland, Australia (Burston et al., 2014). It is currently being used in many different studies, such as that of the Venice Lagoon (Menel Lemos, 2014), San Francisco Bay Delta (Van der Wegen, 2014) and a global tide and storm surge model (Verlaan, 2014).

This chapter briefly describes the basic concepts of the D-Flow FM model, as was done for PCR-GLOBWB in the previous chapter. More information, including a complete overview of the involved numerics, can be found in its technical reference manual (Deltares, 2015a). However, it should be noted that, just like the model itself, this document was still in active development during the writing of this thesis.

4.2 Shallow-water equations

D-Flow FM solves the shallow-water equations in one, two and/or three dimensions, depending on the type (or section) of the model grid that is being calculated. The depth-averaged, homogeneous shallow water equations are given by (Deltares, 2015a; Kernkamp et al., 2011):

$$\frac{\partial H}{\partial t} + \nabla \cdot (H\vec{u}) = q$$

$$\frac{\partial \vec{u}}{\partial t} + adv(\vec{u}) + g\nabla\zeta + c_f\vec{u}\|\vec{u}\| + 2\Omega \times \vec{u} = d$$

in which H is the total water depth, $\nabla \equiv \left[\partial_x, \partial_y\right]^T$, T is the horizontal gradient operator, ζ is the water level relative to a reference plane, $\vec{u}$ is the depth-averaged horizontal velocity vector, $adv(\vec{u})$ is the advection term and Ω is the earth rotation vector. The right-hand side q contains source terms

[14] http://oss.deltares.nl/web/delft3d/d-flow-flexible-mesh
[15] https://publicwiki.deltares.nl/display/nghs/Projects-Flexible+Mesh

and d contains external forcing. The constants g and c_f denote the gravity constant and bottom-friction coefficient, respectively. The Ω term is important for coastal applications but often omitted in river-related studies, since it is related to the Coriolis effect which has little effect on river systems (Lane, 1998).

4.3 Flexible mesh and unstructured grids

What makes D-Flow FM stand out from other shallow-water solvers is its flexible mesh. It allows the use of different grid-types, so that one model can use a structured, curvilinear or unstructured grid, or a combination of these in either Cartesian or spherical coordinates. As stated by Kernkamp et al. (2011), the need for such a model, with a locally variable grid resolution, arose from the desire to more accurately simulate the flow of water in topographically complex areas. It allows the user to set up a model with a high resolution grid only in areas where this is required, keeping the rest of the model in a lower resolution. This should improve the modelling accuracy in complex areas while keeping the computational restraints relatively low.

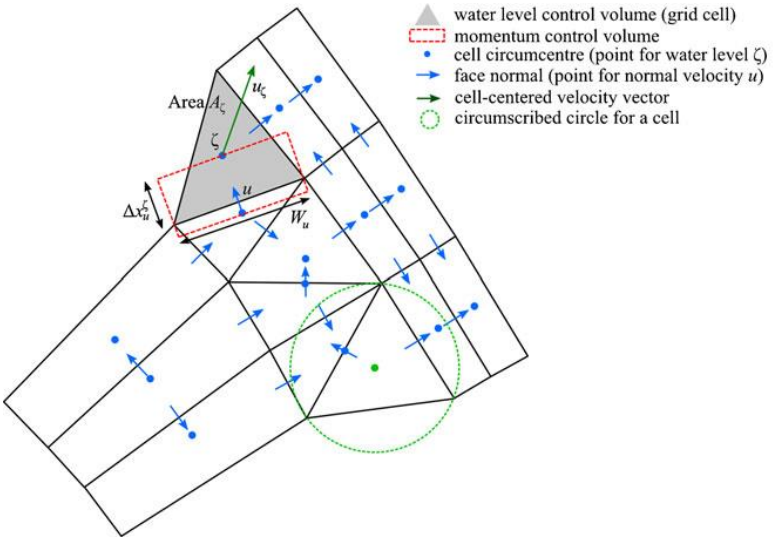

Figure 13: A small section of an unstructured grid made up of triangles and quadrangles (Kernkamp et al., 2011)

An example section of an unstructured grid is shown in Figure 13 on the left. It shows how two sections made up of different quadrangles can be joined together by triangles of variable size and shape. The symbols match those of the equation described in the previous paragraph.

Curvilinear grids were a great step forward in the possibilities of numerical flow modelling, but some of their drawbacks are hard to deal with. For example, when a curvilinear grid is used to represent a meandering river channel, the gridlines will be focused in the inner bends of the channel, resulting in unnecessarily small grid cells (Kernkamp et al., 2011). An unstructured grid would be able to overcome most issues associated with structured and curvilinear grids. There are currently a lot of developments related to unstructured grids applied to hydrodynamic simulations, such as ADCIRC (Dietrich et al., 2010; Westerink et al., 2008), TELEMAC (Hervouet, 2007; Postma & Hervouet, 2007) and UnTRIM (Casulli & Walters, 2000; Casulli & Zanolli, 2002). As always, each model has its own strengths and weaknesses. The novelty of D-Flow FM lies in the fact that it allows a grid with polygon-shaped cells of arbitrary degree and size, as well as a combination of 1D, 2D and 3D elements (Kernkamp et al., 2011; Verwey et al., 2011). This gives great flexibility when designing a model grid. For example, a model of an estuary could now have river tributaries modelled in 1D, floodplain sections in 2D and the estuary itself modelled in 3D.

For river channels that are not meandering a lot, Kernkamp et al. (2011) realized that curvilinear grids might still represent the best possible modelling solution and they state that “flow gradients in the channel length direction are often smaller than those in the channel cross direction, which suggests application of grid cells that are elongated and aligned in the flow direction. This can only be

achieved by a curvilinear grid." In this case, a curvilinear grid would have less grid cells in total than an unstructured triangular grid, while it would have a higher resolution in the cross-flow direction. This would optimize computational efficiency while maintaining high accuracy.

4.4 Grid creation concepts

As stated above, D-Flow FM allows the creation of a grid with relatively small cells in areas where this is required (e.g. within river channels and around areas that are susceptible to flooding, such as lakes, wetlands and low-lying floodplains), while keeping the rest of the model grid at a relatively low resolution to maximize computational efficiency. The manual creation of such a flexible grid, with different cell sizes and shapes depending on the specific features of an area, requires a lot of time and effort. While manual creation might be the best option for projects that are only concerned with one specific area, especially when this area is relatively small, this is not an option for large-scale and global studies. While this study is primarily concerned with the Niger basin, it also investigates a possible global application, which rules out the manual creation of a grid (because it would involve too much work to manually create a grid for all river systems). Fortunately, D-Flow FM has several options to automate the grid creation process.

An automatically generated grid is not only a necessity for this study, it also has the advantage that there are no human errors involved in its creation and it ensures that every location on earth is treated in the exact same manner. Finally, if this is so desired, it is still possible to manually adjust the grid after its automatic creation, giving it all the flexibility of manual creation. One of the most promising options for this study is Courant-based grid refinement, which has been used to create a grid for the Dutch Continental Shelf Model [DCSM] (Kernkamp et al., 2011), see Figure 14 below, and which is also being used in the global tide and storm surge model that is currently in development (Verlaan, 2014). This automatic grid refinement uses Courant number theory to refine an existing grid, with more refinement occurring in areas associated with shallower water depth values. This can clearly be seen in Figure 14, where the resolution of the grid increases as it gets closer to the shore.

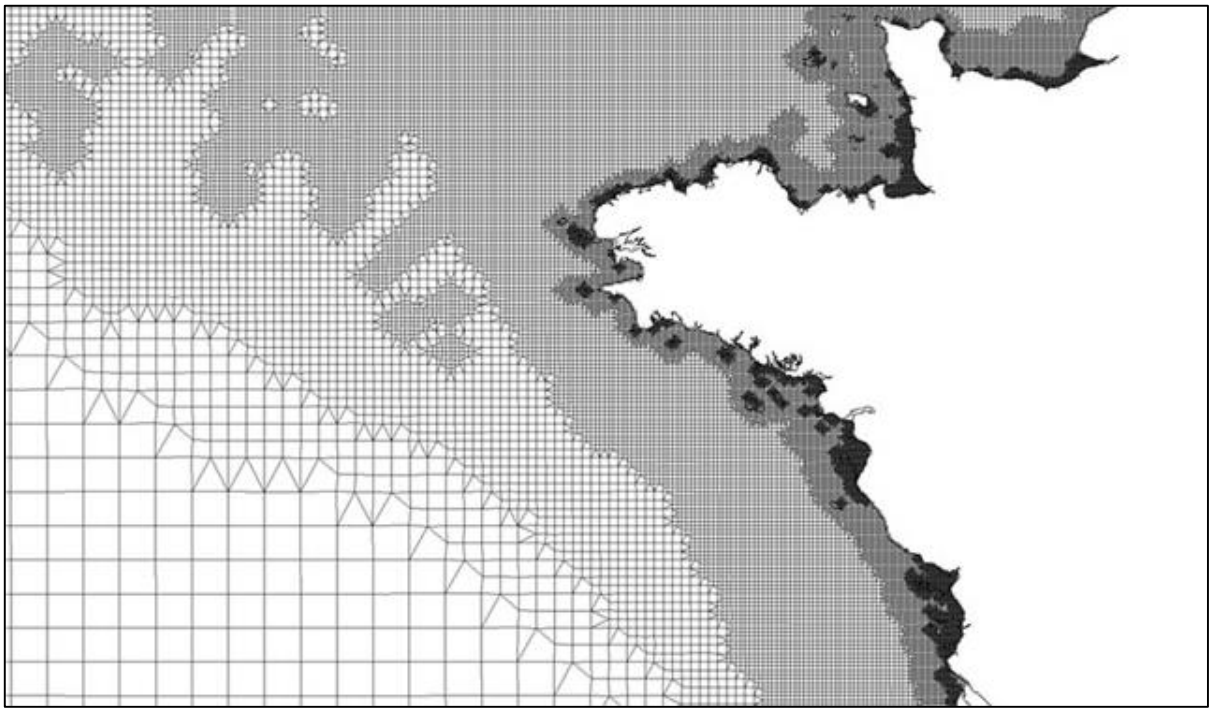

Figure 14: Part of the Courant-based grid used in the Dutch Continental Shelf Model (Kernkamp et al., 2011)

Such a grid is desirable in coastal applications, as shallower areas represent regions with stronger influences from currents and waves, and thus require a higher grid resolution to accurately model these processes.

4.4.1 Courant number theory

The Courant number is part of the Courant-Friedrichs-Lewy (CFL) condition (Courant et al., 1928), which is a necessary (but not always completely sufficient) condition for the stability of numerical approximations of partial differential equations, such as those described before in paragraph 4.2. The principle behind the CFL condition is that, considering the movement of a fluid, there should be a balance between the timestep used in the numerical calculation, the size of the grid cell over which it is transported and its velocity. If the timestep is too large, the fluid might travel a distance that is longer than the size of the grid cells and miss information required for the numerical approximation, which can lead to oscillations and instability. This is illustrated for a simple one-dimensional case in Figure 15 below, in which α is the (dimensionless) Courant number.

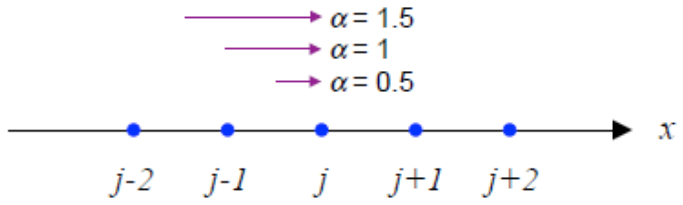

$$\alpha = u\frac{\Delta t}{\Delta x}$$

Figure 15: Concept of the Courant number for a simple one-dimensional case (Schär, n.d.)

With u being the velocity, Δt the timestep and Δx the cell length (which is the distance between two adjacent points j in Figure 15). From this figure it can be seen that it is necessary to limit the Courant number to make sure that the information of all grid cells is being considered in the calculation. This is often done by limiting it to one $(\alpha \leq 1)$, which in the example above would be exactly equal to the distance between two points, so that:

$$u\frac{\Delta t}{\Delta x} \leq 1$$

It also shows that, when Δx decreases (because of the use of smaller grid cells), Δt has to decrease as well to still fulfill this criteria (assuming the velocity u stays the same). This has clear implications for the creation and use of a grid in models using numerical approximations of partial differential equations, such as D-Flow FM, in that a higher resolution grid will require smaller timesteps and thus increase the time required to perform a simulation.

4.4.2 Automatic grid refinement

The velocity in the equation of the Courant number depends on a lot of different factors, including the method used to approximate the full Saint-Venant equations. When the shallow water approximation is used in coastal applications, this often means that one considers gravity waves, which are a function of the gravitational acceleration g and the water depth H:

$$\sqrt{g \cdot H} \cdot \frac{\Delta t}{\Delta x} \leq 1$$

When information on H is available, for example through bathymetric data (and the assumption of a constant water level), the above equation can be used to automatically refine a grid. This is done by specifying a maximum allowed timestep for Δt, so that Δx becomes the only unknown variable and

can then be calculated for every cell within the total grid. For example, if the specified maximum timestep is 400 seconds, the grid width Δx at an area with a water depth of 10 meters would be (assuming $g = 10\ m/s^2$):

$$\Delta x = \sqrt{g \cdot H} \cdot \Delta t_{max} = \sqrt{10 \cdot 10} \cdot 400 = 4000\ m$$

Consequently, the resulting grid width Δx will be different for locations with different water depths; lower water depths give smaller mesh grid widths. By using this as a refinement criterion the entire grid can be refined automatically. D-Flow FM also automatically connects cells of different sizes with triangles (see also Figure 14).

However, this exact procedure cannot be applied directly to studies of river systems, because it is not possible to obtain an estimate of water depths H for every location within a study area. While elevation data of an area can be obtained relatively easily, usually in the form of a Digital Elevation Model (DEM), this cannot be directly linked to water depths. And even if this would be possible, the desired grid resolution of a river system model is opposite to that of a coastal model; it requires a higher resolution in areas associated with higher water depth values, as these indicate the location of channels, lakes and low-lying floodplains. Therefore, another type of terrain model, which could overcome these issues, is required to use the Courant-based grid refinement for river systems.

4.4.3 Height Above Nearest Drainage (HAND)

DEMs are very useful to determine the flow of water on land, since this is (partly) controlled by gravitational energy gradients resulting from the spatial variation of elevation levels (Moore at al., 1992). However, it is not directly possible to relate these elevation levels to the potential presence of surface water. A relatively new terrain model, which can do just that and is very suitable for the previously described purpose, was developed by Rennó et al. (2008) and named the Height Above Nearest Drainage (HAND) model. It was originally intended for terrain classification and the creation of landscape classes representing different soil environments in Amazonia (Nobre et al., 2011; Rennó et al., 2008). The idea behind this was that local topography has a strong link with the degree of saturation of the soil, since the soil near a (flowing) stream will very likely have a (permanently) high degree of saturation. Classical DEMs, which show absolute height above sea level, are not suitable to derive these local-scale environmental factors. Instead, it is essential to know the elevation of all points draining to a certain point on a stream relative to the elevation of this point on the stream. The difference between a DEM and HAND map are shown in Figure 16 on the next page. Channels are better visible in the bottom image of this figure, which represents the HAND map. It can also be seen that all channels have a HAND value of zero, indicating that the terrain is essentially 'flattened' and the DEM's reference against sea level is replaced with that of the nearest (hydrologically connected) channel.

Derivation of a HAND map requires knowledge of flow directions within the area, which can be derived from DEMs using a variety of methods (Zhou & Liu, 2002). One of the most simple and widely used methods for determining flow direction is the D8 Flow Algorithm, which was initially proposed by O'Callaghan & Mark (1984). This method describes the flow from each point on a grid towards the steepest downward slope, which is assumed to represent the downstream flow direction. The result is a Local Drain Direction grid (LDD, see also Figure 10 on page 25). In an LDD, a point that does not have any neighbours with a lower elevation is defined as a pit and this either represents an area where water cannot flow out of (i.e. in the case of an internally draining basin), or the outflow point of the channel into the sea. Since errors in DEMs can lead to a wrong derivation of an LDD, many

different methods exist to adjust a DEM prior to the calculation of an LDD and/or adjust an LDD after its creation (e.g. Chen et al., 2012; Zhou & Liu, 2002). This is also done to make sure that small elevation increases do not stop the flow of water completely, as these would simply fill up with water after which the overflow would continue to proceed downstream. LDDs which have been adjusted with this in mind are often referred to as hydrologically sound or correct LDDs. The HAND algorithm requires such a hydrologically correct LDD.

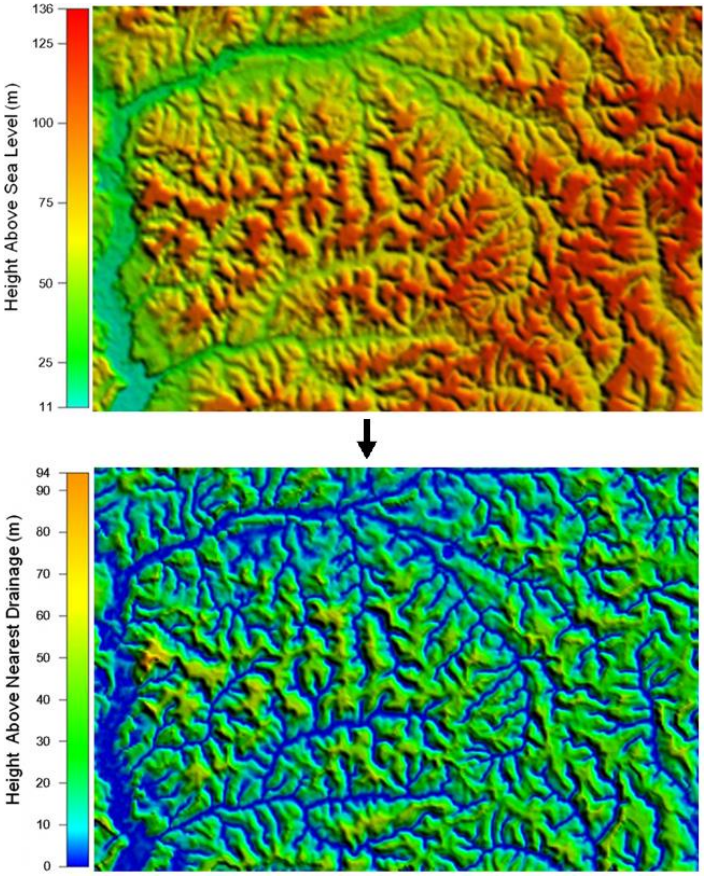

Figure 16: A classical DEM (top) and the HAND map derived from it (bottom) (Nobre et al., 2011)

The HAND algorithm has already been used for other purposes than those described by its original authors (Nobre et al., 2011; Rennó et al., 2008). For example, Alfaya et al. (2012) used HAND to derive floodplains of a section of the Amazon River. The map of the floodplains they created with the HAND algorithm showed a high level of agreement with a previously published map. While they also stated that it was relatively easy to derive floodplains in their study area, due to its rather simple topology, it was concluded that the combination of DEM data with the HAND descriptor is a promising approach to floodplain mapping.

The above information gave rise to the idea that the HAND algorithm could be used to facilitate the automatic creation of a grid for river systems in D-Flow FM (Winsemius, pers. com.). A HAND grid would meet the criteria required for this; it has lower values in hydrodynamically more interesting areas (e.g. channels), which should result in a higher resolution grid in those areas and a decrease in resolution as HAND elevation increases. Using HAND, it would also be possible to reduce the total size of the model grid. For example, it can be assumed that all cells with a HAND value above 30 meters will most likely never be inundated due to river flooding, since these have an elevation of 30 meters above their nearest hydrologically connected channel and it is unlikely that water levels will rise this high. These cells could then be removed from the model grid. An example of the HAND procedure is described in Appendix A. The creation of the D-Flow FM grid for this study is described in the next chapter.

4.4.4 Assigning elevation values

The grid of D-Flow FM requires elevation values to properly represent the study area, which should include an accurate representation of river channel geometry and floodplain elevations. However, such data sets do not have global coverage and also do not exist for the Niger basin. Therefore, this study should use a DEM with global coverage, such as that from the Shuttle Rader Topography Mission (SRTM) or related products (e.g. HydroSHEDS). As stated by Neal et al. (2012) this dataset was conveniently obtained during the dry season in the Niger Inner Delta (February), which means

that lake levels were below average and there were no large inundated areas. The limited vegetation cover in this region also avoids the problem of tree canopies increasing elevation values, which is an issue often found in these radar-derived DEMs (Baugh et al., 2013; Sanders, 2007).

However, even though the DEM was obtained during the dry season, there was still water present in the river channels and the lakes of the Inner Delta, which prevent an accurate representation of channel and lake geometry, since radar cannot penetrate water surfaces. Because water surfaces produce very low radar backscatter, this can lead to water bodies being not well defined and to appear relatively "noisy" (Lehner et al., 2008). This issue is widely recognized and well documented, but still poses a serious problem for hydrodynamical studies that use these type of DEMs, which has led to the development of various techniques to overcome this issue (Getirana et al., 2009; Gichamo et al., 2012; Sanders, 2007; Yamazaki et al., 2012).

All of these methods attempt to create a better representation of river channels and water bodies, while some also attempt to do this for floodplains, and this always involves adjusting the original DEM in some way. In order to get a better representation of channels, a technique called stream burning is often applied (e.g. Callow et al., 2007; Getirana et al., 2009), which was first introduced by Hutchinson (1989). This technique 'burns' the DEM at locations where a channel is thought to be, lowering the elevation values there by a certain amount. Without such modifications, the channels might be less deep than in reality, which would result in an overestimation in the occurrence and extent of floods. The specific method to deal with this problem in this study is described in the next chapter (paragraph 5.4 on page 43).

5 D-Flow FM grid generation

5.1 Introduction

One of the most important aspects of D-Flow FM for this study is the creation of a grid which will have a strong impact on model results; it should be able to capture the complex flow and inundation patterns that are occurring within the Niger Inner Delta, requiring relatively small grid cells in this area (i.e. a high resolution). At the same time, the total study area is quite large (the Niger basin covers approximately 2.3 million km^2, see paragraph 2.1 on page 15), so most of the model grid should have a relatively low resolution to keep computational restraints low. Finally, the grid should be created automatically, as this is required for the possible application of the coupled PCR-GLOBWB D-Flow FM model at a global level or as a rapid setup tool. For this purpose the HAND algorithm is used, of which the theoretical background has been explained in the previous chapter.

5.2 HAND model of the Niger basin

The HydroSHEDS (Lehner et al., 2008) DEM of 15 arcsec resolution (approximately 0.004° degrees or 450x450 m) was used to construct a HAND grid of the study area. The HAND algorithm requires the specification of a threshold value for the accumulated upstream area that indicates where a channel is considered to begin. This is hard to determine automatically and as such several different threshold values were used to create different HAND grids, which were subsequently analysed. Two threshold values, namely those with 250,000 and 500,000 upstream cells, were identified as having the highest potential for this specific DEM and study area.

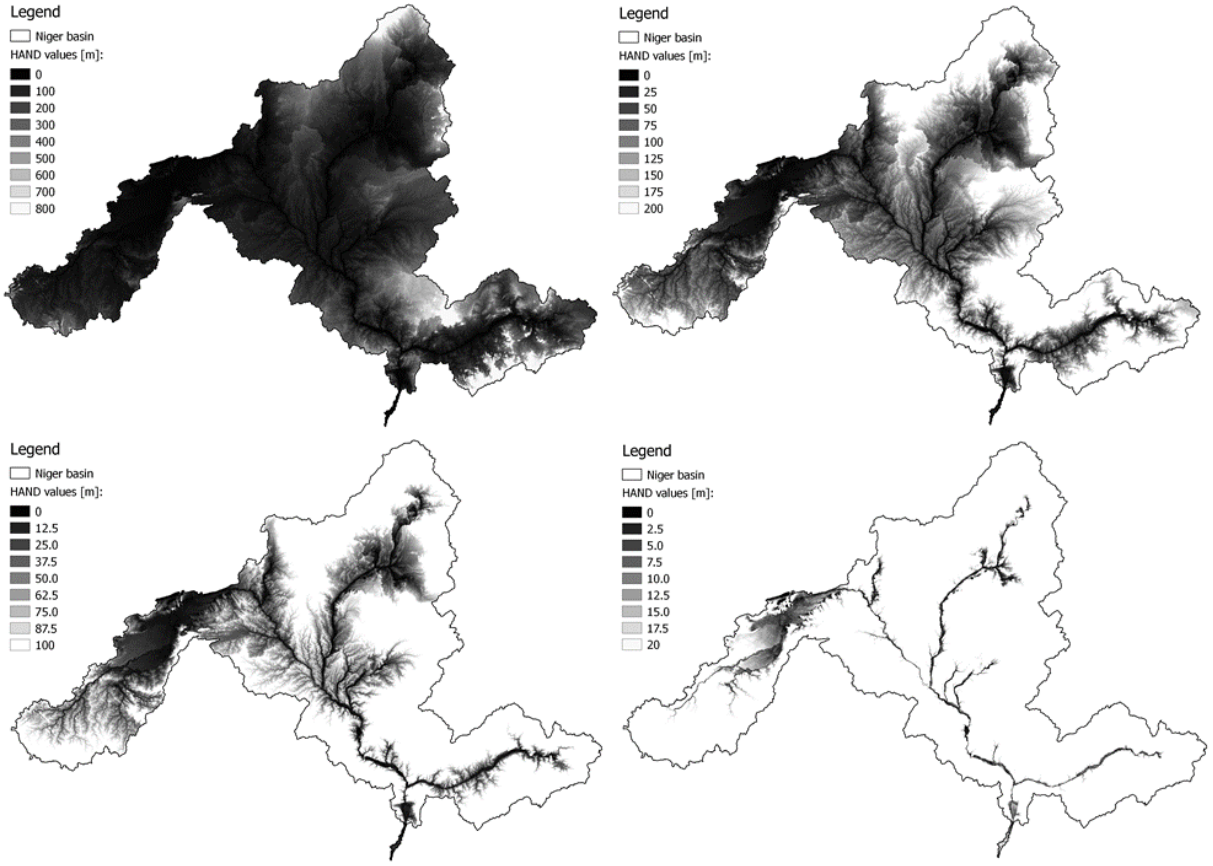

Figure 17: HAND grids of the Niger basin with a threshold of 500,000 upstream cells and elevation limits of 800 meters (top left), 200 meters (top right), 100 meters (bottom left) and 20 meters (bottom right)

The HAND grid with a threshold value of 500,000 upstream cells is shown in Figure 17 on the previous page, with four different limits on HAND values to highlight the potentially interesting areas for hydrodynamics. A limit of 20 meters was used to derive the extent of the model grid; all locations outside of this area are assumed to be irrelevant for the modelling of hydrodynamical processes. As can be seen from the figure, this will keep the extent of the D-Flow FM grid relatively small compared to the area of the entire basin.

Two D-Flow FM grids were created from the HAND grids using the two above mentioned threshold values and the limit of 20 meters. These were inspected with the aim of finding the threshold value that would result in the best model grid. However, it was discovered that both versions had potential advantages and disadvantages that were deemed of too great importance to ignore. One of these issues is illustrated in Figure 18 below; it shows the HAND grid of the most northern section of the Niger Inner Delta with its large lakes (e.g. Lac Faguibine and Lac Télé, see Figure 4 on page 17), with only HAND values of zero visualized to see where it indicates the presence of channels and/or lakes.

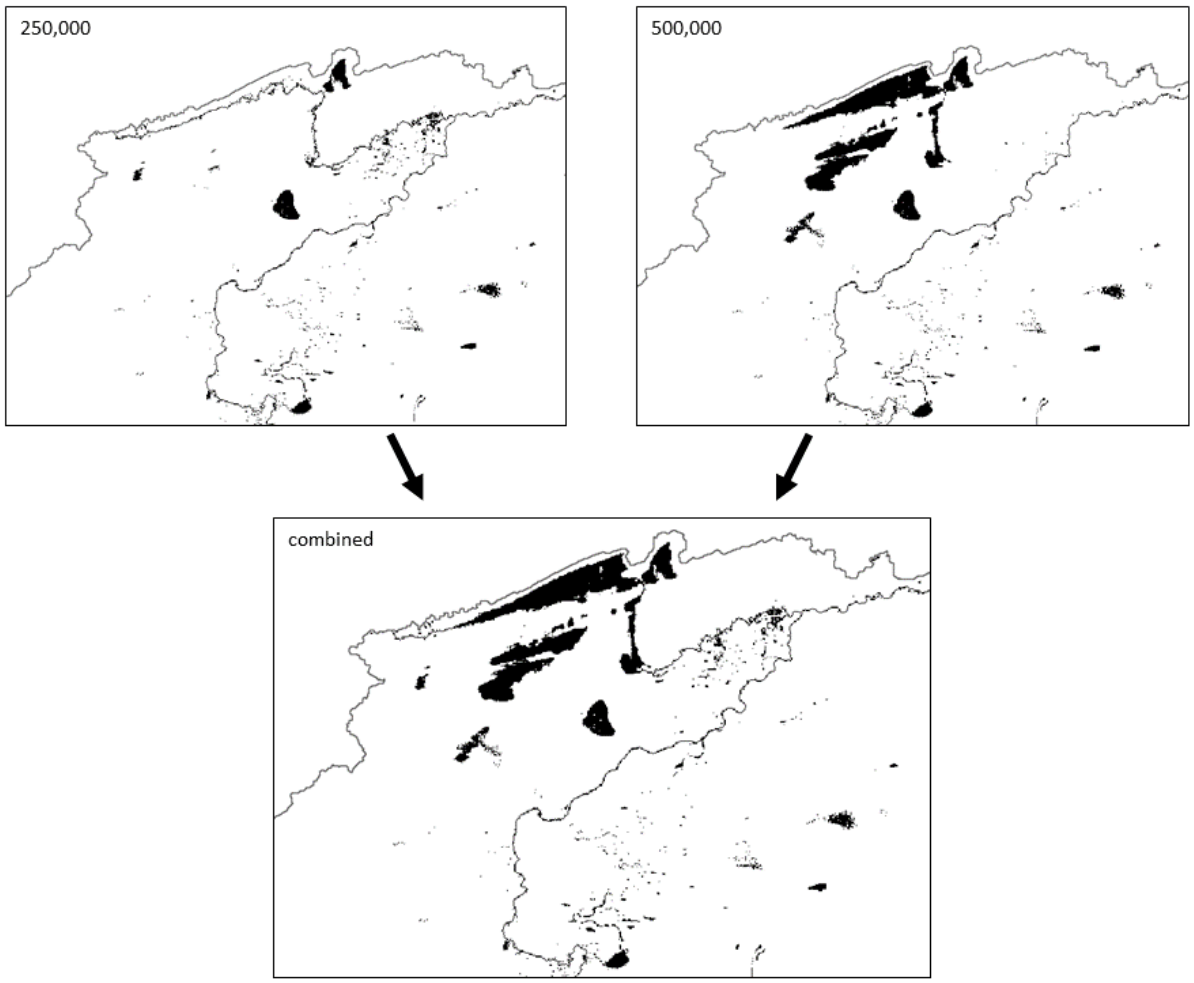

Figure 18: HAND grids of the northern lakes within the Inner Delta with only HAND values of zero shown. The grey line close to the most northern lakes indicates the boundary of the Niger basin.

From this figure it can be seen that the HAND grid with the 500,000 threshold does represent the lakes themselves, but there are no channels linking them to the main branch of the Niger River. The HAND grid with the 250,000 threshold on the other hand does have a channel towards the most northern lake, but not the lake itself. This highlights a drawback of the HAND algorithm itself; when a stream is identified it will follow the LDD and assign zero values along the way, while it ignores possible other channels or lakes that the LDD is unable to represent (at least when the standard D8

LDD is used). Also, small channels, such as those connecting lakes, will not always be picked up by the HAND algorithm. The fact that both versions of the HAND grid have their own advantages brought about the idea to combine them into a single grid, rather than choosing one over the other. This was done by taking the minimum of both grids, so that both the channels and the lakes would be properly represented. The resulting combined grid is shown in the bottom of Figure 18.

5.3 D-Flow FM grid refinement based on HAND

The D-Flow FM grid itself was created in a few steps. First, a uniform, structured grid with a resolution of 12 arcmin was created in D-Flow FM. This grid was then refined automatically by loading in the HAND map and using the Courant-based grid refinement until the smallest cells had a resolution of approximately 22.5 arcsec (requiring eight refinement steps and resulting in a total of roughly 135,000 cells). The grid is shown in Figure 19 below, with the axes representing latitude and longitude coordinates (using the WSG84 / EPSG4326 projection).

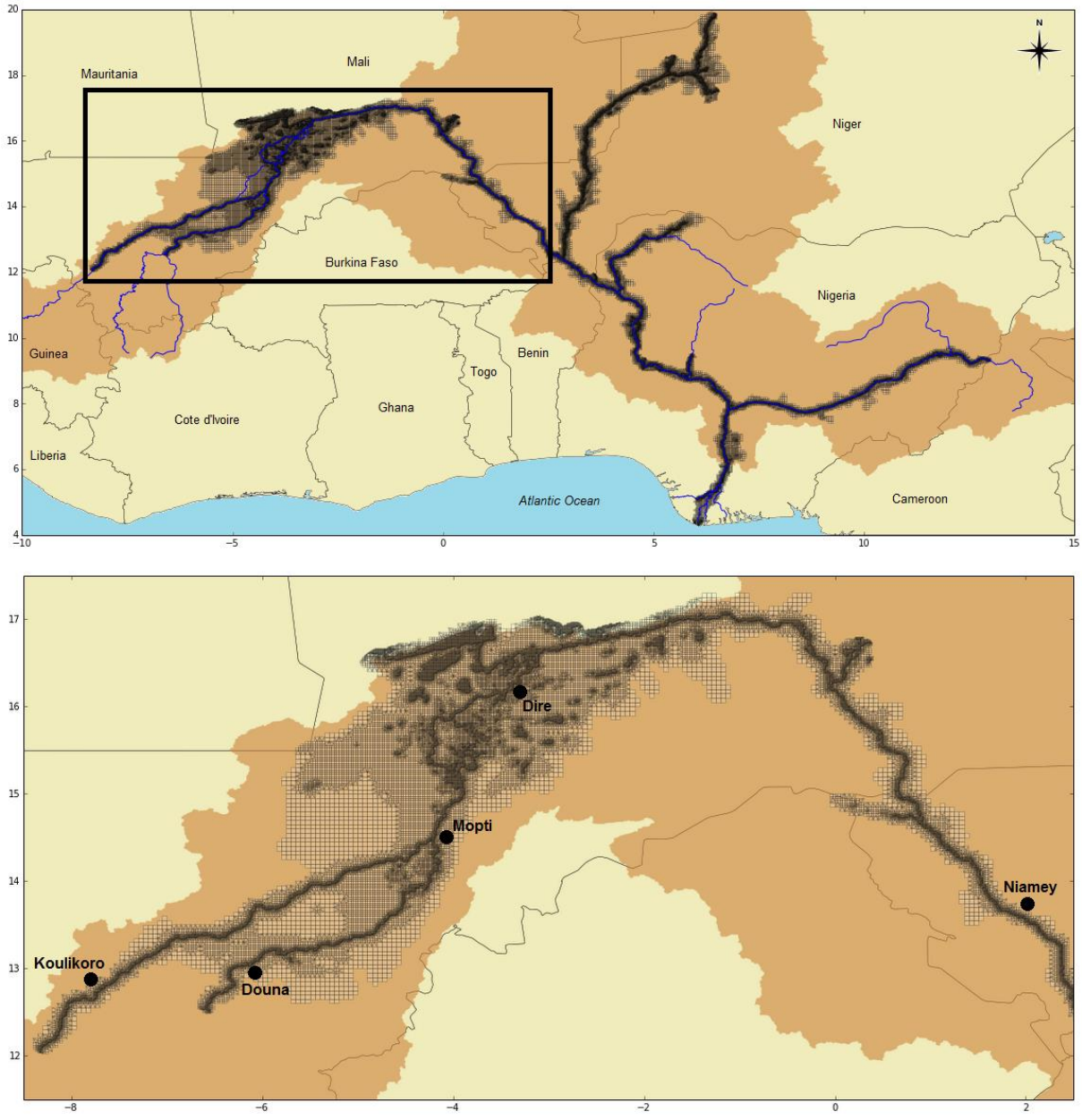

Figure 19: D-Flow FM grid created with HAND, complete grid (top) and zoomed in section around Inner Delta (bottom). Axes represent latitude/longitude coordinates of the WSG84 / EPSG4326 projection.

It should be noted that the grid shown in Figure 19 already received some manual adjustments. This included cutting a small part of the upstream sections representing the Niger and Bani rivers, to make sure that the gauging stations of Koulikoro and Douna were located close to the edges of the grid. This was done for two reasons: (1) to be able to create a stand-alone D-Flow model forced with discharge data from these gauging stations and (2) to be able to investigate the modelled discharge of the coupled model that is entering the D-Flow model, by comparing this with the observed values at these locations. All steps that were carried out to generate the D-Flow FM grid are described in Appendix B.

From the top image of Figure 19 it can be seen that this automatically created grid includes all major streamlines. Areas located far upstream are not included, because a relatively high threshold value is used with the HAND algorithm. This is exactly as intended, as these areas are probably not relevant for the detailed simulation of hydrodynamics, because they are unlikely to experience large flooding. What also stands out is the relatively large size of the region representing the Niger Inner Delta, while the rest of the grid is located close to the river channels. This is because of the small elevation differences within this region, which cause a lot of cells to have HAND values in the order of a few meters. This also makes it very susceptible to flooding and thus shows the strength of the automatic approach using HAND in creating a grid that represents hydrodynamically interesting areas.

It can also be seen that the D-Flow FM grid includes a large branch that starts in north-western Niger and flows roughly southwest until it joins the Niger River slightly downstream of Niamey, while the streamlines don't seem to indicate the presence of a river here (see also Figure 3 on page 15). This section was created because the HAND grid had values there (see Figure 17 on page 39), but this does not necessarily indicate that there is an active river system at that location. The HAND grid uses the LDD to define flowpaths, which simply checks downslope directions. This area however, is part of the Sahara and receives very little rainfall, which makes it relatively inactive in a hydrological sense and it would not be necessary to include it in the D-Flow FM grid to simulate hydrodynamics. That is why this branch was manually removed at a later stage of the study.

The bottom image of Figure 19 makes it a bit easier to distinguish between the different cells of the grid, although the cells in river channels and lakes can still not be seen because of their small size. This image does reveal interesting patterns within the region of the Niger Inner Delta, with a relatively large amount of cells having a very high resolution. However, by comparing this figure with Figure 4 on page 17, it can be seen that the grid still misses some of the smaller side-channels, especially the one that branches off the Niger just downstream of Ke-Macina (also known as the Diaka River). This stream is also clearly visible on satellite images of the area. It is not included in the grid because the HAND algorithm follows the LDD, which follows the main branch of the Niger River as this has the steepest downward slope. This is a limitation of the LDD method, and as such also of the automated grid creation used in this study. Regarding a potential global application, this will most likely only be of concern in areas such as the Niger Inner Delta (e.g. wetlands, marshes, large braided rivers and other deltas), where the flow of water is not restricted to a single channel, since the main river channel seems to be represented very well in the grid.

Regarding river channels, it was recommended by Kernkamp et al. (2011) to use curvilinear grids that are elongated and aligned in the main flow direction whenever possible. It would be difficult to achieve this with an automated procedure, which is why the creation of such a grid was not attempted in this study.

5.4 DEM smoothing and stream burning

The D-Flow FM grid is assigned the elevation values from the HydroSHEDS 15 arcsec resolution DEM, which is derived from the original Shuttle Rader Topography Mission (SRTM). This specific DEM was chosen for a number of reasons; first of all, it represents averaged values from the original 3 arcsec resolution DEM, which smooths out irregularities and errors that are often present in a DEM (Neal et al., 2012; Sanders, 2007). Second, the resolution is high enough to be used with the designed setup of the D-Flow FM grid, while its file size is small enough to be easily loaded into D-Flow FM without the need to split it up into multiple parts. Finally, the HydroSHEDS DEMs have received some adjustments that are thought to improve the data quality over the original SRTM DEM, such as void-filling. HydroSHEDS also includes hydrologically conditioned DEMs, in which further adjustments were made that include stream burning. However, these DEMs are not suitable for the modelling of floods and inundation dynamics because the stream burning of the Niger River has resulted in unrealistically deep channels (e.g. depths of over 20 meters). This is demonstrated in Appendix C.1.

Since this means that a non-burned DEM has to be used, it is required to apply burning techniques to better represent river channels and water bodies (as explained in paragraph 4.4.4), and there are a lot of possible methods to do so. It was not possible to devote a lot of time into the investigation of burning methods for this study. Instead, a relatively simple method was devised that focused only on a better representation of the main channels, which are transporting the largest part of the total water downstream.

The method is designed with two goals; (1) smoothing the DEM to make sure that elevation is consistently decreasing in a downstream direction (removing 'obstacles' represented by elevation increases in the flowpath) and (2) burning the DEM to make sure that the riverbed has a lower elevation than its surroundings and channel bathymetry is included. The algorithm starts at one (or more) user-specified upstream location(s), and follows the LDD in the downstream direction, while checking elevation values along the way. When a point is encountered with an elevation value higher than its predecessor, its elevation value is set to be equal to that of its predecessor. This ensures that the flowpath has no elevation increases. Burning is then done by simply lowering each point by a user-specified value.

Figure 20 on the next page shows the elevation profile along the total path travelled from the specified upstream point, as well as a specific section of this path in more detail, in which the original DEM data, the smoothed DEM and the burned DEM are all visualized. The irregularity of the original DEM can clearly be seen; there are a lot of small variations and local increases of elevation, even though the general trend is a decrease in elevation. The local increases of elevation block the flow of water, either forcing it in another direction or, when that is not (or no longer) possible, increasing the water levels up to the point that allows overflow. This could lead to an overestimation of inundation and an underestimation of the speed with which water flows downstream. In the two-way coupled model, both of these things would result in an overestimation of evaporation and infiltration from the floodplains. The smoothing and burning of the DEM was carried out after first tests showed that doing so was absolutely critical to obtain at least somewhat realistic results with two-way coupling. An example of model results without this smoothing/burning is shown in Appendix C.2.

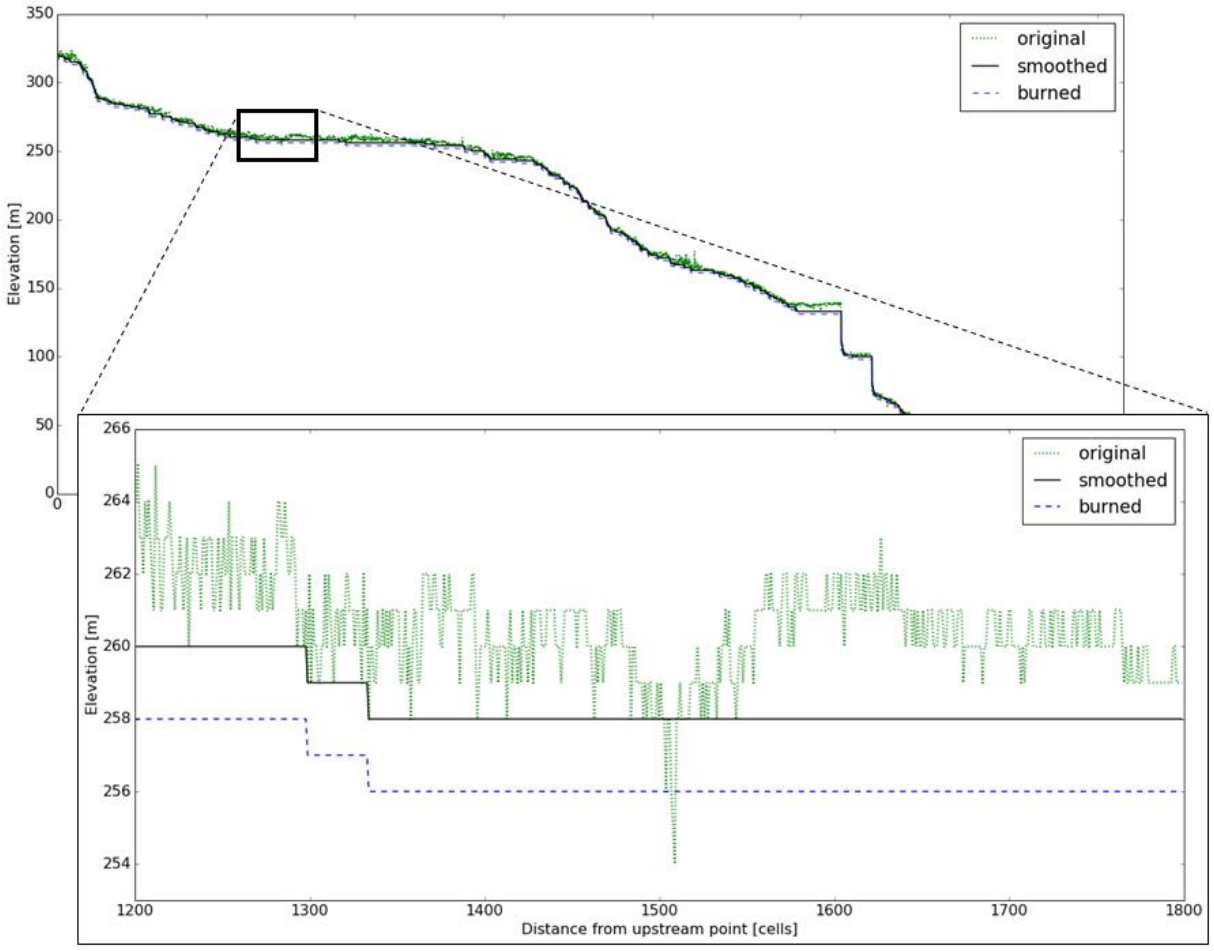

Figure 20: Elevation profile along the flowpath with adjustments made by smoothing and burning

From Figure 20 it can be seen that the smoothing algorithm has removed the irregularities and ensures that the DEM is consistently decreasing in the downstream direction. It can also be seen that it does not always follow the original DEM when elevation is decreasing, especially when this decrease is relatively large (for instance, the deep depression near the upstream distance of 1500 cells has been ignored). This functionality was added to the algorithm after first tests showed that it would otherwise lead to an extremely deep river channel, in some locations up to 16 meters below the surrounding area, which was thought to be just as unrealistic as the original DEM. The method works by checking for 'large, sudden drops' in elevation (decreases above a user-specified value, which was set at 2 meters) and then assesses whether this is realistic or not. This is done by comparing the elevation at this point with that of the next four locations; if the current value is equal to or larger than the average of the next points, it is assumed to be realistic and the algorithm proceeds to this point without making any changes to the DEM. However, if the current value is lower than the average of the next points, the DEM is adjusted by substituting this average instead of the current value, up to a maximum equal to the elevation value of the previous cell, as follows:

$$\bar{h} = \frac{1}{4} \cdot \sum_{j=i+1}^{4} h_j$$

$$\begin{cases} h_i = \bar{h} & if\ \bar{h} \leq h_{i-1} \\ h_i = h_{i-1} & if\ \bar{h} > h_{i-1} \end{cases}$$

In which h is the elevation at a certain point i and $\bar{h}$ is the average elevation of the next four points.

The value applied in the burning is based on the only study related to channel depths of the Niger River that could be found (Krekeler, 2012), which lists values between two and four meters at several locations. Since the smoothing algorithm already increases the channel depth at certain locations, it was decided to apply an additional burning of only two meters.

The applied smoothing algorithm is explained in more detail in Figure 21 on the next page. This figure shows a schematic of an elevation profile along a hypothetical flowpath, highlighting two possible issues that the smoothing algorithm attempts to solve; a local increase in elevation and a sudden drop in elevation that could be the result of an error in the data. The local elevation increase is simply lowered to the same level as its predecessor, while the sudden drop in elevation a bit further downstream is recognized as a potential error and filled up. The final product is a DEM with a smoothed flowpath that does not contain any elevation increases in the downstream direction.

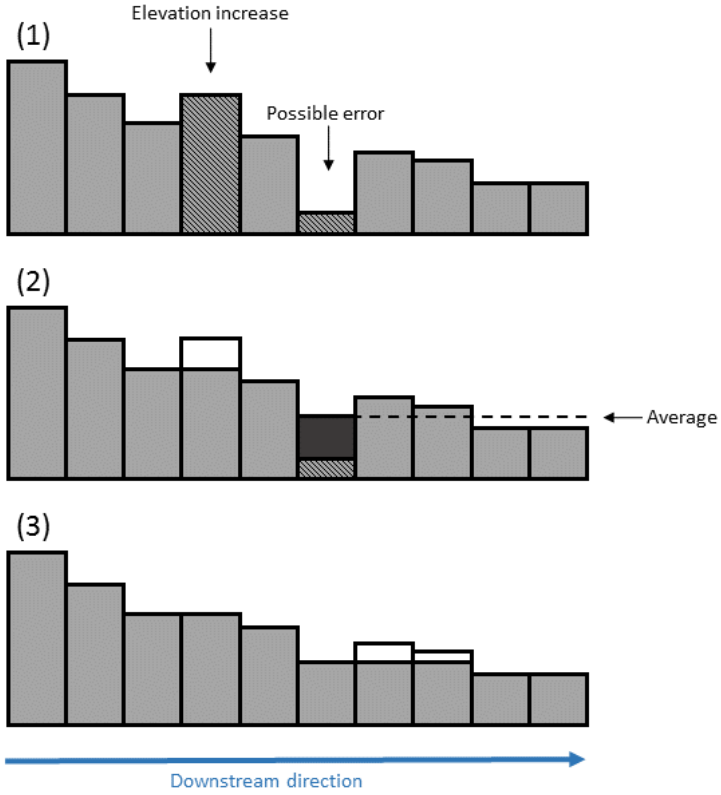

Figure 21: Schematic of an elevation profile along a hypothetical flowpath with the different steps of the smoothing algorithm; (1) original situation, (2) decrease of local elevation increase and filling of possible error to the average of the next four locations and (3) final elevation profile after last adjustments

6 Model coupling

6.1 Basic Model Interface

As stated in the introduction, the models will be coupled using the Basic Model Interface (BMI). This is described by Peckham et al. (2013) as a component interface, which is a set of functions that is completely standardized regarding its names, arguments and return values. This implies that, even though the source code might be different for each model, the same named BMI function can be used for different models to achieve the same goal. The source code of the BMI itself will still be different for each model, as it depends on the internal structure of the model and the language in which it is written, but its input (a string with the variable's name) and output (an array with all the values) are of the same type. Besides this, BMI also contains functions which allow the manipulation of the way the model is run, bypassing the normal time loop of the model. This is essential for coupling, as most models usually run for a specified time period and cannot be interrogated while they are running, which prevents the exchange of variables between models.

As mentioned before, a BMI was already in place for D-Flow FM at the start of this study. This was not the case for PCR-GLOBWB, so the BMI for the model was created as part of this study. The complete BMI contains a long list of functions, out of which the most important functions are briefly described below.

6.1.1 BMI *initialize*

The *initialize* function starts up the model by reading data from a configuration file, opening output files and initializing the first set of variables. This allows the user to retrieve or change these variables using other BMI functions and makes it possible to use the *update* function.

6.1.2 BMI *update*

This function updates the model, by advancing it a specified time step. Any timestep is possible, as long as it is within the model's own capabilities. It is also possible to run the model normally, by having it simulate the full time period as specified in its configuration file. Only advancing it a single time step (i.e. one day in the case of PCR-GLOBWB) allows the exchange of information between other models, making a coupled model setup possible.

6.1.3 BMI *get_var*

This function retrieves the data stored within a specified variable, returning it either as a text string or an array, depending on how it is stored internally within the model. For PCR-GLOBWB specifically, this means that variables stored as PCRaster maps are converted to arrays, to allow a more convenient exchange of information between this model and D-Flow FM.

6.1.4 BMI *set_var*

The *set_var* function overwrites the data stored within a specified variable by a specified input, which should match the shape of the original data. This allows the user to make changes to a model while it is running, which is essential for the coupling. Information retrieved from a variable of one model with the *get_var* function can be used, possibly after some adjustments or conversions, to overwrite a related variable in the other model using this *set_var* function.

It should be noted that the g*et_var* and *set_var* function do not exactly follow the standard set by Peckham et al. (2013), as the original BMI made a distinction between 1D, 2D and 3D arrays, while

the functions used in this study work for variables with data of any shape. This was done because the BMI of D-Flow FM used this format, and it was decided to have a similar BMI for PCR-GLOBWB. In this sense, they are more similar to the *get_values* and *set_values* function of the overlying CMI (Component Model Interface), which was created by Peckham et al. (2013) to serve as a "plug and play" interface for any model with a BMI. This is a technicality and does affect the functioning of the BMI used in this study in any way. For more information on the CMI, the reader is referred to Peckham et al. (2013).

6.2 Coupling of model grids

Coupling requires that the models are able to exchange information. This implies that each cell of one model should give information to cell(s) of the other model, and vice versa. In order to achieve this, a lookup table is created that specifies which cells of the models should exchange information. Since D-Flow FM has cells of different sizes and shapes, and these might not completely fall within the larger cells of PCR-GLOBWB, the coupling of the model grids is based on the assumption that the location of the centroid of a D-Flow FM cell determines to which PCR-GLOBWB cell is will be coupled.

All cells of D-Flow FM are non-self-intersecting and closed polygons with *n* vertices. To calculate the centroid of such a cell, first the total area of the cell A is calculated as:

$$A = \frac{1}{2} \cdot \sum_{i=0}^{n-1} (x_i \cdot y_{i+1} - x_{i+1} \cdot y_i)$$

In which x_i and y_i are the x and y coordinate of the i-th vertex. The location of the centroid in (x,y) coordinates can then be calculated as (Bourke, 1988; Nürnberg, 2013):

$$C_x = \frac{1}{6 \cdot A} \cdot \sum_{i=0}^{n-1} (x_i + x_{i+1})(x_i \cdot y_{i+1} - x_{i+1} \cdot y_1)$$

$$C_y = \frac{1}{6 \cdot A} \cdot \sum_{i=0}^{n-1} (y_i + y_{i+1})\,(x_i \cdot y_{i+1} - x_{i+1} \cdot y_1)$$

In which C_x and C_y are the x and y coordinate of the centroid. This is calculated for all individual cells so that all cell centroids are known. A D-Flow FM cell is considered coupled to a PCR-GLOBWB cell if its centroid is located within the bounds of the PCR-GLOBWB cell. Figure 22 on the next page shows the coupled model grids, with the top image showing the complete grids of both models and the middle image showing the coupled cells only. From this figure it can be seen that there are a lot of PCR-GLOBWB cells that are not coupled; these will work just as the stand-alone model and are not influenced by the coupling. It can also be seen that almost all D-Flow FM cells have been coupled, which is good because these require input from PCR-GLOBWB to simulate the flow of water within the Niger River. However, there are small regions where some D-Flow FM cells have not been coupled, indicated by a red circle in the top image of Figure 22. This is simply caused by the fact that there are no PCR-GLOBWB cells at those locations. The reason behind this is related to the resolution of this grid, which at 30 arcmin gives a different extent of the Niger basin. The coupled cells of the 5 arcmin version of PCR-GLOBWB, shown in the bottom image of Figure 22, give a more complete coverage.

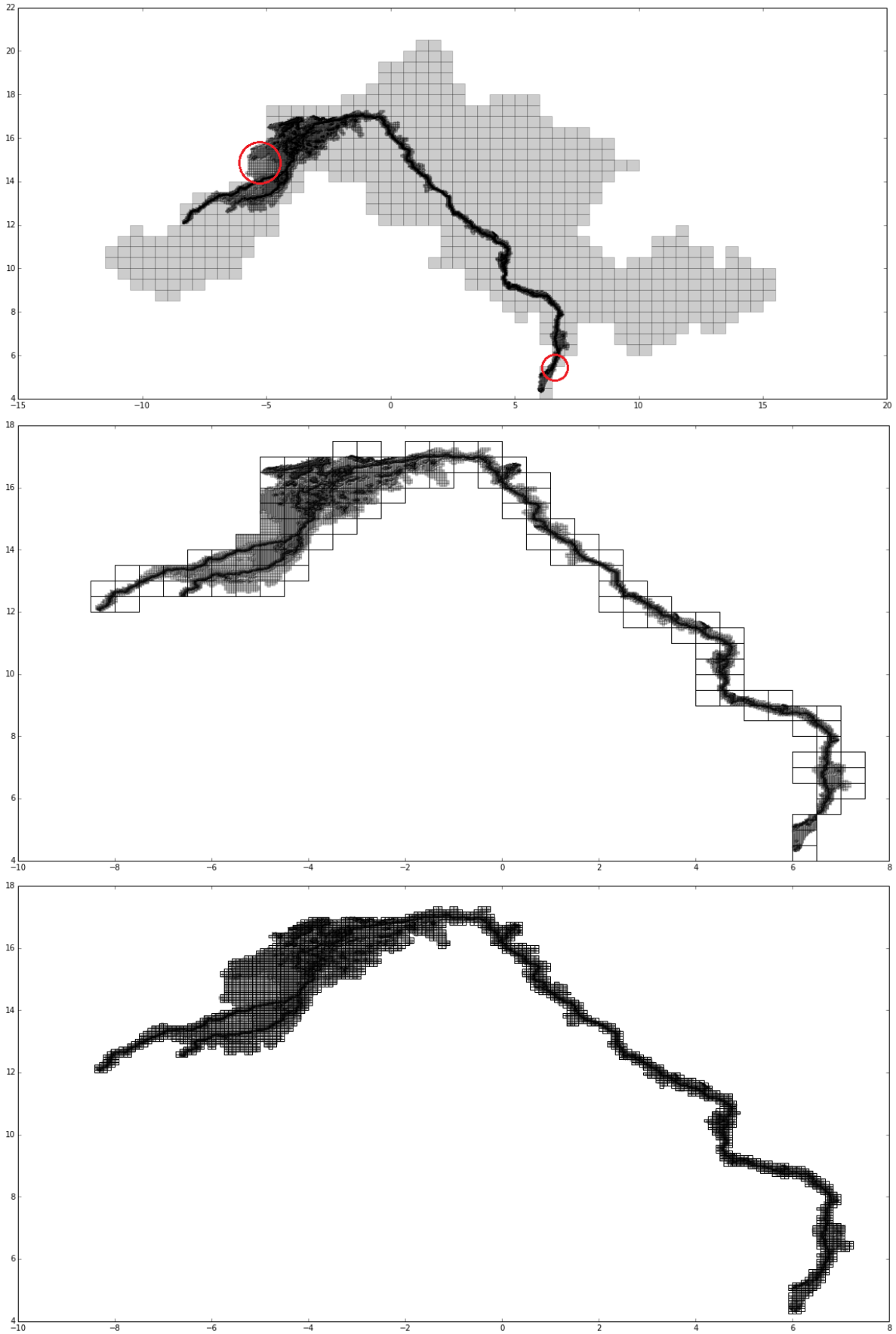

Figure 22: Coupled model grids with the complete grids of D-Flow FM and PCR-GLOBWB at 30 arcmin resolution (top), the coupled cells of these grids (middle) and the coupled cells with PCR-GLOBWB at 5 arcmin resolution (bottom). Cells can appear stretched horizontally due to the ratio of the axes (WSG84 / EPSG4326 projection).

Comparing the grids shown in Figure 22 with the grid of Figure 19 on page 41 (which was created directly from the HAND map) shows that almost all tributaries of the Niger River have been removed. This was done to increase computational efficiency, as the tributaries were significantly slowing down the simulation speed of the model while their effect on results at the specified gauging stations was negligible. As can be expected, only the far downstream station of Lokoja, near the confluence with the Benue River (see Figure 3 on page 15), was affected. Since this study focusses only on the Niger Inner Delta and the gauging stations upstream of Niamey, this was considered acceptable. This procedure reduced the total number of D-Flow FM cells from roughly 135,000 to 91,000.

6.3 General principles and used methods

As stated before, the coupling of the models requires the exchange of information. This information is stored within the variables of both models, which can be handled using the BMI functions described earlier. Successfully coupling the models also involves a number of other procedures which are described below.

6.3.1 Adjusting the LDD of PCR-GLOBWB

Regardless of the type of coupling (i.e. one-way or two-way), the D-Flow FM model needs input from PCR-GLOBWB in order to simulate the hydrodynamics of the study area. PCR-GLOBWB has a variable that keeps track of the amount of water in channels (channel storage), from which discharge is calculated when it is routed over the LDD. After a routing update, discharge represents the amount of water that has passed a cell and channel storage represents the amount that has arrived at a cell. This implies that, if channel storage would be used as coupling variable, the same volume of water that was already routed in PCR-GLOBWB would be added to D-Flow FM, where it would flow even further downstream during the same day. Therefore, discharge should be used as coupling variable instead, to make sure the timing of the flow is correct.

However, the routing within PCR-GLOBWB poses a problem for the coupling. Once water has entered D-Flow FM it should no longer be active in PCR-GLOBWB, as this would not only double the amount of water in the coupled model, it would be added to D-Flow FM again at a next timestep (and this process would be repeated at every consecutive timestep). The exchange of surface water data from PCR-GLOBWB to D-Flow FM should happen once, after which it should be removed from PCR-GLOBWB. This could be done by writing an elaborate scheme that tracks where all discharge comes from, so that, for coupled cells, only discharge that is generated within the cell (e.g. from runoff) is used as input, while discharge coming from upstream cells is ignored. This would then also require a method to distinguish between cells on the edges of the coupled grid, as these would require upstream discharge as input. This would be quite complex, especially because a lot of cells are located on the edges of the domain, but still have upstream connected cells that are also coupled. It would also involve a lot of changes to be made to the code of PCR-GLOBWB, in order to be able to track the discharge. Therefore, such a scheme has been dismissed and instead a more simple solution has been found.

This solution involves the adjustment of the LDD used in PCR-GLOBWB. Instead of having to write an elaborate scheme that tracks discharge and distinguishes between different types of cells in PCR-GLOBWB, changing the LDD values of all coupled cells to represent pits would have the same effect; it makes sure that channel storage is removed when it is added to D-Flow FM. This method is easier to implement and also more efficient in a computational sense. The original and adjusted LDDs of PCR-GLOBWB are shown in Figure 23 below, in which the shape of the coupled grid from Figure 22

can clearly be seen. This figure also gives a good indication of how the coupled model will function; all flowpaths lead to a pit cell, where the discharge of PCR-GLOBWB will enter the D-Flow FM model and its corresponding volume will be removed from PCR-GLOBWB.

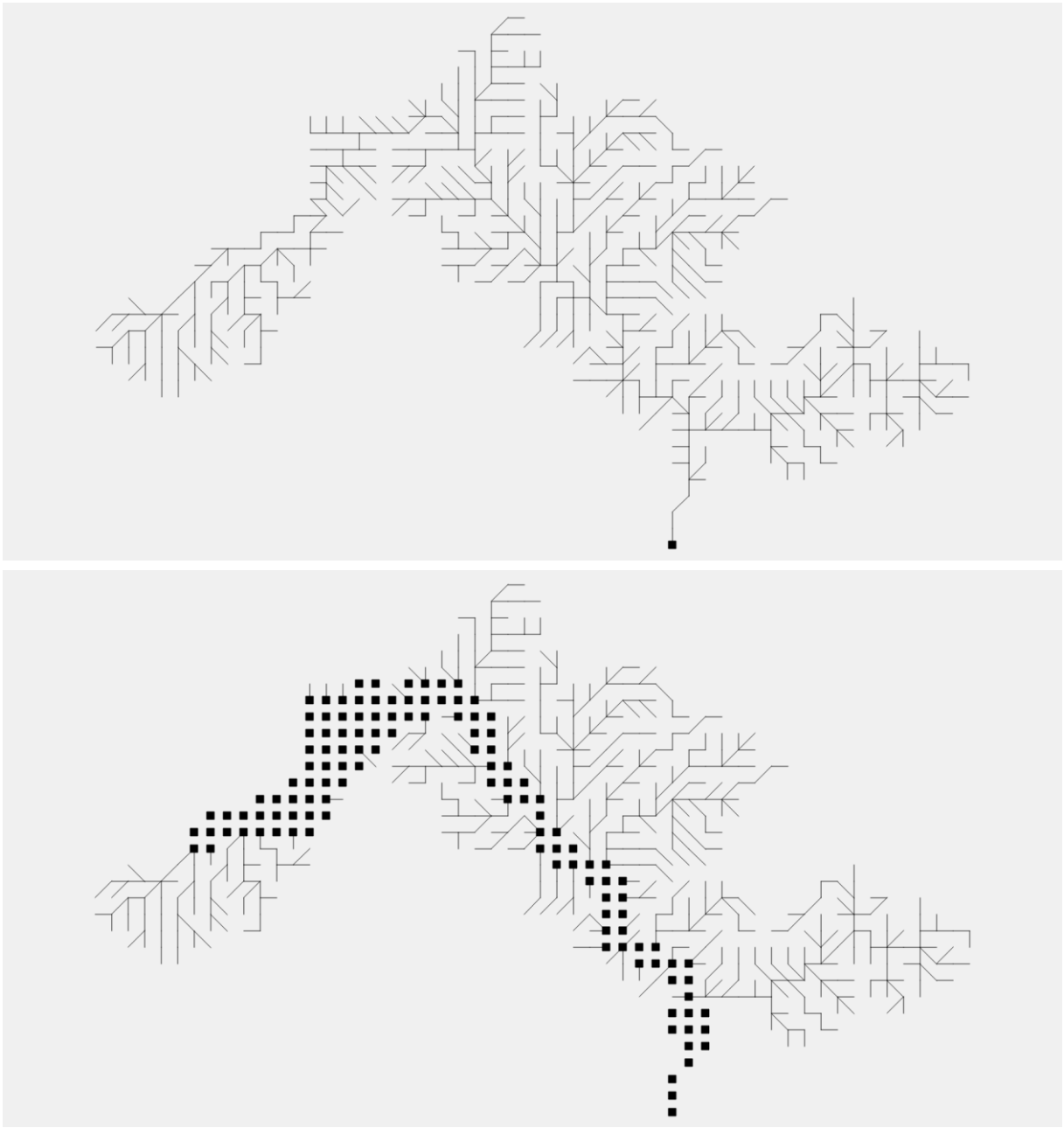

Figure 23: Original (top) and adjusted (bottom) LDD of Niger basin in PCR-GLOBWB at 30 arcmin resolution

However, during the spin-up of PCR-GLOBWB, the model should still have its original LDD, as water otherwise cannot travel downstream. Once the spin-up is completed, BMI functions can be used to adjust the LDD within the active model. The functioning of this adjusted LDD was tested to make sure it was working as intended. This is briefly described in Appendix C.3.

6.3.2 Dividing output of PCR-GLOBWB over D-Flow FM cells

Because of the equations with which D-Flow FM operates (see paragraph 4.2 on page 31), it is using water levels as its working variable. This means that any changes to the amount of water within the model, for example due to discharge input from PCR-GLOBWB, needs to involve the adjustment of this variable. Therefore, any input into D-Flow FM needs to be converted to water levels. Luckily, this

is straightforward; discharge can be converted to a daily volume and then divided by D-Flow FM's cell area to obtain a water depth (which can be added to the current water level). However, this raises the question of how exactly the total volume from the larger PCR-GLOBWB cell should be divided over the smaller D-Flow FM cells. For reference, a single PCR-GLOBWB cell (at 30 arcmin resolution) with its coupled D-Flow FM cells is shown in Figure 24 below.

Given this example, it is possible to come up with a number of possible schemes that determine how to divide the volume coming from PCR-GLOBWB over all the D-Flow FM cells. For instance, it could be stated that only the smallest cells, which are the best representation of the main river channel, should receive input from PCR-GLOBWB's discharge. Another approach would be to use the topography of the area and come up with a similar scheme based on elevation values. It would also be possible to check the current water levels within these cells and distribute the additional water based on this. A combination of these is also an option, while a very simple method would be to just divide the water evenly over all cells. In the end, it was decided to try two different methods: (1) the just mentioned simple approach, in which the total volume is divided by the number of coupled D-Flow FM cells with every cell receiving the same volume, and (2) an approach based on the fact that the smallest cells best represent the main river channel and thus only these cells should receive the discharge output from PCR-GLOBWB.

While the first, simple approach distributes the total volume evenly over all cells, this does not mean that the water depth that is to be added to D-Flow FM is the same for every cell, since their areas can be very different. This simple method has the benefit that it is relatively simple to implement, but it might lead to longer simulation times because D-Flow FM will need to calculate the flow of water within more cells. Water that enters the larger cells, which represent areas with larger HAND values and thus higher elevations relative to the nearest dchannel, will flow downstream and most likely end up in the smaller cells after a while. The second approach is not as simple to implement and requires some additional calculations beforehand, but it might be computationally more efficient and also give a better representation of reality.

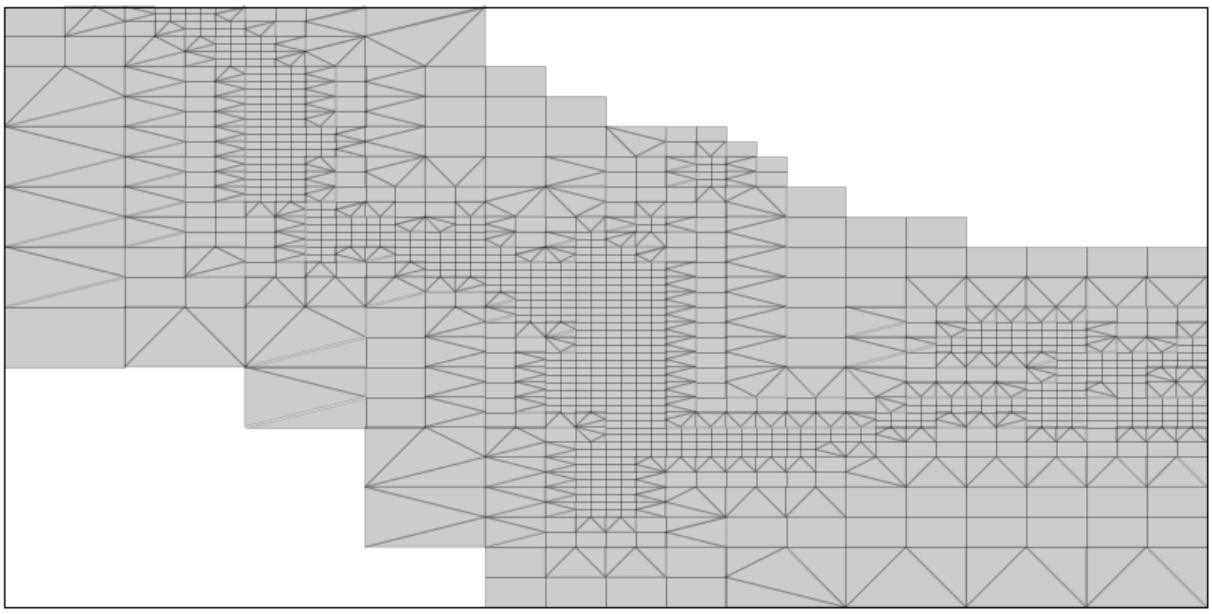

Figure 24: D-Flow FM cells within a coupled PCR-GLOBWB cell of 30 arcmin resolution

6.3.3 Identification of river and floodplain cells

The smallest cells within the D-Flow FM grid represent areas with the lowest HAND values. Since a HAND value of zero is assumed to represent part of a channel or water body, the smallest cells in the grid can also be assumed to represent this. In order to use these cells for the partitioning of the incoming volume from PCR-GLOBWB they will need to be identified (i.e. a lookup table will be created that allows computationally efficient use of this principle). This is done by setting a threshold value for the cell area, so that all cells with an area below this value are designated to be river cells. A more detailed overview of this method is described in Appendix C.4.

An overview of all D-Flow FM cells identified as river cells is shown in Figure 25 below. It can be seen that the main channels of the Niger and Bani rivers are included and fully connected. The lakes within the Niger Inner Delta are also clearly visible.

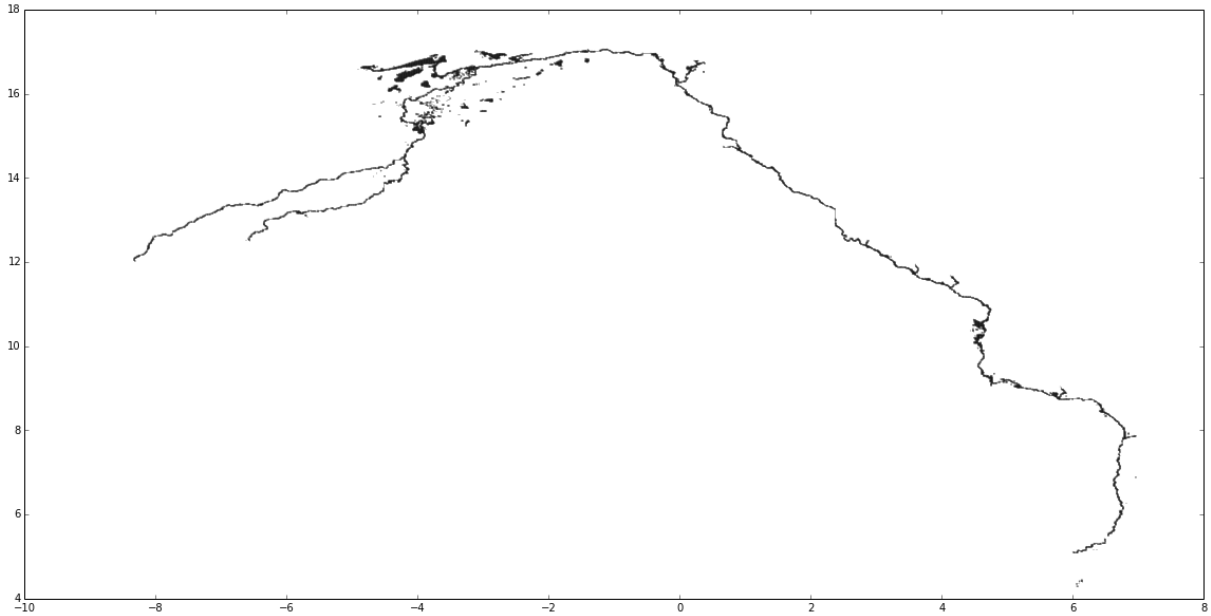

Figure 25: Cells identified as river cells within the D-Flow FM grid

Figure 26 on the next page shows the cells identified as river cells for the example cell shown in Figure 24. It can be seen that indeed only the smallest triangle- and square-shaped cells are included. It can also be seen that there are a few loose patches of cells, which are not connected to the main channel. These might represent small lakes, but since they are identified as river cells they will receive a part of the discharge input from PCR-GLOBWB, which reduces the amount of water that directly goes into the main channel. This might be an unrealistic representation of reality, because these lakes would normally not receive water from the river unless it flooded. However, especially in the case of these small lakes, the reduction of discharge input for the river channel might be small. This issue was not investigated further, but it should be kept in mind when reviewing the results of the coupled model.

Figure 26 also shows the cells that were not identified as river cells within the same example cell, which are assumed to represent the floodplain area (the shown PCR-GLOBWB cell has a total of 1541 D-Flow FM cells coupled to it, out of which 679 were identified as river cells and 862 as floodplain cells). These floodplain cells should not receive the discharge input from PCR-GLOBWB, but instead could be used for other purposes (e.g. receiving runoff from PCR-GLOBWB). The exact use of these cells depends on whether one-way or two-way coupling is used and this will be described in their respective paragraphs.

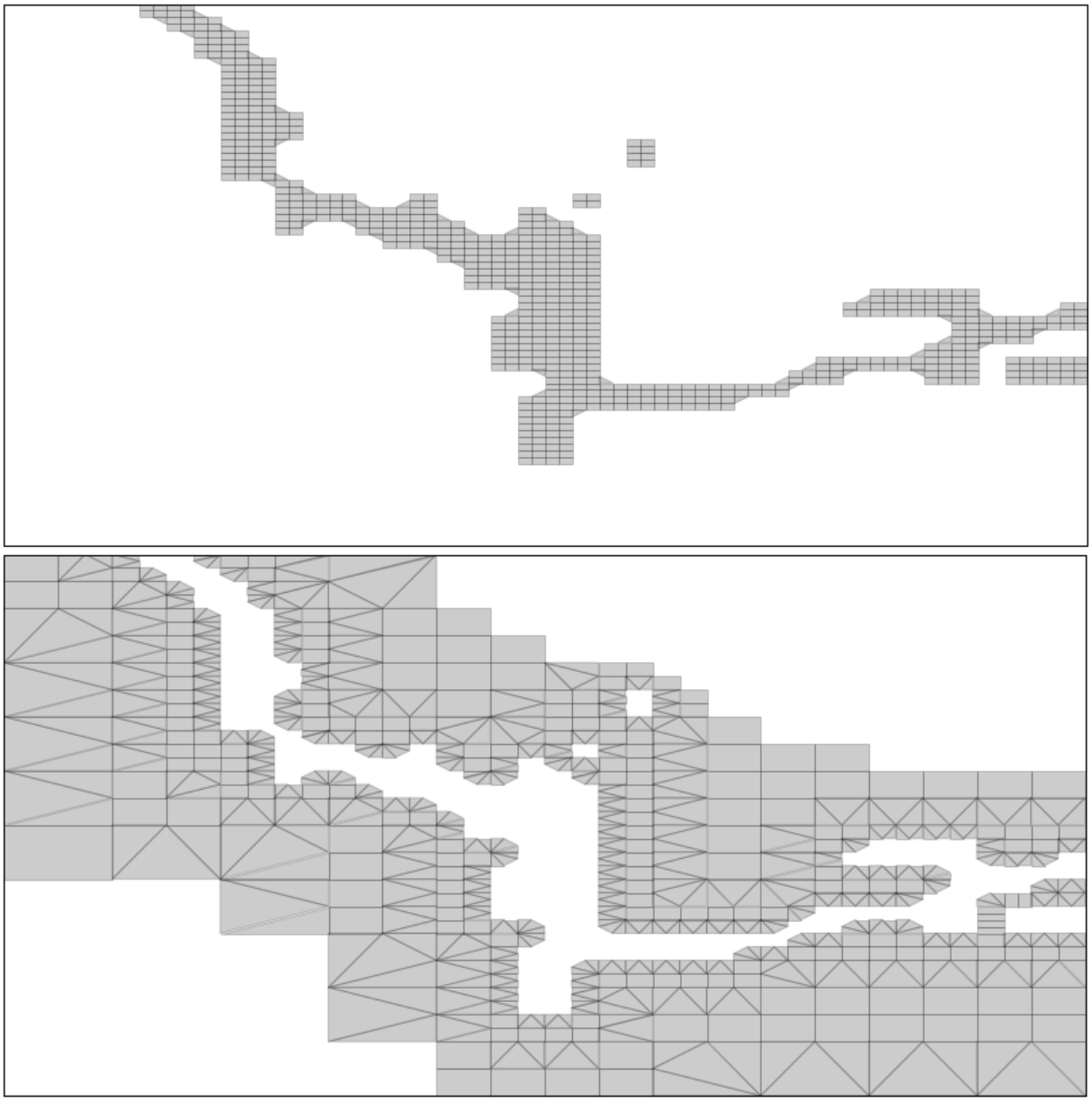

Figure 26: River cells (top) and floodplain cells (bottom) of the example cell shown in Figure 24

6.3.4 D-Flow FM update steps

There is one final issue involving the general exchange of information that needs to be addressed, which is the timestep used to exchange the information. PCR-GLOBWB works on a daily timestep, but D-Flow FM needs to use a much smaller timestep to accurately solve the shallow water equations. Adding the total output of PCR-GLOBWB to D-Flow FM at the start of its own update would be unrealistic, because it is unlikely that this input is concentrated within such a small timeframe (which would create an unrealistically large flood wave). Instead, smaller portions of the total volume should be added to D-Flow FM at specific intervals over the day, which raises the question of how many such intervals should be used. In light of the previously mentioned argument of realism, one could argue to have as much of these as possible within an update of a day. However, this is not ideal either because it would severely slow down the simulation speed of D-Flow FM. One of the strengths of the model is that it uses adaptive timestepping; from its user-specified initial, minimum timestep it will search for a maximum possible timestep based on the current flow conditions and Courant number theory. Thus, setting a relatively short update interval would essentially limit the effect of

adaptive timestepping, as this would reset at the start of every update, causing the timestep to revert back to the initial, minimum value. This implies that a balance has to be found between a realistic update and one that still utilizes the adaptive timestepping, to make sure that the model is both realistic and computationally efficient.

This issue has been investigated by running the D-Flow FM model for several different update values, with the same total volume as input. The result for three of these values (and a user-specified maximum timestep of 600 seconds) can be seen in Figure 27 below, which shows the discharge a couple of cells downstream of the inflow point. In this figure, the 'shock' that is introduced by using a large update value, such as 14,400 seconds, can clearly be seen; discharge strongly increases after which it slowly declines until the next update. The relatively small update value of 600 seconds (equal to the user-specified maximum timestep value) does not have this problem, but it did have the negative side-effect of relatively slow computation speeds. Since the model should be able to simulate several years or even decades, computation speed is an essential component and should be taken into account. Therefore, an update value of 1800 seconds (i.e. 30 minutes) was chosen to be used in the final setup of the model. This update value is also included in the figure and shows a discharge pattern relatively similar to that of the 600 seconds update, although some small oscillations can be seen. But it does not diverge far from the 600 seconds line, and this pattern persisted after the period shown in the figure.

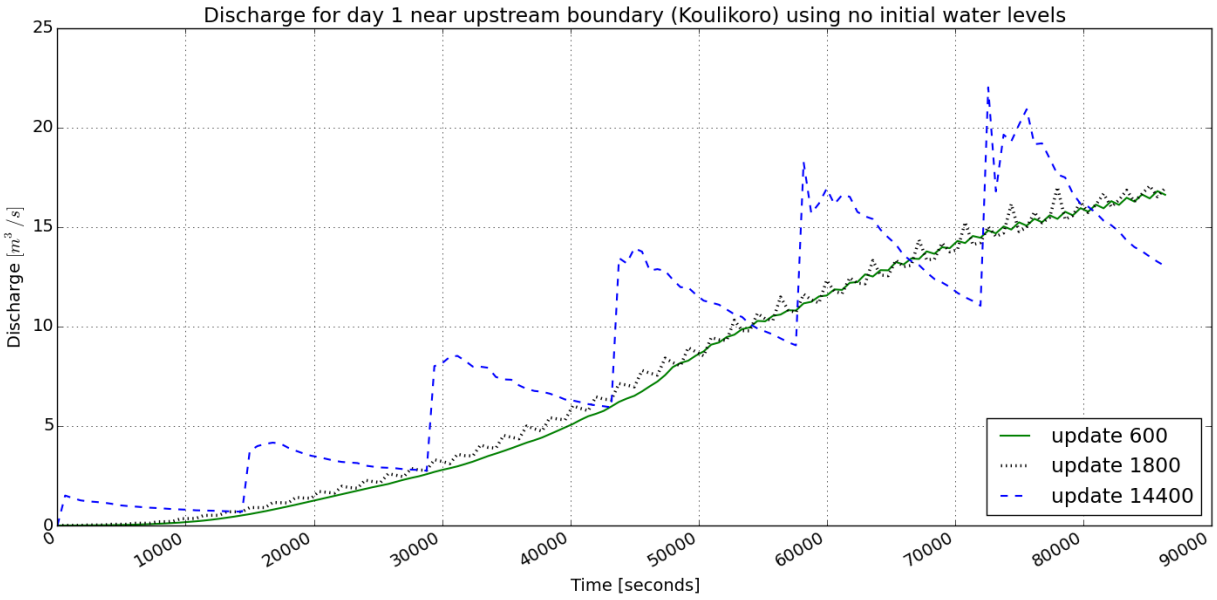

Figure 27: Discharge as modelled by D-Flow FM using three different update steps (600, 1800 and 14400 seconds)

6.3.5 D-Flow FM boundary conditions

With D-Flow FM coupled to PCR-GLOBWB, the model does not require any boundary conditions that would otherwise be used to handle the input into the model. However, there should be a boundary condition that handles the outflow. This could be done by creating a boundary at a location downstream of the Niger Inner Delta using observed data series of discharge or water levels (i.e. at a GRDC gauging station), but this might influence model results. The idea behind the coupled model is that it would function without the use of any discharge or water level data, using only datasets with a global coverage that are not bound to specific locations. Therefore a boundary condition is chosen that would not have a large impact on model results and that would be easy to set up for any other basin in the world; a zero water level boundary at the sea. This ignores possible tidal fluctuations,

storm surges and other related processes, but their effect will be limited to the most downstream section of the river and should not influence the river flow at the locations that will be investigated during this study.

6.4 One-way coupling

With a one-way coupled model PCR-GLOBWB gives relevant information to D-Flow FM, but there is no feedback. Since D-Flow FM handles the hydrodynamics of surface water, the input from PCR-GLOBWB should contain information about this. As stated before, discharge should be a part of this, because it describes the flow of water within channels and thus comprises one of the most important aspects of hydrodynamics. There is one other variable with data related to surface water and that is the amount of water on top of PCR-GLOBWB's upper soil layer. Table 1 below shows how these variables are used to add data to the relevant cells of D-Flow FM.

Table 1: Exchange of information between PCR-GLOBWB variables and D-Flow FM cells for one-way coupling

Description	PCR-GLOBWB variable	Simple distribution	River/floodplain scheme
Water on top of soil	topWaterLayer	All cells	Floodplain cells
Discharge through channel	discharge	All cells	River cells

6.4.1 Flowchart of one-way coupling

A flowchart depicting all processes and BMI functions of the one-way coupled model is shown in Figure 28 below.

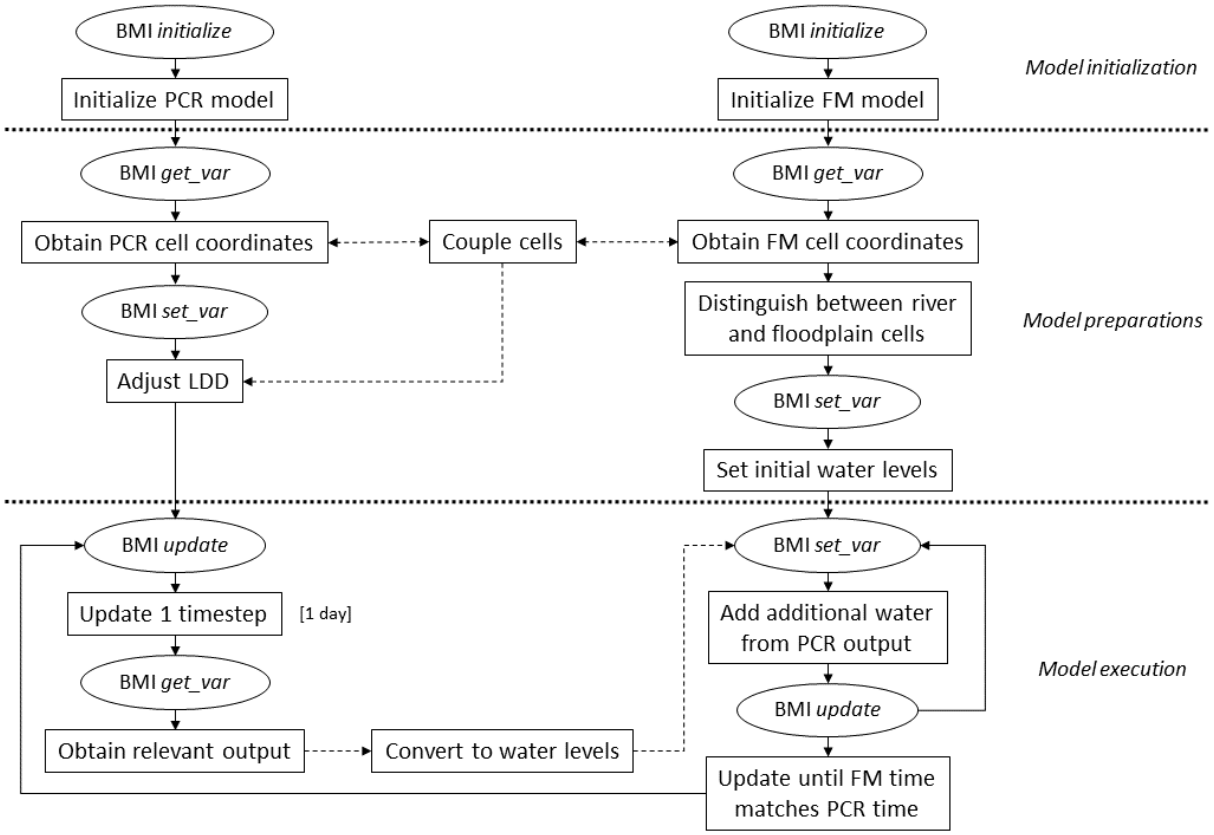

Figure 28: Flowchart depicting the processes and BMI functions involved in the one-way coupled model, with everything related to PCR-GLOBWB on the left and D-Flow FM on the right. BMI functions are represented by round text boxes, the result of these functions or other actions by rectangular text boxes, a next step in the model chain by solid arrows and the exchange of information between models or intermediate coupling functions by dashed arrows.

6.4.2 Remarks on one-way coupling

As stated before, one of the ideas behind the coupling is that the source code of both models is left untouched, so that they can be further developed individually without having to consider the other model or the coupling functions. This is achieved by using the setup for one-way coupling described here; it only requires the addition of BMI for both models and the coupling functions described in this chapter.

It should be noted that the one-way coupled model will not give an accurate representation of reality, as possible losses of water (e.g. through evaporation and infiltration) are not accounted for in the coupled section of the model grid. This means that water that has entered D-Flow FM can only flow downstream; it cannot be removed from the system in any way other than it reaching the outflow boundary near the sea. This will obviously lead to an overestimation of discharge, water levels and inundated areas. However, the one-way coupled model can still be used to assess the functioning of the coupling procedures by comparing results with the two-way coupled model.

6.5 Two-way coupling

The two-way coupling is essentially an extension of the one-way coupling; the exchange of information now takes place in both directions, from PCR-GLOBWB to D-Flow FM and vice versa. This creates a loop in which each model can influence the other. As such, PCR-GLOBWB, which is unable to simulate floods and inundation, will receive information about these processes from D-Flow FM, so that infiltration, evaporation and other hydrological processes can be taken into account. This should ensure a more realistic representation of the natural system, and as such it is expected to improve model results over the use of a single stand-alone model or the previously described one-way coupling.

PCR-GLOBWB is not designed to incorporate the effects of inundation and this means that certain processes cannot be accounted for by simply exchanging information between the models. For instance, the evaporation of open water on the land surface is currently only calculated for the fraction of a cell considered to be a paddy (i.e. one of the irrigation land cover types, see paragraph 3.2). This means that simply supplying PCR-GLOBWB with the amount of inundated water will not work, because it will not properly calculate evaporation. As such, changes will have to be made to the source code of PCR-GLOBWB, to make sure that all relevant processes are handled in a good way. This goes against one of the principles of the coupling, but no other solution for this issue could be found. To minimize the impact of the adjustments to the code, it has been designed in such a way that there is no effect unless certain variables are explicitly changed using BMI functions.

6.5.1 Inundated area, evaporation and infiltration

Theoretically, making some minor adjustments to the source code that handles the evaporation within PCR-GLOBWB would be enough to allow two-way coupling in which all relevant processes are accounted for. However, PCR-GLOBWB calculates stores and fluxes over the entire cell, and this poses a problem. To illustrate this, a hypothetical situation is shown in Figure 29 on the next page. The total volume contained within the wet D-Flow FM cells should be passed to PCR-GLOBWB so that hydrological processes can be accounted for. This would spread out the volume over the larger PCR-GLOBWB cell and lead to a substantial overestimation of evaporation and infiltration, because they are calculated over the entire area. It would be more realistic if these processes were instead only calculated for the inundated area that was simulated by D-Flow FM.

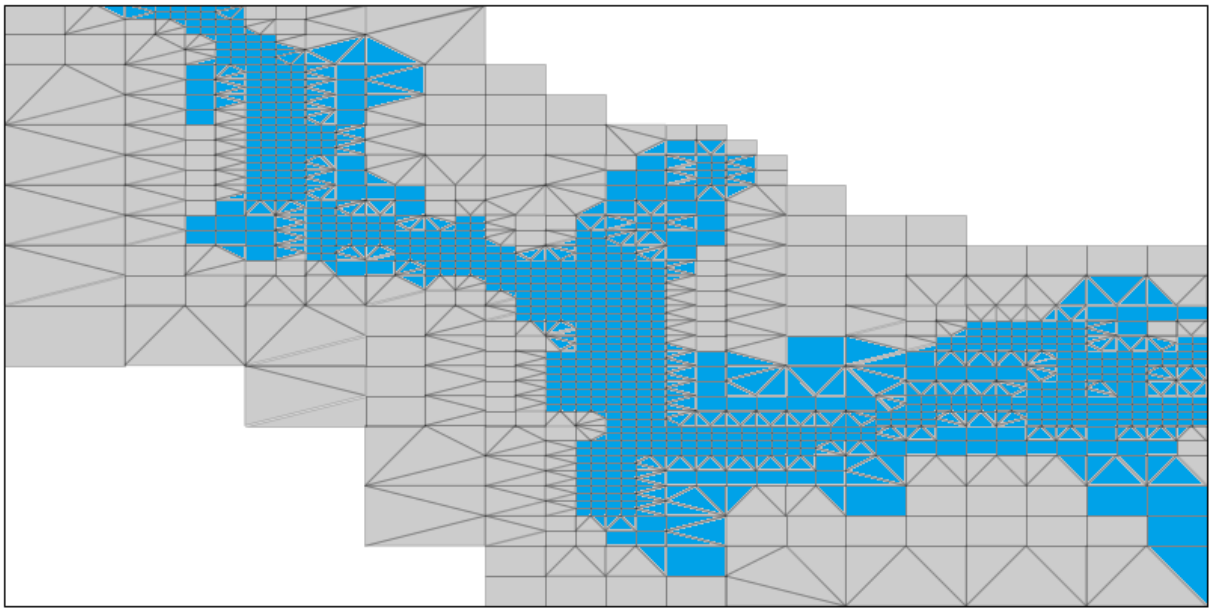

Figure 29: Example of wet D-Flow FM cells within a coupled PCR-GLOBWB cell of 30 arcmin resolution

This issue is solved by accounting for the inundated fraction in each coupled PCR-GLOBWB cell. In practice this means that, for every coupled cell, the total volume and inundated area are calculated, with the inundated fraction calculated by dividing the total inundated area by the area of the PCR-GLOBWB cell. The inundated fraction is then used in the calculations of hydrological fluxes affected by inundation, which means that a sub-grid scheme is introduced that should allow a more accurate representation of what has been simulated by the D-Flow FM model. Hydrological fluxes affected by precipitation should still be calculated over the entire cell. It should be noted that this sub-grid scheme still calculates an average water depth within the PCR-GLOBWB cell, and as such the higher resolution information on specific water depths within D-Flow FM is not used.

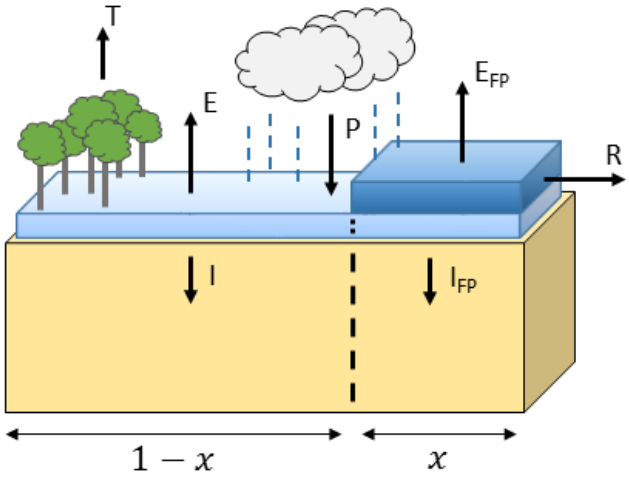

$$I = f_I(V) \cdot (1 - x)$$
$$I_{FP} = f_I(V_{FP}) \cdot x$$
$$I_{total} = I + I_{FP}$$

Figure 30: Schematic representation of hydrological processes within PCR-GLOBWB's land surface, after adjustments for two-way coupling

The adjusted processes within PCR-GLOBWB are visualized in Figure 30 above, with the dark blue layer of water representing the additional water coming from D-FLOW FM. The general subgrid-scheme equations are shown next to it. In these, I stands for infiltration, $f_I(V)$ is the original function to calculate infiltration dependent on V (the amount of water on top of the soil), x is the inundated fraction and the subscript FP stands for floodplain. This uses infiltration as an example, but it is the

same for any other fluxes calculated here. The symbols in the figure are otherwise equal to those used in the similar Figure 8 on page 23. The subgrid-scheme creates two separate stores representing the amount of water on top of the upper soil layer. The fluxes that are dependent on these stores are calculated separately using the inundated fraction as shown in the equations on the previous page. This approach required even more adjustments to the source code of the model, which were again designed in such a way that the model would still be able to run normally, with the adjustments only becoming active after explicitly stating this using BMI functions.

6.5.2 Runoff, discharge and the river/floodplain scheme

As stated earlier in this chapter, two approaches are used to add the relevant output from PCR-GLOBWB to D-Flow FM; a simple approach, where all output is divided over all cells, and a river/floodplain scheme, in which a distinction is made between D-Flow FM cells and certain cells only receive the output of certain variables. Runoff generated in PCR-GLOBWB will be added to the channel storage and thus ends up as discharge. This includes all water on top of the upper soil layer that does not evaporate or infiltrate during the daily update step. This implies that all water that has entered PCR-GLOBWB from D-Flow FM will evaporate, infiltrate or become discharge. As such, a lot of information is still lost using the river/floodplain scheme, because water that was inundating floodplain cells in D-Flow FM might end up as discharge in PCR-GLOBWB, which would be added to the river cells of D-Flow FM. Another issue is related to the fact that the water depth in D-Flow FM is averaged over the inundated area when it is added to PCR-GLOBWB. When all water from the model, including that within the river cells, is added to PCR-GLOBWB's variable representing water on top of the upper soil layer, this again spreads out the water a lot and exposes all of it to the processes of infiltration and evaporation. This will lead to an overestimation of these fluxes and a large reduction of the volume of water within the river channel.

These issues were corrected by making further adjustments to the source code of PCR-GLOBWB, so that, for all coupled cells only, runoff is no longer being added to the channel storage. This makes a clear separation between river cells and floodplain cells (and their relevant processes) possible; water in D-Flow FM's river cells can be added directly to PCR-GLOBWB's channel storage, which is not spread out over the entire cell, while water in the floodplain cells can be added to PCR-GLOBWB as described before. This also makes sure that only the relevant processes for each store are calculated. PCR-GLOBWB includes riverbed infiltration and water body evaporation, which only affect the channel storage. These are also dependent on the water body fraction of PCR-GLOBWB, which includes rivers, lakes and reservoirs. It can be argued that the river cells of D-Flow FM should instead make up this fraction. An analysis of the values for the coupled cells within the study area showed that the fraction calculated from D-Flow FM river cells was consistently larger than that calculated within PCR-GLOBWB. Therefore, to properly account for riverbed infiltration and water body evaporation, it was decided to adjust the source code for this as well, to allow the water body fraction to be updated using BMI functions. This also means that the inundated fraction, as described above, should only be calculated using floodplain cells and should ignore river cells.

The relevant information of how all variables are used in the two-way coupling is shown in Table 2 on the next page, in which variables in italic are the newly introduced variables for the two-way coupling described above. While this table, as well as Table 1 on page 56, also lists how variables would be handled using the simple distribution method, tests revealed that this led to unrealistic results and it was therefore decided to only use the river/floodplain scheme for this study.

Table 2: Exchange of information between PCR-GLOBWB variables and D-Flow FM cells for two-way coupling

PCR-GLOBWB → D-Flow FM:			
Description of PCR-GLOBWB variable	**PCR-GLOBWB variable name**	**Add to D-Flow FM cells (simple)**	**Add to D-Flow FM cells (river/floodplain scheme)**
Water on top of soil	topWaterLayer	All cells	Floodplain cells
Surface runoff	landSurfaceRunoff	All cells	Floodplain cells
Discharge through channel	discharge	All cells	River cells
D-Flow FM → PCR-GLOBWB:			
Description of D-Flow FM variable	**Adjust or add to PCR-GLOBWB variable (simple distribution)**	**Adjust or add to PCR-GLOBWB variable (river/floodplain scheme)**	
Water in floodplain cells	topWaterLayer	*floodplainWaterLayer*	
Water in river cells	topWaterLayer	channelStorage	
Inundated fraction	*inundatedFraction*	*inundatedFraction*	
River fraction	-	dynamicFracWat	

6.5.3 Gains and losses

So far, it has been assumed that data stored within certain variables had to be added from one model to the other. This is indeed the case with one-way coupling, in which no losses are occurring. With two-way coupling however, losses will be occurring and this requires a method to account for them. Since D-Flow FM contains information of a higher resolution than PCR-GLOBWB, it would be good to leave the current state of D-Flow FM untouched until output of PCR-GLOBWB is known and water levels can be adjusted. This is done by calculating the difference between the volume that is added from D-Flow FM to PCR-GLOBWB and the volume calculated as output of PCR-GLOBWB after one timestep:

$$\Delta V_{FM}^{t} = V_{PCR \rightarrow FM}^{t} - V_{FM \rightarrow PCR}^{t-1}$$

in which V is a total volume, t is the timestep in days, the subscripts FM and PCR stand for D-Flow FM and PCR-GLOBWB, respectively, and the arrow subscript denotes the direction in which a volume is handed from one model to the other. This is calculated for every coupled PCR-GLOBWB cell. The change in the total volume within the D-Flow FM cells coupled to a PCR-GLOBWB cell (ΔV_{FM}, hereafter to be named 'delta volume') will be positive if the output of PCR-GLOBWB exceeds the input from D-Flow FM, in which case this delta volume is added to the D-Flow FM cells using the methods described before. If the output of PCR-GLOBWB is less than the input from D-Flow FM, this indicates that the hydrological processes within PCR-GLOBWB resulted in a reduction of total surface water. In this case, the delta volume will be negative and should be removed from the current volume within D-Flow FM. Two algorithms considered to be good for this purpose are described below.

Algorithm 1: removal by total volume

This algorithm starts by finding all wet D-Flow FM cells within the coupled PCR-GLOBWB cell, and assigns an equal part of the total delta volume to each of these. A certain water depth is then removed within each cell (calculated by dividing the volume by the cell's area), after which a check is performed to make sure this did not result in negative water depths. This will often be the case, as it does not check how much water was within each cell. The negative water depths are then set to zero

and the total volume that would be required to do so is calculated, which represents the volume that should still be removed from the model. At this point the algorithm goes back to its starting point and checks which cells are still wet after this first iteration. This is repeated until the volume that is to be removed has reached zero and there are no cells with a negative water depth remaining. The basics of this algorithm are visualized in Figure 31 below.

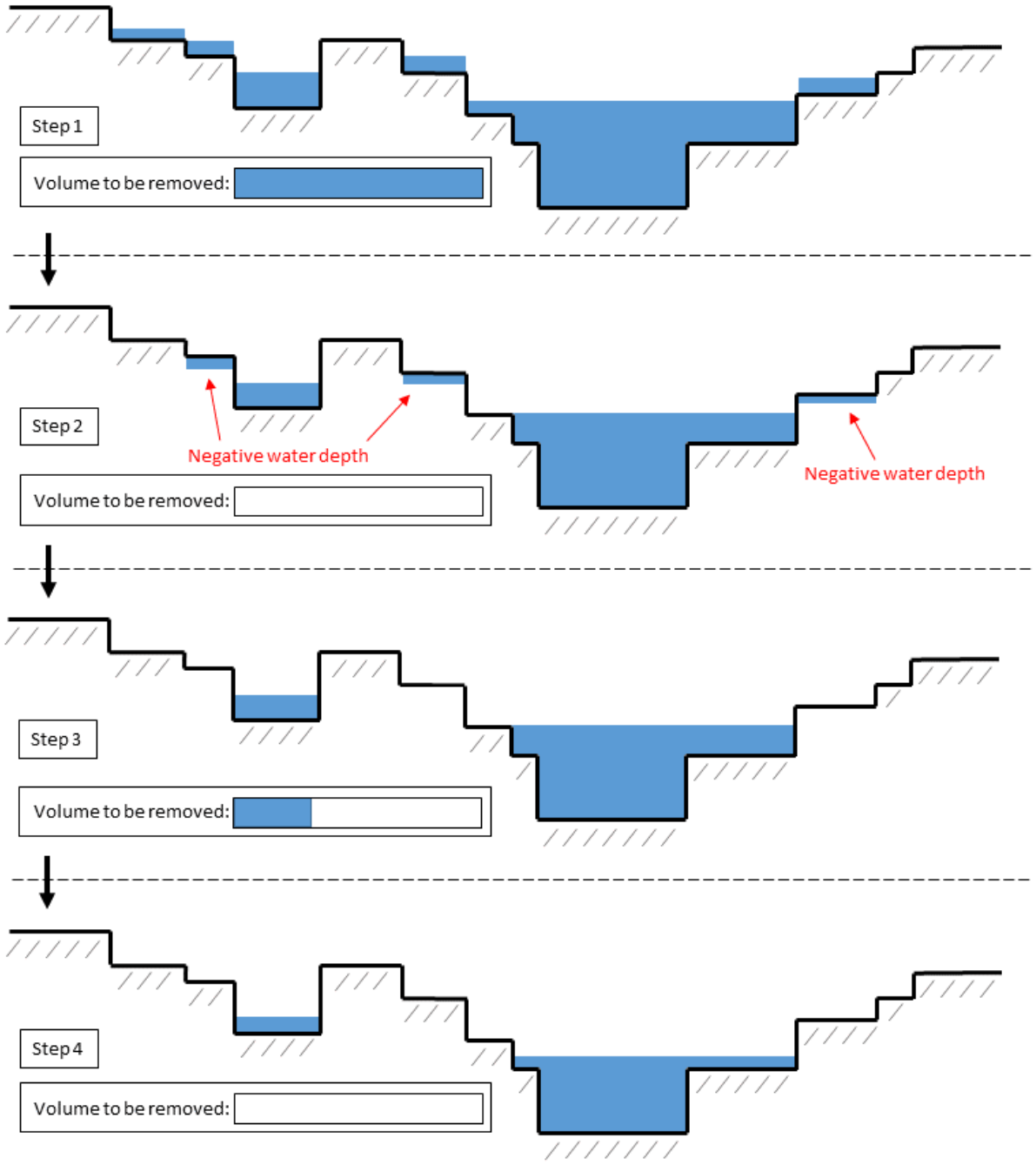

Figure 31: Schematic representation of a cross-section of the D-Flow FM grid and how algorithm 1 (removal by total volume) is used to handle negative delta volumes

Algorithm 2: removal by minimum water depth

The second algorithm also starts by finding all wet cells and then calculates the minimum volume within a single cell. The idea is then to remove this volume from all wet cells, which will not lead to any negative water depths. Beforehand, the total volume that is about to be removed is calculated and compared with the total delta volume, to make sure that this is not exceeded. If this is not the

case, the volume is indeed removed from all wet cells (as well as from the total delta volume to keep track of the re-maining delta volume) and these steps are repeated until the remaining delta volume has reached zero. This is visualized in Figure 32 below. However, it is unlikely that the remaining delta volume will exactly reach zero in this way. It is more likely that the volume that is about to be removed will exceed the remaining delta volume, which poses a problem, because there is no straightforward way to calculate the exact volume that can still be removed from all wet cells. To solve this, the first algorithm is used whenever this issue is encountered.

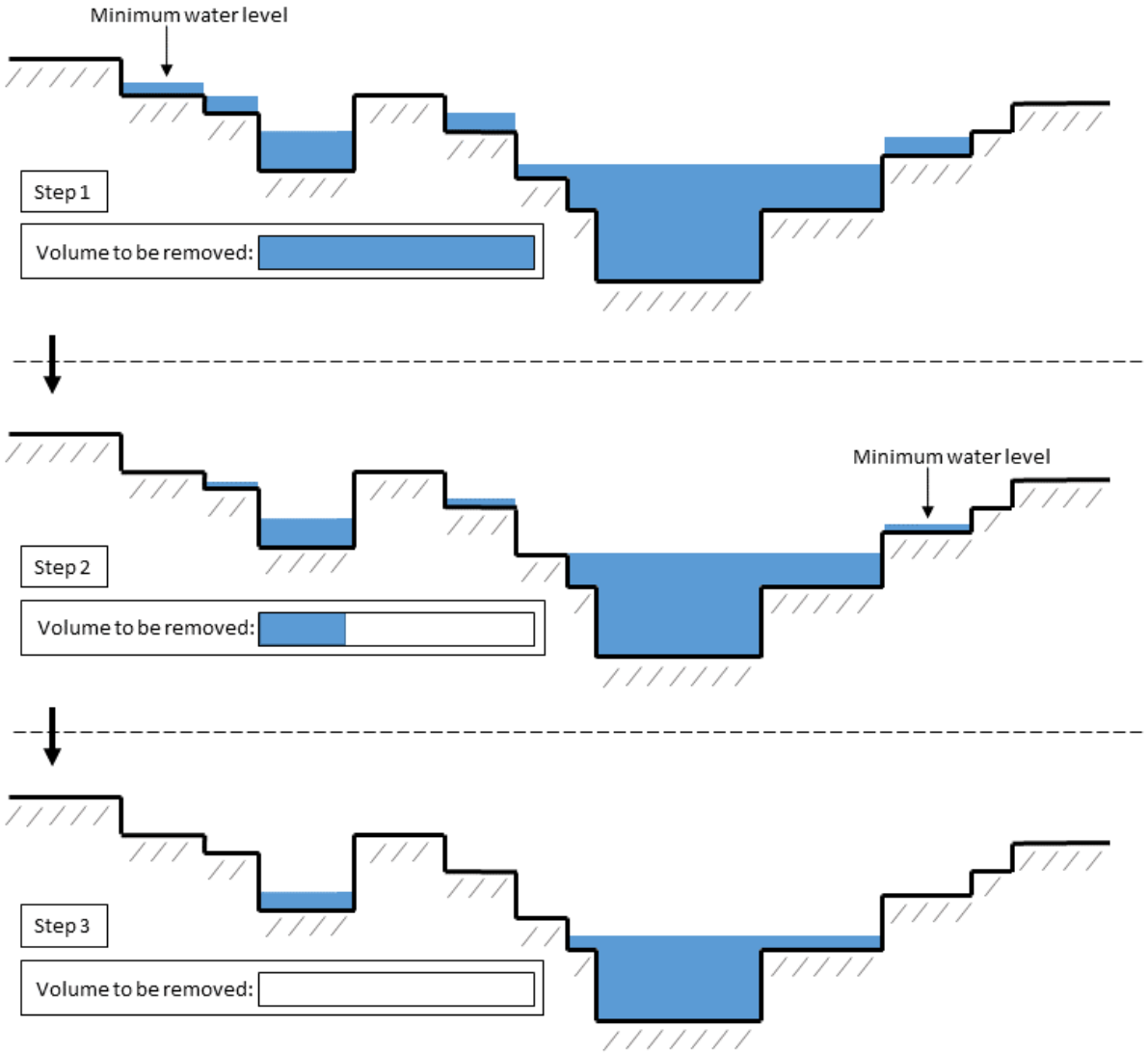

Figure 32: Schematic representation of a cross-section of the D-Flow FM grid and how algorithm 2 (removal by minimum water depth) is used to handle negative delta volumes

Tests of both algorithms revealed a similar performance, with relatively equal calculation times and very small differences between the delta volume and the total removed volume (i.e. a maximum difference in the order of $1 \cdot 10^{-8}\ m^3$). This made it difficult to choose one algorithm over the other. In the end, it was decided to use algorithm 2 because it resulted in slightly less remaining wet cells after a full update, which was thought to be beneficial for computational efficiency.

6.5.4 Water bodies in PCR-GLOBWB

PCR-GLOBWB includes different types of water bodies, such as lakes and reservoirs, with their own storage. This storage is dependent on the channel storage, with PCR-GLOBWB following these four

steps during routing: (1) move channel storage to water body storage for relevant cells, (2) calculate outflow of water bodies and add this to channel storage, (3) perform channel storage routing and (4) move water body storage back to channel storage for the relevant cells. This does not work well with the current setup of the coupled model, which assumes that all channel storage will be removed within the coupled grid (because of the adjusted LDD with pits at all coupled cells, see paragraph 6.3.1). If there are water bodies present within the coupled cells, the channel storage there will not be removed because it is moved to the water body storage before routing. This interferes with the flow of water in D-Flow FM, because it implies that water being added to PCR-GLOBWB from D-Flow FM might end up in the storage of water bodies.

As such, this will reduce the output of PCR-GLOBWB, which can result in large negative delta volumes and the subsequent removal of a lot of water from D-Flow FM cells coupled to PCR-GLOBWB cells with a water body. This is repeated at every timestep of the coupled model; during the next update of D-Flow FM, water located in upstream cells will flow into these cells, after which it will be added to the water body storage of PCR-GLOBWB. This process continues until the capacity of a water body is reached, at which point it will suddenly start discharging enormous amounts of water, resulting in large positive delta volumes and a flood wave entering D-Flow FM. This is very unrealistic behaviour that should be avoided.

The D-Flow FM model does not explicitly contain water bodies. Lakes are only included as large areas of small cells and while these cells are thought to represent generic water bodies in the two-way coupling method using the river/floodplain scheme, they are not a realistic representation of lakes because their bathymetry is unknown (and consequently no burning of the DEM was carried out at their locations). As such, they are probably not as deep as they are in reality. Reservoirs have the same issue, but this is not the only problem related to these water bodies. PCR-GLOBWB includes a reservoir scheme that handles the outflow, but such a scheme is not available for D-Flow FM. This means that reservoirs in D-Flow FM are basically large flat areas with a sudden, steep drop in elevation at their most downstream end. This is of course also not a good representation of reality, but it should not have a strong impact on the results of this study as the only two large reservoirs within the D-Flow FM grid are located relatively far downstream of the gauging station of Niamey (roughly 600 km), which is the most downstream station being used for this study.

In light of all of the above, it has been decided that it would be relatively complex to explicitly include all types of water bodies within the coupled model, while having water bodies only represented in PCR-GLOBWB leads to the aforementioned problems, which should be avoided. Therefore, a final set of adjustments were made to the source code of PCR-GLOBWB, allowing the removal of water bodies within the coupled grid using BMI functions. This ensures that all water being entered into PCR-GLOBWB from D-Flow FM is accounted for and does not end up in a store that interferes with the flow of water within the coupled model. It should be noted that this does mean that there is no proper representation of water bodies within the coupled grid, which could negatively affect results.

6.5.5 Initial groundwater storage

Tests of the two-way coupled model revealed an issue with the groundwater storage of PCR-GLOBWB. Since the stand-alone model does not simulate floods, the only source of infiltration is precipitation, and this means that the recharge of groundwater is also limited to this source. However, since large floods are occurring within the Niger Inner Delta on a yearly basis, this represents an additional source of infiltration (and groundwater recharge), which is taken into

account with the coupled model. The initial groundwater storage in the coupled model, as a result of the spin-up of the stand-alone PCR-GLOBWB, is not based on this, which means that it is underestimated. The effect of this is clearly visible in Figure 33, showing the groundwater storage within the Niger Inner Delta during testing of the two-way coupled model.

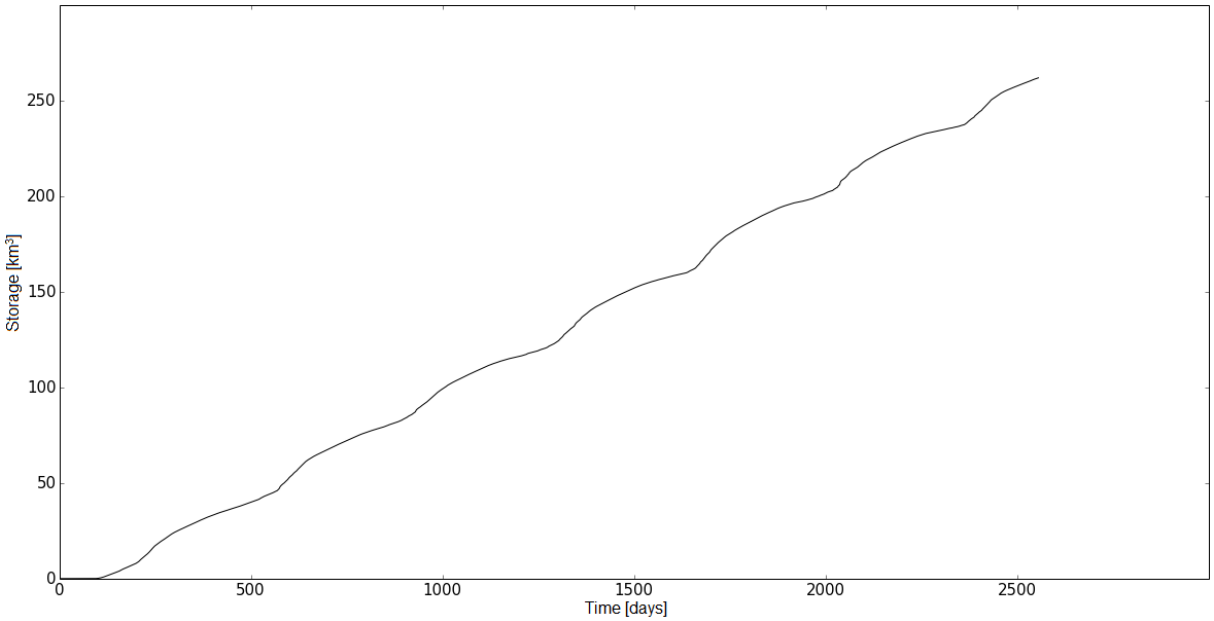

Figure 33: Groundwater storage modelled during tests of the two-way coupled PCR-GLOBWB D-Flow FM model

The groundwater storage is continuously increasing and there is no indication that this is slowing down. This would imply that the coupled model would also need to spin-up to achieve more stable initial conditions. However, the test run from which this result was obtained simulated a time period of seven years, which took over seven days in real-time. Given the fact that the increase in storage is not slowing down, the spin-up period for initial conditions should probably be a lot longer than seven years, which would substantially increase the total simulation time. This was not possible during the timeframe of this study and instead another solution was conceived; using BMI to adjust the initial groundwater storage at the start of a coupled model run. With the groundwater recharge rate known from tests, the average groundwater storage can be obtained by dividing this value by the recession coefficient of the aquifer (Van Beek, pers.com.):

$$S = \frac{R}{k}$$

in which S is the average groundwater storage, R is the recharge and k is the recession coefficient.

6.5.6 Flowchart of two-way coupling

A flowchart depicting all processes and BMI functions of the two-way coupled model is shown in Figure 34 on the next page.

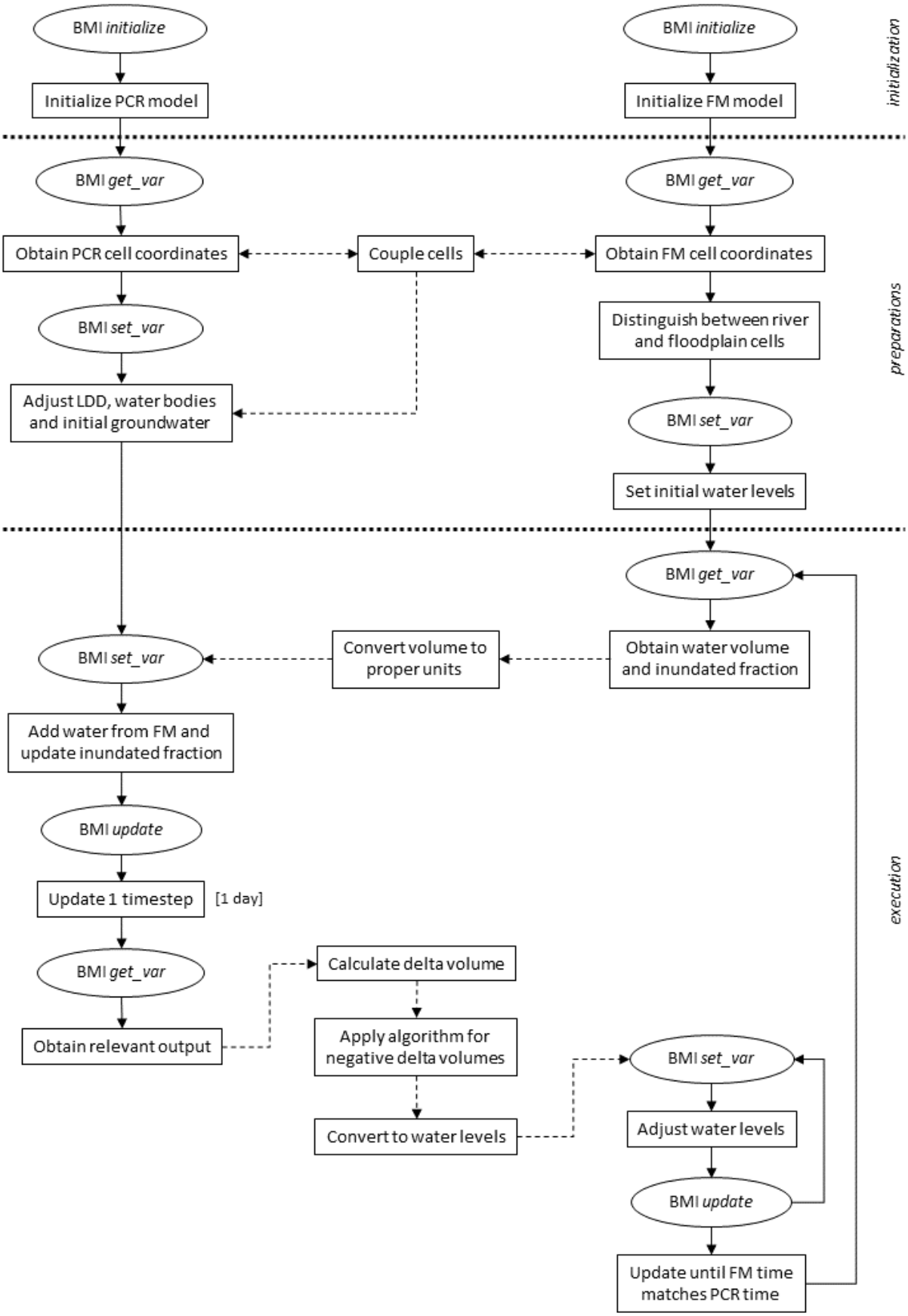

Figure 34: Flowchart depicting the processes and BMI functions involved in the two-way coupled model, with everything related to PCR-GLOBWB on the left and D-Flow FM on the right. BMI functions are represented by round text boxes, the result of these functions or other actions by rectangular text boxes, a next step in the model chain by solid arrows and the exchange of information between models or intermediate coupling functions by dashed arrows.

7 Results

7.1 Model setups

In order to assess the potential of the coupled PCR-GLOBWB D-Flow FM model, several different model setups have been created, so that their results can be compared with each other and with results from other studies. This includes the stand-alone models of PCR-GLOBWB and D-Flow FM, to assess the influence these have on the coupled setups. PCR-GLOBWB has the option to choose between two different grid resolutions (i.e. 5 or 30 arcmin) and two different routing methods (i.e. accuTravelTime or KinematicWave), as was described in chapter 3, giving a total of four possible model setups for the stand-alone PCR-GLOBWB model. The stand-alone D-Flow FM has one model setup, in which upstream discharge boundary conditions using GRDC data are applied instead of meteorological input. The coupled model setups include one 1-way coupled model and two 2-way coupled models, out of which the second 2-way coupled model is an adjusted version in which the infiltration of flooded water is disregarded and upstream discharge for the Niger and Bani rivers is obtained from GRDC data instead of PCR-GLOBWB. The latter is done because PCR-GLOBWB is not able to accurately simulate the upstream discharge of these rivers, leading to inaccurate inputs into the coupled model, and because tests of the standard 2-way coupled model revealed extremely high infiltration values (related to the increase in groundwater storage described in the previous chapter), which removed so much surface water that the river completely dried up before it reached the end of the Inner Delta. Without the distraction of these issues, this setup will allow for a better assessment of other issues related to the modelling of the Niger River, and the Niger Inner Delta in particular. All coupled models use PCR-GLOBWB at 30 arcmin resolution because the coupled models with 5 arcmin resolution turned out to be too computationally intensive. However, one run with a shortened time period could be carried out to still make a comparison of results possible.

This gives a total of nine model setups which will be assessed in this chapter:

1. Stand-alone PCR-GLOBWB at 30 arcmin resolution using the accuTravelTime routing method
2. Stand-alone PCR-GLOBWB at 30 arcmin resolution using the kinematicWave routing method
3. Stand-alone PCR-GLOBWB at 5 arcmin resolution using the accuTravelTime routing method
4. Stand-alone PCR-GLOBWB at 5 arcmin resolution using the kinematicWave routing method
5. Stand-alone D-Flow FM using GRDC discharge data at specified upstream locations
6. One-way coupled model with PCR-GLOBWB at 30 arcmin resolution
7. Two-way coupled model with PCR-GLOBWB at 30 arcmin resolution
8. Two-way coupled model with PCR-GLOBWB at 30 arcmin resolution, without infiltration of flooded water and using GRDC discharge data at specified upstream locations
9. Two-way coupled model with PCR-GLOBWB at 5 arcmin resolution

7.1.1 Model parameters and settings

Both PCR-GLOBWB and D-Flow FM are run with their default settings, without carrying out any sort of calibration. There are several reasons for this; not only would doing so be beyond the scope of this research, it would also distract from the coupling itself and the (inter)comparison of models. PCR-GLOBWB is run using the two natural land cover types (i.e. no irrigation) and domestic and industrial water demand was not included. This allows a better focus on the most important hydrological processes.

Two important parameters in PCR-GLOBWB are *minTopWaterLayer* and *manningsN*, which represent the water level that is allowed to stay on top of the upper soil layer at the end of a timestep and the Manning's roughness coefficient for river channels, respectively. Any water level above the value of *minTopWaterLayer* is added to the runoff. This value is set to zero, as this is the default setting for the two natural land cover types, which means that any water still remaining on the upper soil layer after the calculation of evaporation and infiltration is added to runoff. The parameter *manningsN* is set to the default value of 0.04 $m^{1/3}$ s^{-1}. D-Flow FM also uses Manning's roughness coefficient, which has a default value of 0.023 $m^{1/3}$ s^{-1}.

PCR-GLOBWB is forced with CRU TS3.21 meteorological data from the Climate Research Units of the University of East Anglia, which are downscaled to daily values using the ERA-Interim/LAND dataset, corrected using data from the Global Precipitation Climatology Project (GPCP). More information on the forcing data of PCR-GLOBWB can be found in Van Beek (2008). All PCR-GLOBWB models use "hot starts" with previously obtained initial conditions, to shorten the total simulation time.

7.1.2 Simulated time period

All models were run for the period 1995-2000 because this was the only recent period with (nearly) continuous discharge data for the most important gauging stations, which allows the validation of results at these stations (the stations used in this study are shown in Figure 3 on page 15 and Figure 19 on page 41). The data of the stations of Koulikoro and Niamey are complete for this time period, while the stations of Douna, Mopti and Dire contain some missing data. Days with missing data are removed from the calculation of model performance indicators (described in the next paragraph). A period of six years was chosen as it was thought to be long enough to overcome any initialization problems, while making sure that the total model simulation time would not become unbearable. Early tests indicated that the 2-way coupled model with PCR-GLOBWB at 30 arcmin resolution would require approximately four minutes to simulate a day, which gives a total of six days to simulate the total time period, when the model was run on a standard laptop with 4 GB memory and a 2.5 GHz Intel i5-2520M processor.

7.2 Model assessment tools

Model results will be compared using various tools, to make sure all relevant aspects are considered during the analysis. Hydrographs at gauging stations give a good indication of modelled discharge and how well this reflects observed values. Model performance indicators give a quick view of the models ability to simulate certain aspects of the flow regime. Since the Niger Inner Delta has a strong impact on this flow regime and on downstream discharge, a hydrological analysis of several important fluxes and stores within this area will be carried out as well. This includes an overview of the inundated area within the delta and, whenever possible, results will be compared with similar properties from other studies on this region. Finally, simulation times are considered as well, as these give an indication of the potential use of the model for global applications. This means the following tools are used to analyse the results of each model:

1. Hydrographs of modelled and observed discharge
2. Model performance indicators, including simulation time
3. Analysis of hydrological properties in the Niger Inner Delta, including inundated area

The analysis of hydrological properties requires PCR-GLOBWB to assess stores and fluxes, and D-Flow FM to assess the inundated area. This means that it will not be possible to consider all of the described tools for stand-alone model runs. The model performance indicators and analysis of

hydrological properties are explained in more detail in the following paragraphs. To make sure that these indicators are not influenced by initial conditions, the first year of the time series is excluded from the calculations, which leaves a period of five years (1996-2000) to calculate each performance indicator.

7.2.1 Model performance indicators

Model performance is assessed by calculating several performance indicators at each of the previously mentioned GRDC gauging stations; the Nash-Sutcliffe model efficiency coefficient, root-mean-square-error, peak flow error and phase error.

The Nash-Sutcliffe coefficient (NSC) compares the modelled output to the observed data and can range between $-\infty$ and 1; a value less than zero indicates that the model predictions are less accurate than simply using the mean of the observed data, while a value above zero indicates the opposite, with a value of 1 indicating a perfect fit between modelled and observed discharge (Nash & Sutcliffe, 1970). The NSC is calculated as:

$$NSC = 1 - \frac{\sum_{t=1}^{T}(Q_{data}^{t} - Q_{model}^{t})^2}{\sum_{t=1}^{T}(Q_{data}^{t} - \bar{Q}_{data})^2}$$

In which Q is the discharge at timestep t, $\overline{Q}$ is the average discharge over the entire time period and T is the total number of time steps.

The root-mean-square-error (RMSE) is another widely used criterion for model performance, which is often applied to hydrological and hydrodynamical models (e.g. Kim et al., 2012; Neal et al., 2012). It gives an indication of the average error in the model predictions and is calculated as (using the same symbols as in the equation for NSC above):

$$RMSE = \sqrt{\frac{\sum_{t=1}^{T}(Q_{data}^{t} - Q_{model}^{t})^2}{T}}$$

While the RMSE gives an indication of a model's overall performance, it says little about its ability to accurately simulate peak flows, which are an important indicator for floods. The peak flow error (PFE) is an indication of the difference between the largest discharge value of a model and that of observations, within a hydrological year's time series. For this study, it is assumed the hydrological year of the Niger River is from April 1st to March 31st, as this period always includes the entire wet season at all of the considered gauging stations. The PFE, as a percentage, is calculated as (Kim et al., 2012):

$$PFE = \frac{|Q_{data}^{max} - Q_{model}^{max}|}{Q_{data}^{max}} \cdot 100$$

The phase error (PE) measures the error in the time at which peak flow is modelled and thus gives an indication of how well a model is able to reproduce the timing of a discharge peak. The PE is calculated as (Kim et al., 2012):

$$PE = \tau_{model} - \tau_{data}$$

in which τ is the day at which the peak flow occurred.

7.2.2 Niger Inner Delta area for hydrological analysis

As stated in chapter 2, there is no clear definition on the borders of the Niger Inner Delta, with different areas reported in previous studies. The area considered to best represent the Inner Delta for this study is shown in Figure 35 below (which roughly corresponds to the area highlighted in Figure 3 on page 15). The extent of this area is based on the studies cited in chapter 2 and on where most of the inundation was occurring during model testing. The area covers roughly 69,000 km^2, which is within the range listed by other studies (for example, Mahé et al. [2009] state an area of 73,000 km^2) and this should thus allow a comparison of relevant values. Within this area, the total fluxes and stores of relevant hydrological properties are calculated (using PCR-GLOBWB), as well as the total inundated area and volume of water within the floodplains (using D-Flow FM). It should be noted that the 5 arcmin version of PCR-GLOBWB had a slightly different area, because of a difference in the size and shape of the Niger basin at different model resolutions. A figure showing the area for models with PCR-GLOBWB at 5 arcmin resolution is included in Appendix C.5.

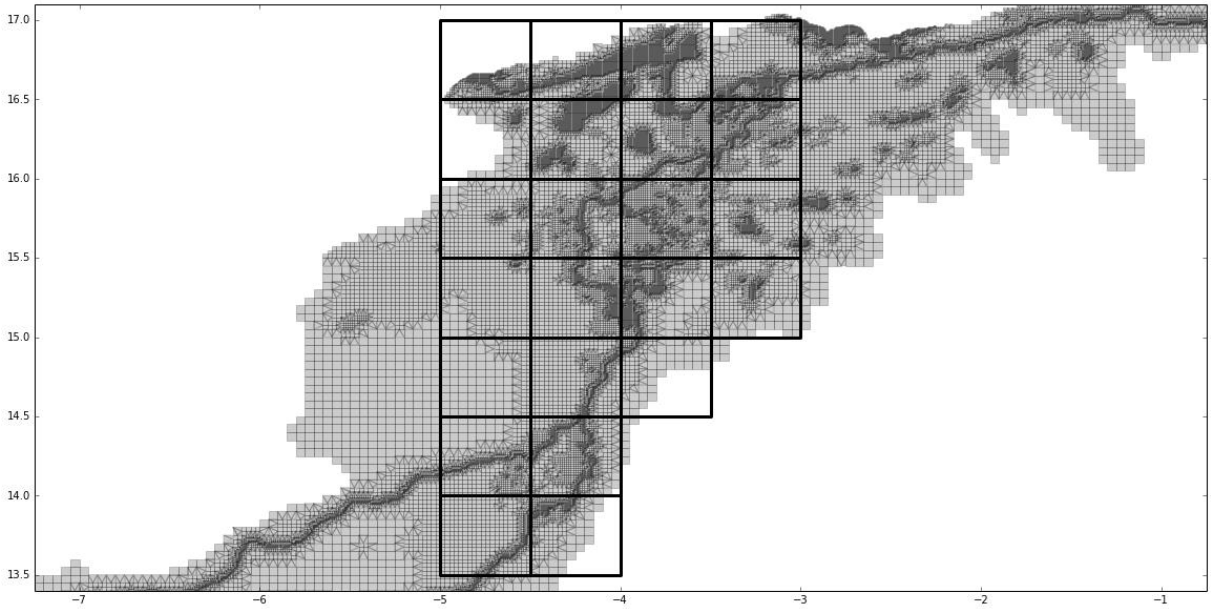

Figure 35: The area of the Niger Inner Delta, visualized by coupled cells of PCR-GLOBWB (at 30 arcmin resolution) overlaid on the D-Flow FM grid.

7.3 Stand-alone PCR-GLOBWB models

The output of PCR-GLOBWB is an important indicator of the input that the coupled models will receive. This output is especially important for the coupled cells located furthest upstream, close to the gauging stations of Koulikoro for the Niger River and Douna for the Bani River. Downstream of these cells the influence of PCR-GLOBWB output is diminished, because D-Flow FM takes over the simulation of surface water. Upstream of these cells however, all calculations are done by PCR-GLOBWB and the discharge that arrives at these cells makes up an important part of the total amount of water that enters the coupled model.

7.3.1 Hydrographs and performance indicators

The discharge simulated by the four stand-alone PCR-GLOBWB models at Koulikoro is shown in Figure 36 on the next page, together with the observed discharge from the GRDC. This reveals a clear difference in the discharge simulated at different resolutions, while the effect of a different routing method seems to be limited. This is probably because this station is located relatively far upstream, where the effect of routing is limited in general. All models overestimate discharge most of the time,

although this is more pronounced in the versions with 30 arcmin resolution, which have a very high minimum discharge. The versions running at this resolution also have extremely large and sharp peaks. The 5 arcmin versions seem to be better at simulating the seasonality of the flow, although the observed discharge is not accurately simulated at this resolution either; minimum flow is overestimated, peak discharge is not accurately simulated and the decline in discharge after peak flow is too slow. Overall, this constitutes a relatively poor performance of all PCR-GLOBWB models, which is reflected in the performance indicators shown in Table 3 on the next page). The hydrograph for the Bani River at the station of Douna, also shown in Figure 36, reveals a similar pattern, although it can be seen that the discharge values are substantially lower.

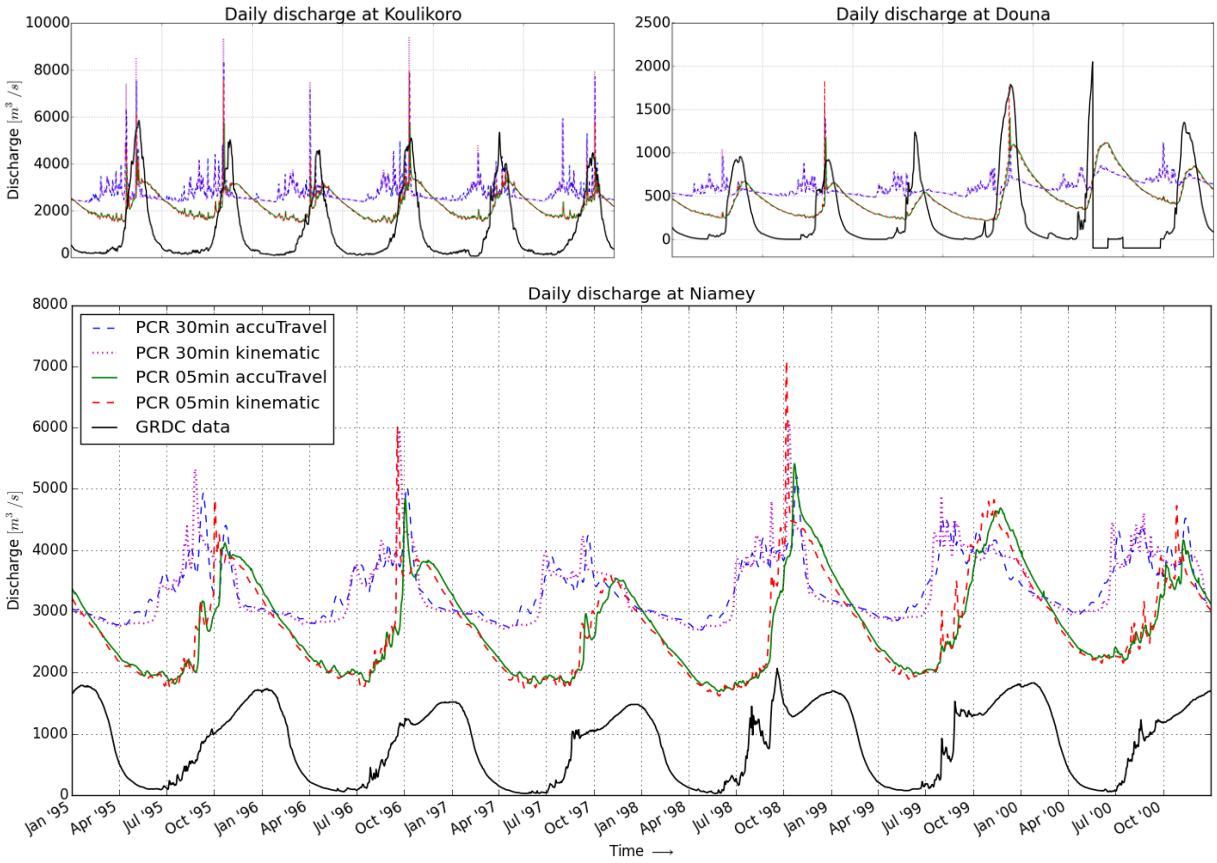

Figure 36: Discharge as modelled by the stand-alone PCR-GLOBWB models and data of the GRDC (period 1995-2000) at the stations of Koulikoro, Douna and Niamey (with missing data, present at Douna, assigned a value of -99)

The results of the same model setups for the downstream station of Niamey are shown in the bottom image of Figure 36 above. This also shows that the largest differences in modelled discharge are caused by different resolutions and not by different routing methods. However, some differences are visible between the routing methods used at the same resolution, which is likely caused by the fact that this station is located further downstream. The kinematicWave method seems to be able to react quicker than the accuTravelTime method; peaks are simulated earlier and have higher values. In fact, during the largest peak flows the results of the kinematicWave method used at the different resolutions show more similarities than the kinematicWave method and accuTravelTime method of the same resolution. But it should be noted that the performance indicators reveal that the simulation of peak flow is better done with the accuTravelTime method.

The general overestimation by all models has increased at Niamey compared to the upstream station of Koulikoro, up to the point that the minimum discharge of all models is exceeding the peak flow of the observed discharge. The 5 arcmin versions seem to have a constant overestimation of

approximately 2000 m^3/s, while the seasonality seems to be modelled relatively well. The 30 arcmin versions have more severe overestimations and a less well modelled seasonality at this station as well. The larger overestimation at this station is probably caused by the fact that the Niger Inner Delta is not accurately modelled in the stand-alone PCR-GLOBWB model, which means losses due to evaporation and infiltration are underestimated. The performance indicators for Niamey are included in Table 3, while Table 5 on page 82 (which displays the performance indicators for all models) also lists those for the stations of Mopti and Dire.

Table 3: Model performance indicators for the four stand-alone PCR-GLOBWB models at Koulikoro, Douna and Niamey*

		Koulikoro		Douna		Niamey	
Model setup	Time	NSC	RMSE	NSC	RMSE	NSC	RMSE
30 arcmin accuTravelTime	2	-1.37	2082	-0.38	523	-17.78	2641
30 arcmin kinematicWave	4	-1.37	2085	-0.38	523	-17.78	2641
5 arcmin accuTravelTime	4	-0.32	1554	0.20	400	-9.80	2002
5 arcmin kinematicWave	23	-0.29	1535	0.24	389	-9.77	1999

Model setup	PFE	PE	PFE	PE	PFE	PE
30 arcmin accuTravelTime	49	-39	45%	-16	179	-73
30 arcmin kinematicWave	61	-40	49%	-20	210	-83
5 arcmin accuTravelTime	21	-7	38%	22	169	-33
5 arcmin kinematicWave	36	-9	50%	16	211	-47

* Time is the total simulation time [h], NSC is the Nash-Sutcliffe coefficient [-], RMSE is the root-mean-square-error [m^3/s], PFE is peak flow error [%] and PE is phase error [days].

7.3.2 Niger Inner Delta hydrological properties

The hydrological stores and fluxes within the area designated as the Niger Inner Delta also show very strong similarities between the models of the same resolution. This is to be expected as the only difference between these models is the used routing method and this mostly affects discharge (which, without the possibility of flooding, will have little effect on other hydrological properties). But while there was a clear difference in discharge between the models using a different resolution, this is not the case for the hydrological stores and fluxes. The evapotranspiration for two model setups, which is shown together with the precipitation in Figure 37 on the next page, reveals very little differences. It does clearly show the seasonality of these fluxes. It can also be seen that evapotranspiration is more evenly distributed than precipitation, which is to be expected as evapotranspiration can draw water from soil stores, which temporarily store excess precipitation. The total yearly fluxes are similar to each other; the input from precipitation (with a yearly average between 320-340 mm) is only slightly larger than the loss through evapotranspiration (with a yearly average between 290-310 mm).

When compared with values listed in other studies, it seems that these fluxes are underestimated by the PCR-GLOBWB models. For example, Mahé et al. (2009) state that rainfall over the area varies between 356 and 682 mm, with an average of 545 mm. There are two possible explanations for this; their study used a larger area to describe the Niger Inner Delta (i.e. 73,000 km^2), which might contain a part of the region that receives more precipitation, or it is caused by the use of different meteorological data (Mahé et al. [2009] refer to Olivry [1995] but this source could not be verified). It is

unknown whether this means that the values of this study are an underestimation or their values are an overestimation. However, it is important to consider this difference when comparing other hydrological properties, as these are influenced by the input from precipitation. The difference in modelled evapotranspiration is more severe, with Mahé et al. (2009) stating an average of 800 mm/year. Again, this might be caused by different definitions of the extent of the Inner Delta, but it seems unlikely that this is the only reason for this large difference. It is probably also caused by the fact that the models are unable to simulate inundation, which is an important source of evaporative losses in this region.

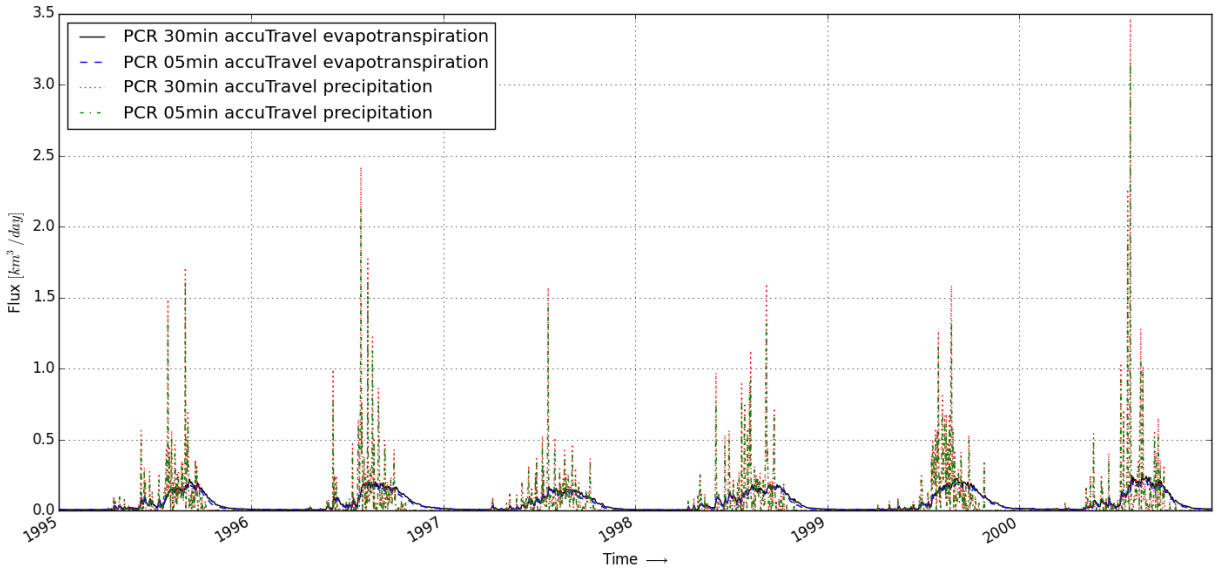

Figure 37: Daily precipitation and evapotranspiration fluxes within the Niger Inner Delta as modelled by the stand-alone PCR-GLOBWB models at 30 arcmin and 5 arcmin resolution using the accuTravelTime routing method

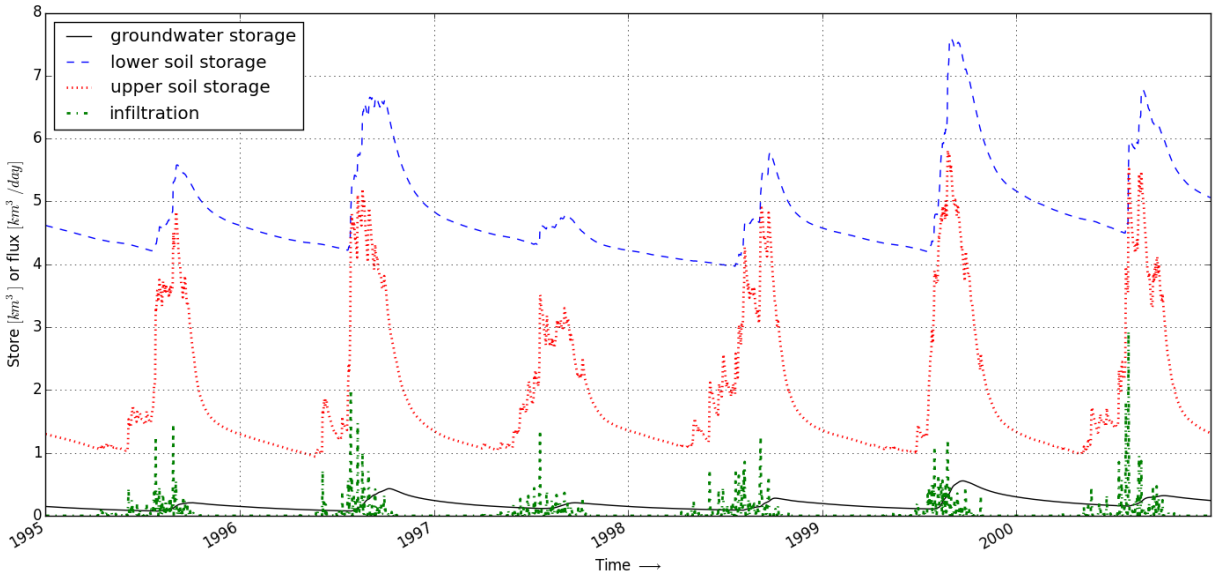

Figure 38: Daily values of groundwater storage, soil storage and infiltration within the Niger Inner Delta as modelled by the stand-alone PCR-GLOBWB model of 5 arcmin resolution using the accuTravelTime routing method

Infiltration and all of the soil stores, including groundwater, are shown in Figure 38 above. It can be seen that infiltration follows a similar pattern as precipitation, which is to be expected as water on top of the soil layers as a result of precipitation is the only water that can infiltrate in the non-coupled PCR-GLOBWB models. The total flux within the Inner Delta is roughly 280-300 mm/year, which is slightly less than that of precipitation. As can be expected, the increase in the soil stores

follows a similar pattern, albeit with a slight delay. When there is no input from infiltration the soil storage decreases again, due to exchange with other stores and losses from evapotranspiration. The seasonality seen in the surface water is thus also seen in the soil layers. The groundwater store is relatively small compared to the other soil stores, with the related fluxes of groundwater recharge and baseflow being only a few mm/year.

7.3.3 Choice of PCR-GLOBWB model setup for coupled models

Based on the results shown above it can be stated that the 5 arcmin accuTravelTime model gives the best overall performance. The results of both 5 arcmin models are definitely better than those of the 30 arcmin models, as can be seen from the hydrographs and the performance indicators of Table 3. The two different routing methods of the 5 arcmin model give relatively similar results, but the accuTravelTime method is substantially faster and seems to give a better reproduction of observed peak flows. However, as stated at the start of this chapter, the coupled models with PCR-GLOBWB at 5 arcmin resolution were too computationally intensive to simulate the entire time period, which is why the 30 arcmin version with the accuTravelTime routing method is used to do this instead. This means that the upstream discharge of the Niger and Bani rivers is simulated relatively poorly, which will affect results of the coupled models.

7.4 Stand-alone D-Flow FM model

The stand-alone D-Flow FM model is driven by upstream boundary conditions instead of meteorological input. Discharge data from the GRDC is used to set discharge boundaries at the most upstream cells of the Niger and Bani rivers, near the gauging stations of Koulikoro and Douna respectively. No time delay is introduced on the data (even though the stations are located a bit downstream of the most upstream cells) because the distance is relatively short and the travel time is unknown. It is otherwise also not expected to have a large impact on results, because the influence of other factors (e.g. the model grid and applied stream burning) is expected to be far greater. The station of Koulikoro has a complete dataset for the chosen period of 1995-2000, but this is not the case for the station of Douna, which has missing data between September 1999 and June 2000. To make sure that the model always receives discharge input, the missing data were adjusted by taking the average of the last three known values and the value at the same date one year earlier (see Appendix C.6 for the resulting hydrograph).

The hydrographs showing the simulated discharge at the stations of Mopti, Dire and Niamey are included in Figure 39 on the next page. From this figure it can be seen that, at Mopti, which is the furthest upstream of the three stations, the timing of the flow is well simulated, as is the flow itself during the dry season. However, the peak flow is severely overestimated, roughly by a factor of two. This implies that there should be substantial losses occurring before Mopti, which is often seen as the start of the Inner Delta. By the time the flow has reached Dire, close to the end of the Inner Delta, the overestimation seems to be less severe (probably due to inundation and the recharge of lakes within the Inner Delta), but the timing of the flow is less well modelled. The modelled discharge shows a delay with respect to the data, which could imply that the used model grid does not give a good representation of the delta, potentially leading to an overestimation of inundation that attenuates the flow. This delay persists until Niamey, although the timing of the peak flow itself seems to be reasonably well modelled. However, the increase in discharge at the start of the wet seasons starts too late, while the decline is too slow. The peak flow, as well as minimum discharge, is overestimated. This is to be expected, because the stand-alone D-Flow FM model does not include

any loss factors. Overall, the hydrographs reveal that the model is able to simulate the flow within the river relatively well, taking into account the issues described here. The coupling to PCR-GLOBWB will make sure that potential loss factors are accounted for, but the timing error is likely to persist because it is related to the model grid.

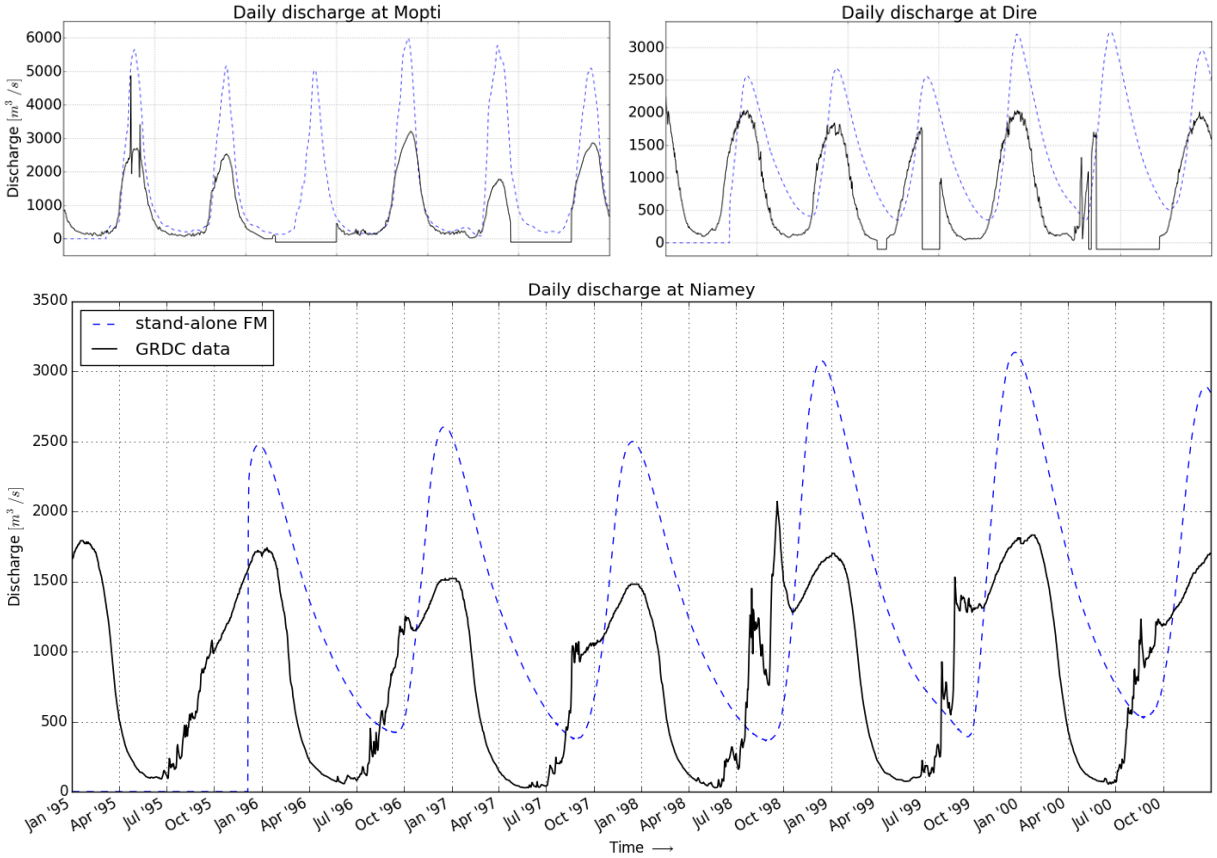

Figure 39: Discharge as modelled by the stand-alone D-Flow FM model and data of the GRDC (period 1995-2000) at the stations of Mopti, Dire and Niamey (with missing data, present at Mopti and Dire, assigned a value of -99)

The performance indicators for the stand-alone D-Flow FM model are included in Table 5 on page 82. These show that results have improved over the stand-alone PCR-GLOBWB models for all of the listed stations. This is as expected, because the model uses discharge boundary conditions which are set using observed discharge values. However, the errors are still relatively large. Since this model did not include PCR-GLOBWB, no hydrological properties of the Niger Inner Delta could be calculated.

7.5 Coupled models

This includes all the coupled models that were run for the full time period (1995-2000), which use PCR-GLOBWB at 30 arcmin resolution: a 1-way coupled model, 2-way coupled and the adjusted 2-way coupled model that has no infiltration of flooded water and uses GRDC discharge data as upstream input for the Niger and Bani rivers instead of PCR-GLOBWB output. The resulting hydrographs for the stations of Mopti, Dire and Niamey are shown in Figure 40 on the next page.

7.5.1 Hydrographs

The effect of the 2-way coupling can be seen in the hydrographs at Mopti; discharge is lowered compared to the 1-way coupling, which does not include any loss factors, and the seasonality is more pronounced. The 2-way coupled model clearly gives a better fit to the observed values. However, the observed values are not accurately replicated by either of the models, but that is to be expected given the incorrect upstream input from PCR-GLOBWB. When this input is correct, as is the case with

the adjusted 2-way coupled model, the resulting discharge looks very similar to that of the stand-alone D-Flow FM model. Since that model uses the same discharge input for the Niger and Bani rivers, but does not include any other sources (i.e. precipitation and discharge from smaller streams) or any loss factors, this implies that the input from other sources is roughly equal to the accounted losses. For this model, these losses include the evaporation of flooded water, as well as the evapotranspiration from the soil stores and infiltration of precipitation.

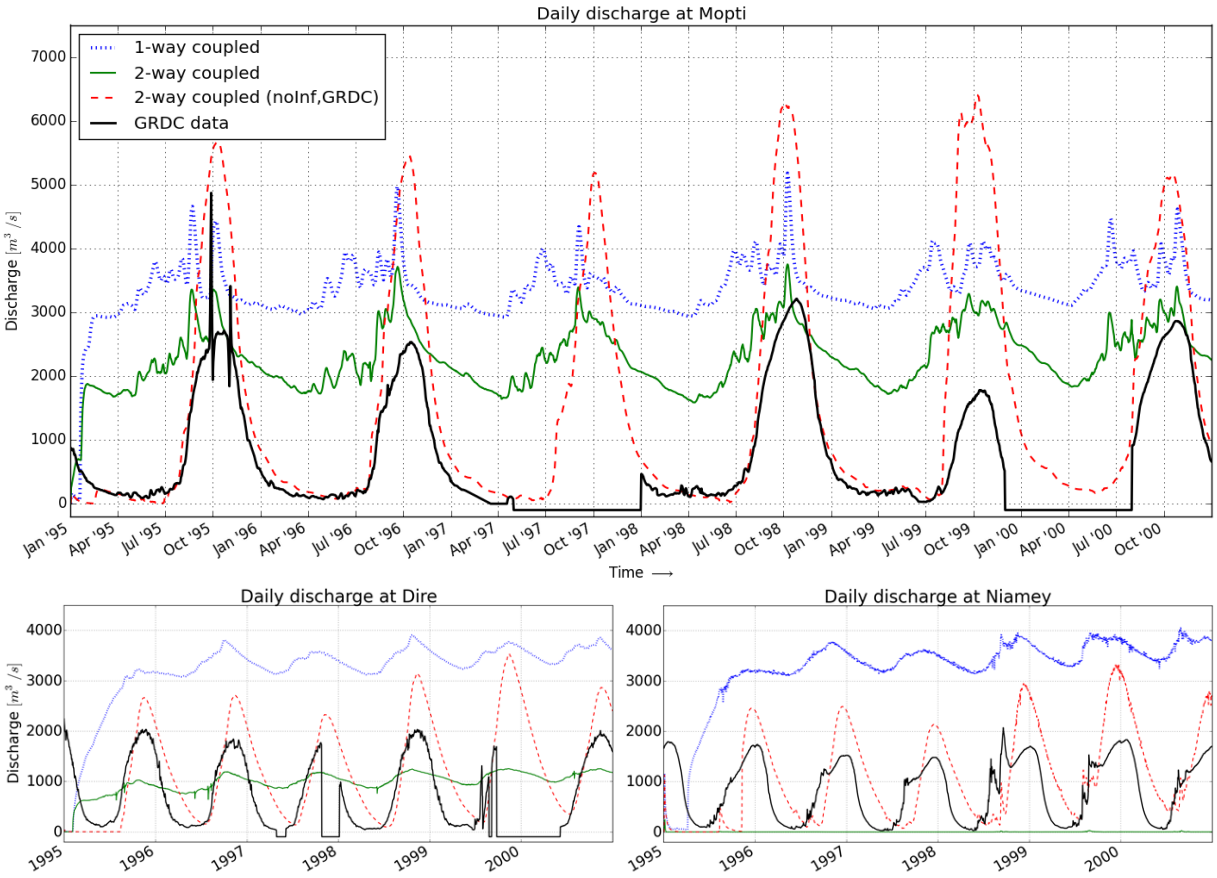

Figure 40: Discharge as modelled by the 1-way coupled model, 2-way coupled model and adjusted 2-way coupled model (without infiltration of flooded water and with upstream GRDC data) for the period 1995-2000 at the stations of Mopti, Dire and Niamey. All models use PCR-GLOBWB at 30 arcmin resolution and the accuTravelTime routing method. Observed discharge of the GRDC is included as well (with missing data, present at Mopti and Dire, assigned a value of -99).

The hydrograph at Dire shows a more substantial difference between the 1-way and 2-way coupled models. The 1-way coupled model gives a severe overestimation of discharge, as any output from PCR-GLOBWB is added to D-Flow FM, while no subsequent losses are taken into account. The 2-way coupled model on the other hand shows the influence of including these losses, with substantially lower discharge values than seen at Mopti. The hydrograph also appears a lot smoother compared to Mopti, without any of the small peaks that were still present there. This must at least partially be caused by the model's representation of the Inner Delta, because this smoothing is also seen in the 1-way coupled model. Inundation of floodplains and the flow into lakes attenuates the flow, reducing many of the small peaks. In the 2-way coupled model, the water on the floodplains and in the lakes is subjected to infiltration and evaporation, which reduces the total volume of the discharge. However, the model seems to be unable to properly simulate the seasonality of the observed values, as the difference between the minimum and maximum discharge is relatively small. The maximum discharge is less than that of the observed values, even though it was larger at Mopti. Minimum flow on the other hand is a lot higher than that of the observed values. This large change in the

hydrograph between Mopti and Dire is not seen with the adjusted 2-way coupled, which implies that this effect is probably caused by the infiltration of water on the floodplains. Infiltrated water can eventually reach the groundwater, and as such, if infiltration is high, peak flows will be reduced while the increase in the groundwater store can lead to a higher baseflow, increasing minimum discharge. It also seems like the average discharge of the standard 2-way coupled model is gradually increasing, although this increase is very small. This could also be related to a baseflow that is still increasing.

The hydrograph of the adjusted 2-way coupled model is relatively similar to that of the stand-alone D-Flow FM model, while there is a lot of inundation taking place between Mopti and Dire. This implies that evaporation of flooded water alone is again roughly equal to the additional input from other sources than upstream discharge and might not able to account for the loss of discharge that should be occurring between these stations. However, as described above, when the infiltration of flooded water is included as well, this leads to a too large reduction of peak discharge and increase of minimum discharge. This could imply that both of these processes are not accurately modelled.

The hydrographs at Niamey show that the discharge of the adjusted 2-way coupled model is still relatively similar to that of the stand-alone D-Flow FM model, although the coupled model seems to be better able to replicate some of the smaller peaks seen in the observed values. This means that these are most likely related to hydrological processes and not to the flow through the Inner Delta itself. The discharge of the standard 2-way coupled model has been reduced to zero, for which floodplain infiltration between Dire and Niamey should somehow be responsible. However, this process does not affect water within the river channel, as this is not subjected to the hydrological processes that are occurring on the floodplains. The relevant processes of riverbed infiltration and evaporation from water bodies are also not large enough to account for the complete removal of discharge between Dire and Niamey. An investigation of the D-Flow FM grid at this section reveals that the smoothing and burning algorithm applied on the DEM (described in paragraph 5.4 on page 43) is not able to properly adjust the flowpath at some locations. This is because the LDD used in the HAND and DEM burning algorithms assumes that water can travel diagonally between grid cells, while D-Flow FM assumes that water has to travel between cell-faces, ruling out diagonal flow (see Figure 41 below).

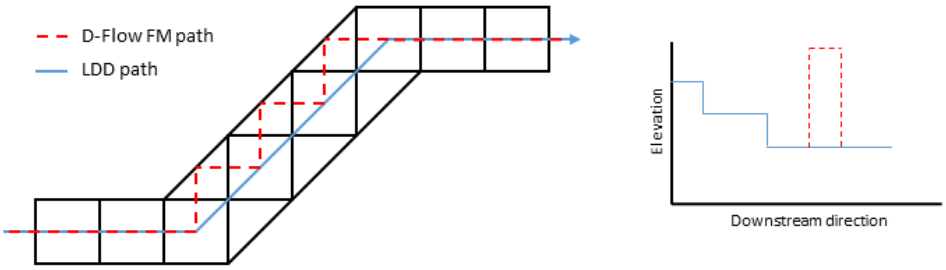

Figure 41: Example of river cells within the D-Flow FM grid, showing the downstream directions of the LDD (used by the HAND and DEM burning algorithms) and D-Flow FM, with the corresponding elevation profiles shown next to it

Therefore, at locations where the river channel is relatively narrow, represented by the width of a single cell in the D-Flow FM grid, and where it has a diagonal downstream direction, there is a discrepancy between the assumptions that created the grid and the assumptions used in the flow simulations. This results in the DEM burning algorithm only burning cells that are connected diagonally, while the flow of water has to go over cells that are missed by the burning algorithm, which will have higher elevation values and thus obstruct the flow. This leads to a similar issue as to why the burning was applied in the first place; flow obstructions can lead to upstream flooding,

which, in turn, allow floodplain infiltration and evaporation to affect water that would otherwise have remained within the channel. This is able to greatly reduce the discharge here. During peak flows some water is able to spill over the obstructions, but this is so little that it is removed by riverbed infiltration and open water evaporation before it reaches Niamey.

7.5.2 Niger Inner Delta hydrological properties

The effect of the different model setups can also be seen from the various hydrological properties within the Inner Delta that are included in Figure 42 on the next page. The inundated area (which is a summation of the area of all floodplain cells with a water depth of at least 10 cm) shows how the absence of any loss factors in the 1-way coupled model leads to a relatively constant area after its initial increase. Only a few small peaks can be detected at times of maximum discharge (around October), while there still seems to be a gradual increase over the entire time period. A somewhat similar pattern can be seen for the standard 2-way coupled model, although with a lot lower values due to the inclusion of loss factors. Only the adjusted 2-way coupled model is able to produce an inundated area with a strong seasonal character, as described in other studies (Dadson et al., 2010; Mahe et al., 2011). As described in chapter 2, there is no consensus of the total area of the Inner Delta, preventing a good comparison of the maximum flooded surface between various literature sources; Mahe et al. (2011) put this at 6,150 km^2, which would be closest to the standard 2-way coupled model, Dadson et al. (2010) state a value of 15,000 km^2, which is close to the adjusted 2-way coupled model, while Schuol et al. (2008) list it as 45,000 km^2, which is closest to the 1-way coupled model, although the difference with the latter is substantial. It should also be noted that it is un-known if these studies made a distinction between river and floodplain cells, as this study did, although it is thought to be unlikely. If river cells would be included in the calculation of the inundated area, the values shown in Figure 42 would be higher.

Looking at the graph of evapotranspiration, it can be seen that most of the time the standard 2-way coupled model has the highest values. This is to be expected, as the 1-way coupled model only contains evapotranspiration of water present in PCR-GLOBWB's soil stores, while the absence of floodplain infiltration in the adjusted 2-way coupled model causes these soil stores to contain less water compared to the standard 2-way coupled model. This can also be seen from the graph of the upper soil storage. However, the largest peaks of evapotranspiration seem to belong to the adjusted 2-way coupled model. This is most likely caused by evaporation of water within the floodplains, since this model has a much larger inundated area than the standard 2-way coupled model.

Infiltration is obviously the highest for the standard 2-way coupled model, with the large peaks being a result of the infiltration of precipitation (that is also included in the 1-way coupled model). Lower soil storage shows a difference between the adjusted 2-way coupled model and the 1-way coupled model, even though both have roughly the same infiltration values. This is probably caused by the fact that the adjusted 2-way coupled model includes evapotranspiration of surface water, which could result in an actual evapotranspiration closer to the potential evapotranspiration, limiting the amount still able to evaporate from this soil layer. Related to the high infiltration rates of the standard 2-way coupled model are its large groundwater storage and high groundwater recharge and baseflow rates. The seasonality that can be seen in so many of the other stores and fluxes is also present in these. The large baseflow values substantiate the claim made before that the relatively high minimum discharge at Dire for this model was influence by baseflow.

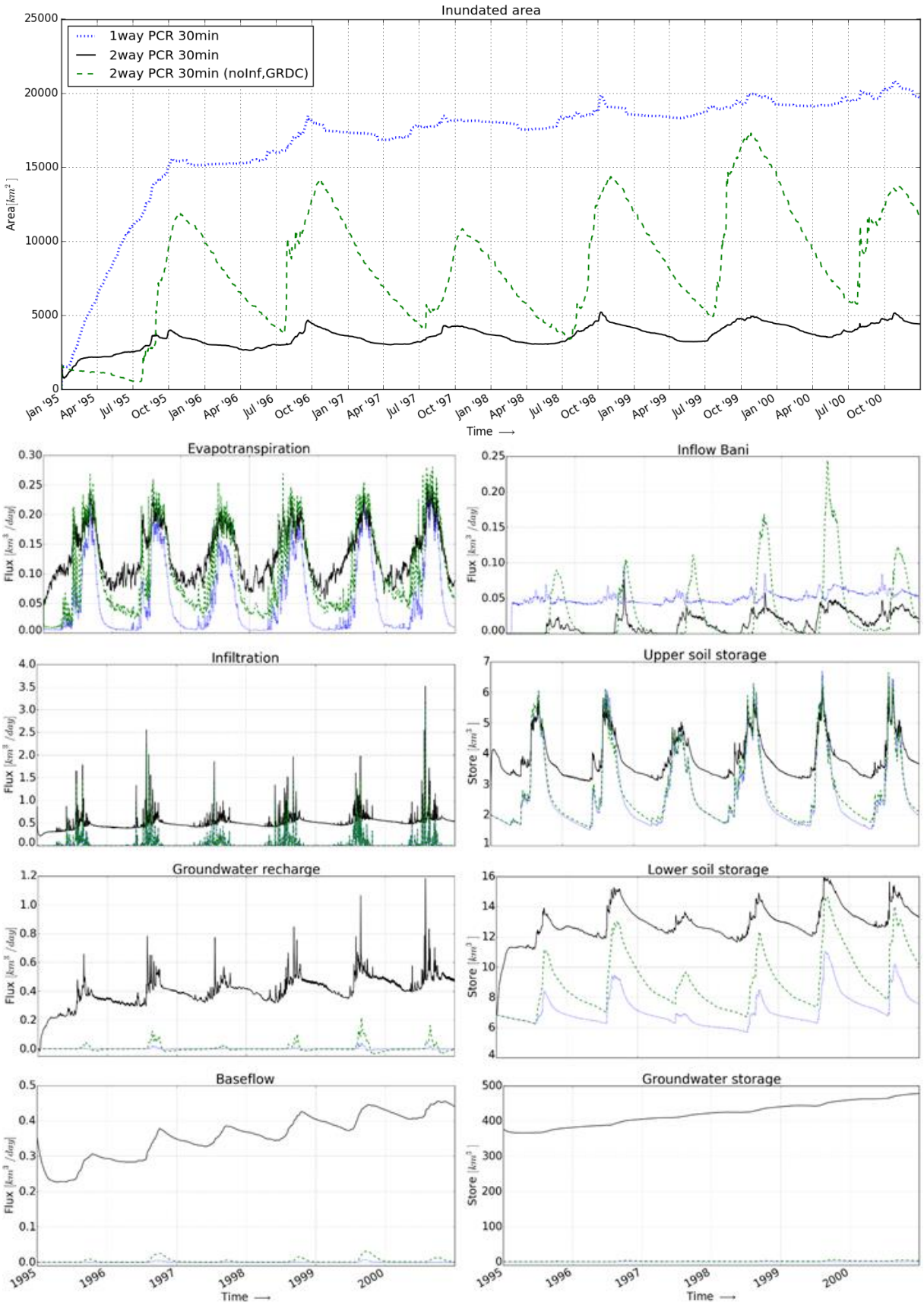

Figure 42: Information on daily values of hydrological properties within the Niger Inner Delta, as modelled by the 1-way coupled model, standard 2-way coupled model and adjusted 2-way coupled model for the period 1995-2000. All models use PCR-GLOBWB at 30 arcmin resolution and the accuTravelTime routing method.

Table 4: Total fluxes per year, averaged over the period 1995-2000

	1-way coupled		2-way coupled		2-way coupled adjusted	
	[km^3/yr]	[mm]	[km^3/yr]	[mm]	[km^3/yr]	[mm]
Inflow Niger	89	1294	70	1015	41	590
Inflow Bani	18	266	5	78	11	161
Inflow total	107	1560	75	1093	52	751
Outflow total	101	1475	16	239	37	539
Precipitation	22	317	22	317	22	317
Evapotranspiration	20	293	48	700	37	541
Infiltration	19	283	190	2763	20	284
Groundwater recharge	0	2	147	2146	2	26
Baseflow	0	2	131	1900	1	19

It can also be seen that the influence of adjusting the initial groundwater storage, as done in the standard 2-way coupled model, is relatively limited; although an initial decrease can be seen, this is followed by the constant increase already described in chapter 6. This implies that the groundwater reservoir keeps filling up, which is the reason why infiltration does not seem to slow down over time; water that infiltrates the soil layers is transported to the groundwater, which creates room for more infiltration within these layers. Finally, it is interesting to note the inflow from the Bani River, in which a clear difference between the two 2-way coupled models can be seen. This shows that there must already be some inundation occurring before the Bani reaches the cells designated as the Inner Delta and that floodplain infiltration is able to greatly reduce the discharge peaks. During low flows, the discharge of the standard 2-way coupled model is slightly higher, which is most likely related to the influence of baseflow.

For a further analysis, the yearly averaged values of all relevant fluxes within the Niger Inner Delta are shown in Table 4 above. These show that the inflow of the Bani River is relatively small compared to that of the Niger River for all models, and that the total inflow is far greater than the input from precipitation. However, as described in the analysis of results of the stand-alone PCR-GLOBWB models, precipitation seems to be underestimated compared to values listed in other studies, while the discharge is overestimated. Still, as described in chapter 2, flow from the rivers should make up the largest part of the input of water into the Inner Delta. It can also be seen that infiltration is indeed a very large flux for the standard 2-way coupled model, as are the related fluxes of groundwater recharge and baseflow. The relatively large difference between groundwater recharge and baseflow is the reason behind the large reduction in discharge seen in this model.

When comparing these values to those listed in other studies it seems evapotranspiration is still underestimated, even for the standard 2-way coupled model with the largest value (700 mm/year); Mahé et al. (2009) state an average evapotranspiration of 800 mm/year and Gourcy et al. (2000) state that this could even be as high as 2000 mm/year. On the other hand, infiltration and groundwater recharge is neglected by most other studies, as these are thought to be of no significance compared to the other fluxes. In fact, Dadson et al. (2010) state that “groundwater recharge rates are extremely low relative to rainfall and evaporation” and Neal et al. (2012) refer to UNICEF (2010) and Pedinotti et al. (2012) to state that “infiltration is believed to be negligible as

borehole surveys have found much of the delta to have a high water table throughout the year and to be underlain by an impermeable clay layer" and "although a groundwater aquifer is thought to maintain flow during the dry season, this can be <1% of the annual peak flow". Mahé et al. (2009) studied general losses from a water balance analysis over the period 1955-1996. They give an average input volume of 47.1 km^3/year, an output volume of 28.4 km^3/year and a loss of 18.7 km^3/year. It can be seen from Table 4 that the adjusted 2-way coupled model comes closest to the input and output values, although both are overestimated. If the loss is also calculated as the difference between input and output, this would give a loss of 37 km^3/year, which is roughly twice as much as the value listed by Mahé et al. (2009).

7.5.3 Performance indicators

The performance indicators for all previously described models at the stations of Mopti, Dire and Niamey are included in Table 5 on the next page. These indicate that both 2-way coupled models improved results compared to the stand-alone PCR-GLOBWB models; NSC values are closer to 1, RMSE is substantially lower, PFE is smaller and PE is closer to zero in almost all cases. However, it can also be seen that the coupled models are substantially slower than the stand-alone PCR-GLOBWB models. Interestingly, the adjusted 2-way coupled model is a lot slower than the standard 2-way coupled model, even though it does not calculates floodplain infiltration. This is related to simulations done in D-Flow FM, which will become slower if the model contains more water (as more grid cells are included in the calculations). That is also why the 1-way coupled model has the longest overall simulation time. Interestingly, it seems results are the best at Dire and they deteriorate downstream towards Niamey, which is most likely caused by the issue of flow directions within D-Flow FM and the LDD (described on page 77).

It can be seen that the 1-way coupled model has a less severe overestimation of peak flows than any of the stand-alone PCR-GLOBWB models, even though no losses of surface water are accounted for in this model. This shows the effect of the higher resolution grid of D-Flow FM, which is better able to simulate flow and inundation patterns within the Niger Inner Delta. The stand-alone D-Flow FM model performs relatively well and it even has the best overall results at Mopti. This indicates that the adjusted 2-way coupled model is not able to accurately simulate the hydrology of the area up to Mopti, as it uses the same discharge input for the Niger and Bani rivers, but does account for hydrological processes through coupling with PCR-GLOBWB. However, at Dire the two 2-way coupled models perform better and at Niamey the adjusted 2-way coupled model has the best performance. Furthermore, it can be seen that all models have a negative PE at Mopti and thus simulate peak flow too early. The relative small negative PE values for the models using upstream GRDC discharge as input could be related to the fact that no time delay is used to account for the distance between the gauging stations and the input points. Finally, even though the performance indicators of the 2-way coupled models show an improvement over the use of the stand-alone PCR-GLOBWB models, they can still not be considered to be good. Even the adjusted 2-way coupled model, which gives the best overall results, still has a negative NSC at Niamey, a relatively large RMSE and an overestimation of peak flow by almost 60%.

Table 5: Performance indicators of all models (with coupled models using PCR-GLOBWB at 30 arcmin resolution)*

Model setup	Time	Mopti		Dire		Niamey	
		NSC	RMSE	NSC	RMSE	NSC	RMSE
Stand-alone PCR 30min accuTravel	2	-6.8	2629	-14.9	2683	-17.78	2641
Stand-alone PCR 30min kinematic	4	-6.9	2645	-14.9	2682	-17.78	2641
Stand-alone PCR 5min accuTravel	4	-3.5	1997	-6.9	1891	-9.80	2002
Stand-alone PCR 5min kinematic	23	-3.5	1992	-7.0	1901	-9.77	1999
Stand-alone FM	30	-0.66	1212	-0.17	730	-1.07	878
1-way coupled	124	-6.99	2659	-15.00	2696	-18.93	2721
2-way coupled	82	-1.79	1571	0.16	618	-1.83	1024
2-way coupled adjusted	120	-1.60	1516	0.16	617	-0.46	737

Model setup	Mopti		Dire		Niamey	
	PFE	PE	PFE	PE	PFE	PE
Stand-alone PCR 30min accuTravel	128	-47	157	-37	179	-73
Stand-alone PCR 30min kinematic	175	-54	200	-47	210	-83
Stand-alone PCR 5min accuTravel	119	-6	142	-21	169	-33
Stand-alone PCR 5min kinematic	171	-17	201	-31	211	-47
Stand-alone FM	138	-5	49	10	65	14
1-way coupled	96	-44	100	-30	125	-42
2-way coupled	50	-21	36	-15	100	-93
2-way coupled adjusted	157	-10	45	10	58	11

*Time is the total simulation time [h], NSC is the Nash-Sutcliffe coefficient [-], RMSE is the root-mean-square-error [m^3/s], PFE is peak flow error [%] and PE is phase error [days].

7.6 Two-way coupled models with different PCR-GLOBWB resolution

Since the 2-way coupled model with PCR-GLOBWB at 5 arcmin resolution could not be used for the full time period, it has not been included in any of the model comparisons so far. Therefore, this paragraph will focus on that model and compare it to the same model with PCR-GLOBWB at 30 arcmin resolution to assess the influence of the different resolutions.

7.6.1 Hydrographs and performance indicators

The hydrographs for the simulated period of 1995-1997 are shown in Figure 43 and the performance indicators for the same period as listed in Table 6 on the next page. It should be noted that the first year is excluded of the calculations of the performance indicators, as was done for all the other models. Since Mopti has missing data for the year 1997 it was decided to only use the hydrological year of 1996 for these calculations, being 1996-03-30 to 1997-04-01, to allow a better comparison between stations.

The hydrographs at Mopti shows a relatively similar pattern as seen with the stand-alone PCR-GLOBWB models of different resolutions at Koulikoro (see Figure 36 on page 71). However, while the 30 arcmin versions had larger discharge values than the 5 arcmin versions there, the discharge values are more equal for the 2-way coupled models here. This shows that the reduction of discharge between Koulikoro and Mopti is larger in the 30 arcmin model than in the 5 arcmin model.

Table 6: Performance indicators for the 2-way coupled models with different PCR-GLOBWB resolutions*

Model setup	Time	Mopti		Dire		Niamey	
		NSC	RMSE	NSC	RMSE	NSC	RMSE
2-way coupled 30 arcmin	36	-2.72	1619	0.25	570	-1.63	885
2-way coupled 5 arcmin	73	-3.72	1735	-1.27	988	-0.54	677

Model setup	Mopti		Dire		Niamey	
	PFE	PE	PFE	PE	PFE	PE
2-way coupled 30 arcmin	47	-24	35	-24	100	-103
2-way coupled 5 arcmin	34	-20	0	65	65	80

* Time is the total simulation time [h], NSC is the Nash-Sutcliffe coefficient [-], RMSE is the root-mean-square-error [m^3/s], PFE is peak flow error [%] and PE is phase error [days].

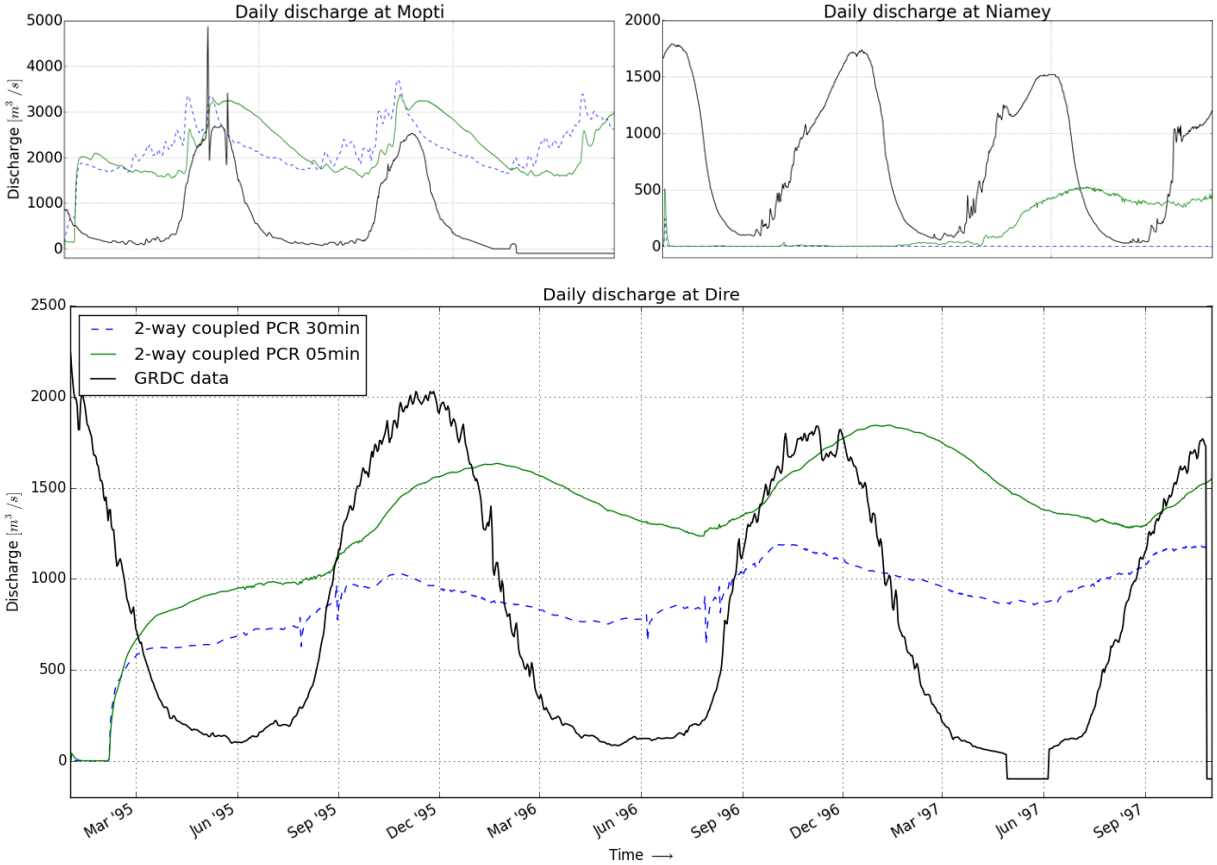

Figure 43: Discharge as modelled by the 2-way coupled model using PCR-GLOBWB at 30 arcmin and 5 arcmin resolution (both with the accuTravelTime routing method), as well as data of the GRDC (period 1995-1997) at the stations of Mopti, Dire and Niamey (with missing data, present at Mopti and Dire, assigned a value of -99)

This effect continues further into the model, so that at Dire the discharge of the 30 arcmin model is always lower than that of the 5 arcmin model. This is probably caused by two resolution-related effects. First of all, when flooding occurs, the 5 arcmin model is better able to distinguish between cells that contain inundation and those that do not. For the 30 arcmin model, even if there is only a small area of the cell covered by inundation, this will trigger the related processes of floodplain infiltration and evaporation. The sub-grid scheme described in the previous chapter does make sure that these processes are limited to the area covered by inundation, but the total storage capacity of the soil layers is much larger for a single 30 arcmin cell than for a few 5 arcmin cells. That means that

the two soil layers are able to withdraw and contain more water in the 30 arcmin model, which reduces discharge. The second resolution-related effect is caused by the assumptions of the river/floodplain scheme that handles the distribution of water between the two models; since all small cells are considered to be river cells, this includes water bodies and other low lying areas, which means that these will also receive a part of the discharge output of PCR-GLOBWB, even if they are not connected to the river channel and might be completely dry in reality. This reduces the volume of water in the river, which reduces discharge, especially if these areas are indeed not connected and the water there will simply infiltrate and evaporate. It also affects the calculation of the fraction of open water with the related processes of riverbed infiltration and open water evaporation, which in turn affect the amount of water within the river channel, potentially reducing its volume even more. This issue occurs a lot less in the 5 arcmin models, since its cells are less likely to include parts of a channel and of a water body because of its higher resolution, as is demonstrated in Figure 44 below.

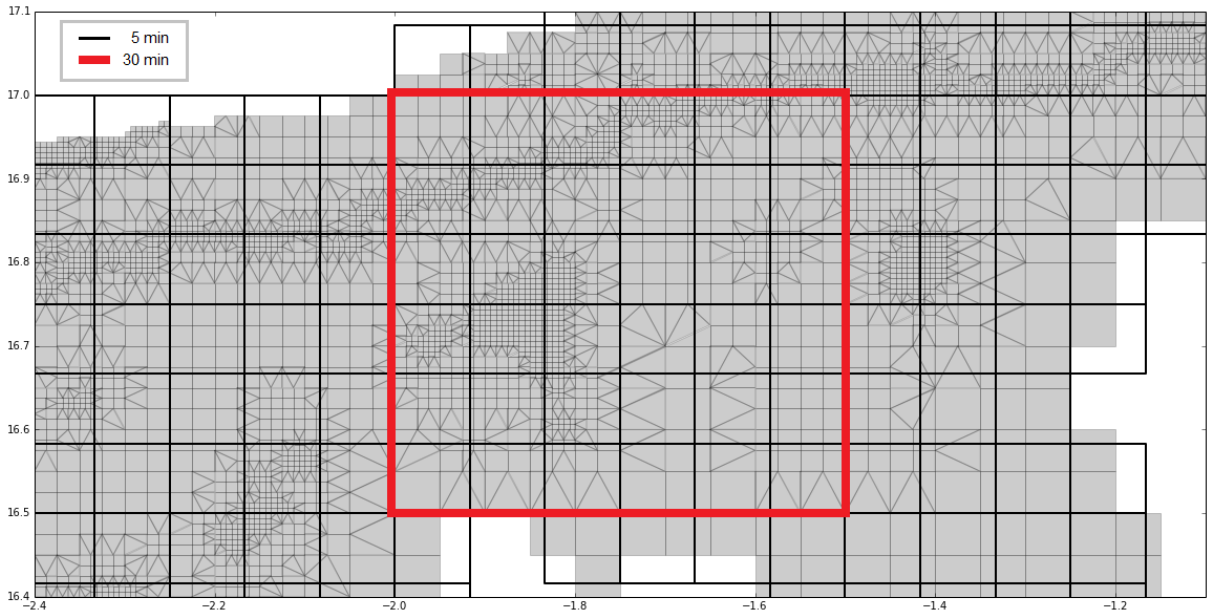

Figure 44: A section of the coupled model grid showcasing how the large PCR-GLOBWB cell of 30 arcmin includes parts of the channel and a water body, while this is not the case for the smaller cells of 5 arcmin resolution

Finally, the hydrograph at Niamey shows that the 5 arcmin model has the same problem of the 30 arcmin model in that discharge has been reduced substantially. However, there is some discharge present in the 5 arcmin model, although it is substantially lower than its values at Dire and only starts to occur during the second half of the simulated time period. The models use the same D-Flow FM grid, so the issue related to the applied stream burning is present in both models. The fact that discharge starts to occur relatively late probably implies that it is related to the resolution effect on the soil stores described above; the flooding, that occurs as a result of the obstruction to the flow due to higher elevation values, will lead to floodplain infiltration which fills up the underlying soil stores, and only when the capacity of these stores is reached and/or baseflow from the groundwater starts to increase, does the discharge increase as well.

From the performance indicators it can be seen that, regarding the NSC and RMSE, results of the 30 arcmin model are better than the 5 arcmin model at the stations of Mopti and Dire. However, peak flow seems to be better simulated with the 5 arcmin model. As can be expected from the

hydrograph, the 5 arcmin model gives the best results at Niamey. Finally, it can be seen that the 5 arcmin model took about twice as long to simulate the same time period.

7.6.2 Niger Inner Delta hydrological properties

Figure 45 below shows several relevant hydrological properties within the Inner Delta and Table 7 on the next page lists the yearly averaged values of all fluxes. It can be seen that there is indeed a difference between the two soil stores of both models, with the 30 arcmin model having higher values at all times. The same is true for the related flux of evapotranspiration, probably because it draws water from the soil stores. Infiltration on the other hand seems to be roughly the same, although the peaks of the 30 arcmin model are always higher than those of the 5 arcmin model. From the average yearly fluxes, it can be seen that the total infiltration is indeed higher for the 30 arcmin model. Baseflow shows a substantial difference between the two models, with that of the 5 arcmin model almost always having higher values even though it has a lot less groundwater storage. This probably implies that the groundwater-related fluxes are concentrated to a smaller area for this model, while they are more spread out for the 30 arcmin model. It can be seen that the groundwater storage of both models is constantly increasing, with the 30 arcmin model having an increase of roughly 15 km^3/year, while this is 10 km^3/year for the 5 arcmin model.

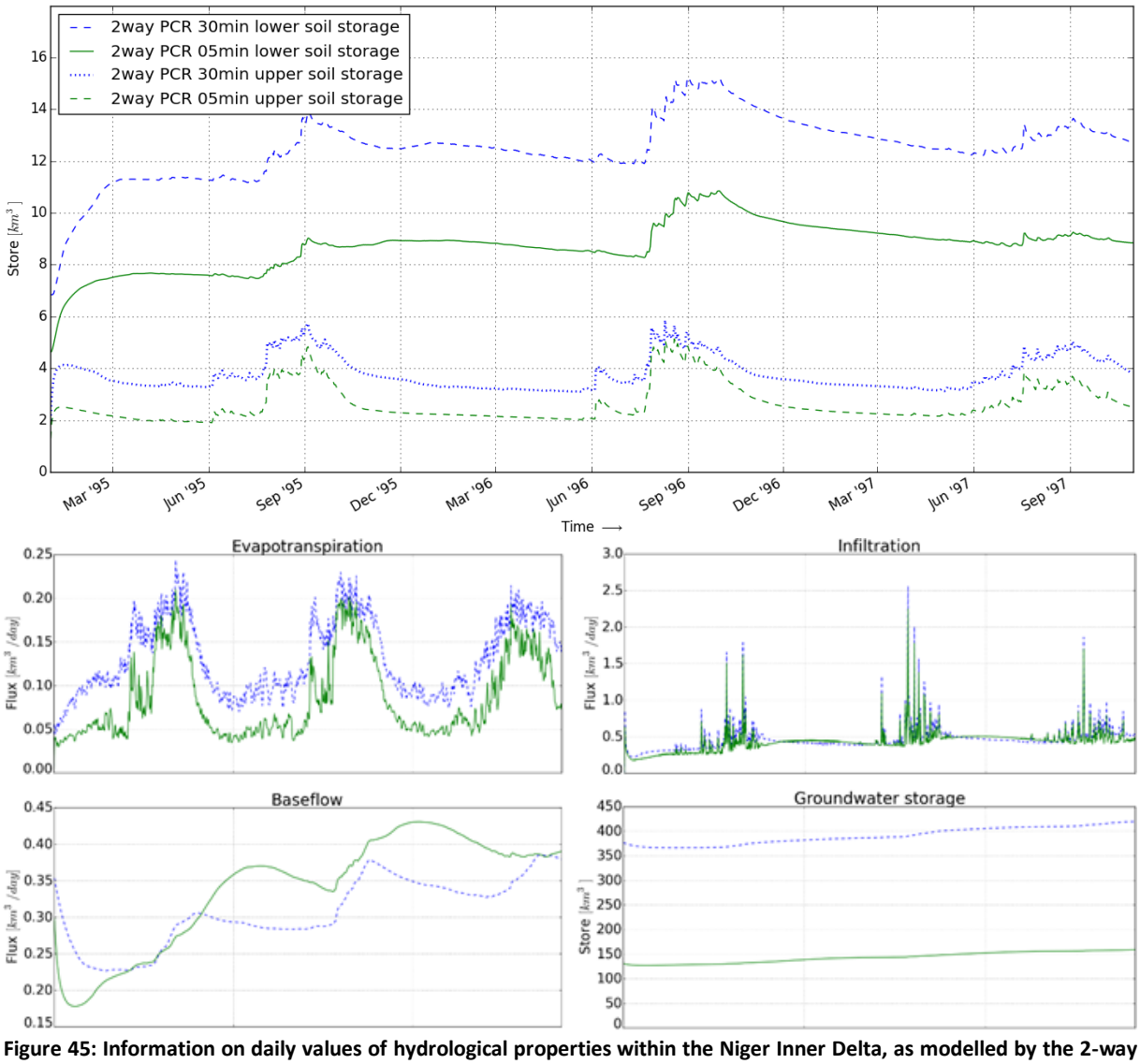

Figure 45: Information on daily values of hydrological properties within the Niger Inner Delta, as modelled by the 2-way coupled models with different PCR-GLOBWB resolutions for the period 1995-1997

Table 7: Total fluxes per year for the 2-way coupled models with different PCR-GLOBWB resolution

	2-way PCR 30min		2-way PCR 5min	
	[km^3/yr]	[mm]	[km^3/yr]	[mm]
Inflow Niger	68	995	66	1104
Inflow Bani	2	32	10	161
Inflow total	71	1027	75	1265
Outflow total	9	131	35	585
Precipitation	21	307	19	317
Evapotranspiration	48	694	31	514
Infiltration	165	2405	150	2530
Groundwater recharge	120	1748	125	2090
Baseflow	106	1541	114	1912

The initial groundwater storage is much higher for the 30 arcmin model, which also reflects the effect of the different resolutions; both initial stores were calculated from groundwater recharge rates for each individual cell (as described in paragraph 6.5.5 on page 63), with high values of groundwater recharge limited to a smaller total area for the 5 arcmin model, resulting in a smaller total volume.

The inflow of the Niger River is slightly less for the 5 arcmin model, which is most likely related to the lower discharge values at Koulikoro for this model, while that of the Bani River is larger, resulting in a larger total inflow. The discharge of the Bani River further upstream, at Douna, was also lower, which implies that there was a larger reduction within the 30 arcmin model (probably caused by the already mentioned resolution-related effects). The outflow of the Inner Delta is much larger for the 5 arcmin model, again showing the effect of the higher resolution on hydrological properties within this area.

It should be noted that some small differences between the models could also be caused by the fact that the area representing the Niger Inner Delta is slightly different for both models, as explained before and shown in Appendix C.5. This is also why, for some of the fluxes listed in Table 7, the value in km^3/year can be larger for one model while the same value in mm is larger for the other model.

7.6.3 Inundated area

As a final comparison between the models, water levels within a section of the Inner Delta are shown for two different dates in Figure 46 on the next page. This also serves as an indication of the inundated area. The chosen dates are thought to best reflect the dry and wet season, although it can be seen from the hydrographs at the station of Dire (which is located just north of this image) that the timing of the peak flow is different between models and that the peak flow of the 5 arcmin model occurs some time later (around February). This means that the image of this model for October might show water levels that are lower than those seen during the actual peak flow.

It can also be seen that the differences between the dry and wet season are relatively small for both models. This is probably caused by the fact the models are not able to replicate the extreme seasonality of the discharge with very low minimum flows and high peak flows. One other factor might be that the conveyance of the channel is underestimated as a result of the relatively simple DEM burning algorithm, so that water is not draining as quickly as it would in reality, resulting in longer lasting inundation.

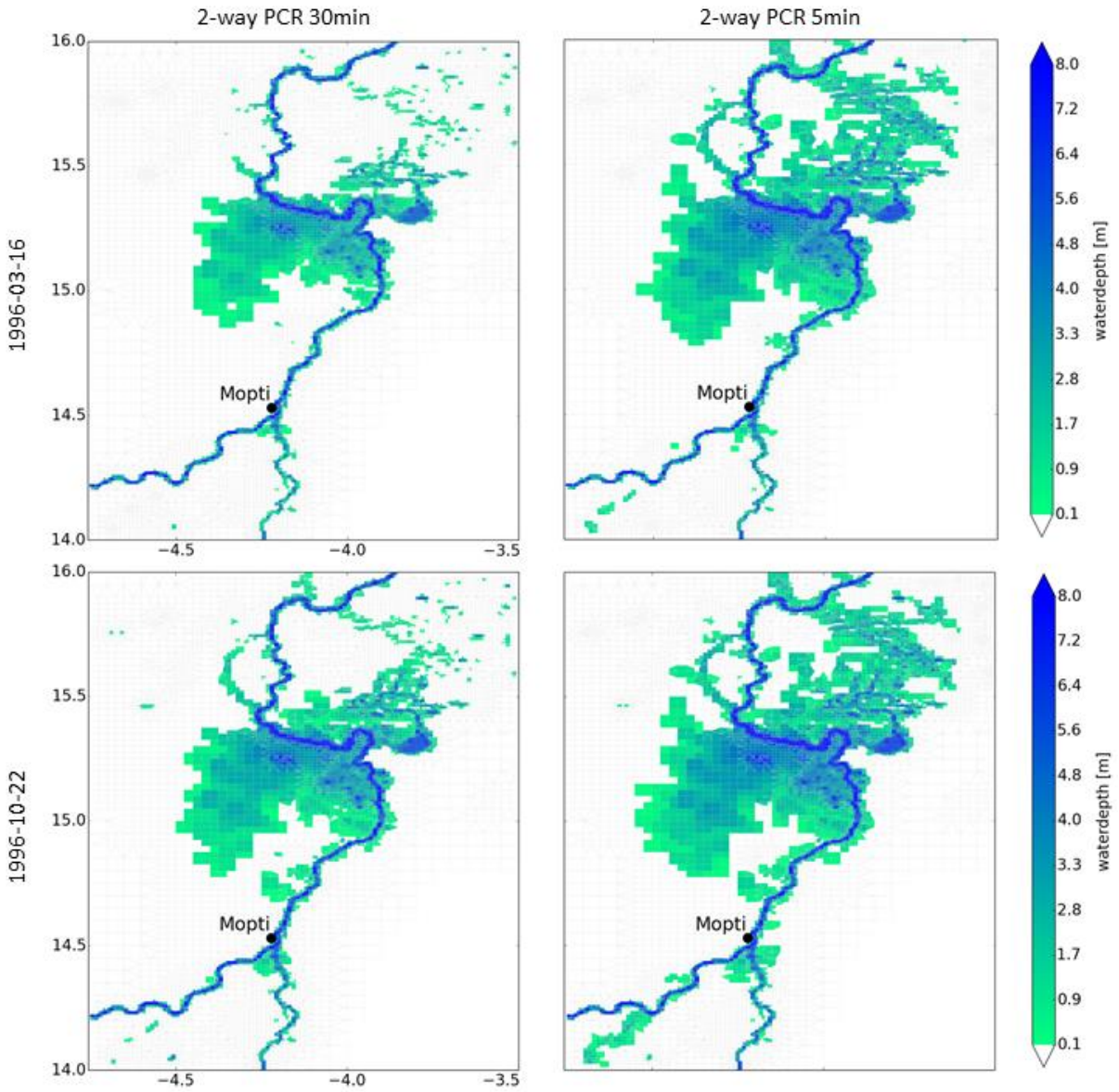

Figure 46: Water levels within the Niger Inner Delta, simulated by the 2-way coupled model with PCR-GLOBWB at 30 and 5 arcmin resolution.

The largest differences in modelled inundation between the dry and wet season are not occurring within the already large inundated area, but instead take place north of this area and around Mopti. It can also be seen that, in the 30 arcmin model, one of the side-channels of the Niger River, that starts just northwest of the large inundated area, is becoming more active during the wet season. The low water levels in this channel reveal that the grid based on HAND and the applied stream burning did not manage to properly include this channel. Similarly, it can be seen that the channel that branches off from the Niger River before Mopti (the Diaka River, already mentioned in paragraph 5.3 on page 41 and visible in Figure 4 on page 17) is not included at all. This is related to the assumptions behind the HAND algorithm and the applied stream burning algorithm that only consider the main channel, ignoring any other channels.

8 Discussion

8.1 Model setups and assumptions

The model results described in the previous chapter depend on a lot of different factors, and by no means has a full analysis of all of these factors been included. For example, all model setups were created with default parameter settings without carrying out any sort of calibration. It can be expected that model results would improve when a calibration is carried out, as parameter values would be better suited to the specific conditions of the study area. The channel roughness coefficient especially can have a large influence on results and there are a lot of studies on the calibration of this parameter (e.g. Mason et al., 2003; Pappenberger et al., 2005). Neal et al. (2012), who also created a model for the Niger Inner Delta, used values in the range of 0.025 - 0.05 $m^{1/3}$ s^{-1}, which were set based on user experience. The default value of PCR-GLOBWB is 0.023 $m^{1/3}$ s^{-1}, while that of D-Flow FM is 0.04 $m^{1/3}$ s^{-1}, so these are close to the values used by Neal et al. (2012). And, as mentioned before, for global applications it would be hard to do a calibration for each specific river basin.

PCR-GLOBWB also allows for a lot of different settings that have not been used, such as the inclusion of irrigation-related land cover types. Since the Niger Inner Delta is used extensively for irrigation (Zwarts et al., 2006) this could be an important factor. However, one of the biggest issues of the tested two-way coupled models is the fact that modelled discharge values are too low compared to observed values and the inclusion of irrigation would probably only lead to even lower discharge values. Similarly, D-Flow FM allows for several different settings related to hydrodynamics, such as the way in which bottom levels for each cell are represented in the model grid. For this study a relatively simple approach was used in which there are no elevation differences within a cell, leading to a staircase representation of elevation, while it is also possible to assign a different elevation value to each of the cell corners. The latter would lead to a more smooth transition of elevation values and would allow D-Flow FM cells to be only partially inundated. Currently, an entire cell will be inundated as soon as some water flows there, which also influences the calculation of the inundated fraction used in the subgrid-scheme for floodplain infiltration and evaporation, as this means that larger cells will lead to larger inundated fractions. When cells can be partially inundated this could give a more realistic representation of inundation and a more accurate calculation of the inundated fraction. This approach has been tested in this study, but it was slowing down the model calculations up to the point that it became useless for the simulation of time periods larger than a few days (which is probably related to the fact that D-Flow FM needs to carry out a lot of iterations to accurately simulate the partial inundation of each individual cell).

The sub-grid scheme using the inundated fraction has one other issue, and although its influence is thought to be relatively small its true influence is unknown; the fraction is static (i.e. it cannot change within a timestep), because water on the floodplains is spread out over the inundated area within PCR-GLOBWB and the model calculates everything on a set daily timestep. In reality the infiltration and evaporation of relatively small puddles could reduce the fraction during the day, which would lead to lower overall infiltration and evaporation values. However, implementing this in the model would require a lot of adjustments to PCR-GLOBWB's source code, as the model is designed to calculate all hydrological properties using a single daily timestep. On a side note, such a scheme, in which the two coupled models can influence each other during their own timestep, could be seen as 'strong two-way coupling', which is explained in more detail in Vaasen et al. (2010). While strong

two-way coupling could be seen as more realistic, it will affect model calculation speed as it requires iterations within the model timesteps.

As was already mentioned before, the method that is used to create the grid of D-Flow FM depends on a LDD map. The often used D8 version of the LDD might not give a good representation of the many side-channels of the Niger River that are located within its Inner Delta, because it only recognizes a single flowpath. The application of the HAND algorithm and the model grid derived from this indeed revealed that the side-channels were not properly included. The stream burning algorithm had the same issue because it also used the D8 LDD, only correcting elevation values within the main river channel. The exclusion of the side-channels affects the ability of the river system to transport water downstream, because all of the water is forced through the main channel. During periods of high flow, this means that flooding will occur at times when the side-channels would have become more active in reality. As such, the D-Flow FM grid used in this study will lead to a delay of discharge and an overestimation of inundation, which in turn could lead to an overestimation of evapotranspiration and infiltration. This is substantiated by the model results described in the previous chapter. It is not straightforward to fix this issue using the current model setup, as it is found in several steps of the grid creation process and it would require the application of a different type of LDD. However, another approach, being the application of a 1D channel network imbedded within the 2D model grid, might be able to overcome the aforementioned problems. A 1D channel network can be derived using other methods than a LDD and D-Flow FM is specifically designed to work with model grids that consist of both 1D and 2D elements. This would also make it easier to specify channel geometry and it would potentially allow the use of different roughness coefficients for the channel and the floodplains. There are already tools in place that could be used to help create such a network, such as the Global Width Database for Large Rivers (GWD-LR) created by Yamazaki et al. (2014). The application of a 1D network was outside the scope of this research, but it is recommended to be investigated by studies that attempt to improve the method described here. However, it should be noted that this will not affect the size of the floodplain cells near the side-channels, as those would still be derived using the HAND algorithm and could thus be relatively large. It might therefore be good to also revise, and potentially improve, the methodology behind the HAND algorithm itself.

Aside from the assumptions behind the applied stream burning method, the chosen level of burning alone will already have a substantial influence on model results and the ability of the models to replicate observed discharge values. If the resulting channel depth is less deep than the river is in reality, this will lead to an overestimation of inundation, and vice versa. The same is true for channel width, which has not been investigated in this study at all. The chosen level of burning is based only on a single report with very sparse measurements, as no other sources could be found. It also applies the same burning value on the entire stretch of the Niger River included within the D-Flow FM grid, while it is unlikely that the channel has a similar depth at all locations. This probably implies that the stream burning algorithm used in this study is too simplistic to properly set the channel geometry within the 2D model grid; aside from the fact that it only considers the main river channel, it is very likely that its dimensions are overestimated at some sections and underestimated at others, obviously influencing results in a negative way. It should also be noted that the resolution of the DEM (15 arcsec) and the smallest D-Flow FM cells (22.5 arcsec) are different. This influences the assignment of elevation values to the grid, because they cannot be assigned directly and need to be interpolated instead, which will probably amplify this issue. However, it did improve results over not

applying such a method at all (as described in paragraph 5.4 and Appendix C.2) and a thorough analysis and testing of existing stream burning methods fell outside the scope of this research. Besides, it is thought that the application of a 1D channel network has a greater potential to properly include channels and channel geometry than the use of a better stream burning algorithm.

The PCR-GLOBWB model includes a scheme for natural water bodies and reservoirs, which was found to interfere with the coupled setup and as a consequence lead to unrealistic results. Therefore, it was decided to remove the representation of water bodies in PCR-GLOBWB within the coupled cells. This makes sure that the simulation of surface water is only handled by D-Flow FM. However, it does mean that these are not properly modelled, as the applied stream burning only focussed on river channels, leaving the water bodies relatively shallow. The effect on reservoirs is more severe, as these have a regulated in- and outflow that is not included within D-Flow FM. It might be possible to include these in the coupled model, for example by splitting up the coupled grid into sections up- and downstream of a reservoir, with the reservoir itself handled by PCR-GLOBWB. This was not attempted in this study, because the reservoirs within the coupled grid are located relatively far downstream of the relevant gauging stations. The inclusion of any reservoirs is therefore unlikely to affect model results, especially given the issue of too low modelled discharge values at the most downstream station of Niamey. However, it is probably good to re-investigate the representation of water bodies in the coupled model in any future studies using the coupling setup described here.

A final note on the used D-Flow FM grid is related to the issue of narrow sections of river cells with a diagonal downstream direction, as illustrated in Figure 41 on page 77. Aside from the problems caused by the discrepancy between the assumptions of the LDD and the flow simulations of D-Flow FM, it also creates a 'staircase effect', which is a notorious issue in structured grids and is one of the reasons why the application of a curvilinear grid is thought to give a better representation of reality (Kernkamp et al., 2011). As described in chapter 4, Kernkamp et al. (2011) state that is recommended to use a curvilinear grid that follows the main flow direction whenever possible. However, it is not possible to create such a grid with the automated grid refinement method used in this study, as it does not account for flow directions. It should also be noted that, as was already stated in chapter 4, curvilinear grids can lead to unnecessarily small grid cells in the inner bends of a meandering river and might therefore not always be the best solution.

The D-Flow FM model uses adaptive timestepping for computational efficiency. However, as stated in paragraph 6.3.4 on page 54, the coupling procedure interferes with this because the model cannot advance its timestep while it is receiving output of PCR-GLOBWB, forcing the adaptive timestepping to restart at its relatively small initial value. Since the daily output of PCR-GLOBWB is divided into smaller timeslices to improve model accuracy, the adaptive timestepping has to restart relatively frequently, which impacts the total simulation time of the coupled model. This study has only carried out a brief analysis on the optimum 'update step', i.e. the timeslice at which D-Flow FM receives a part of the output of PCR-GLOBWB, making it hard to say whether the chosen update step is indeed the most ideal. If computational efficiency is a concern for future studies using this coupled model, it might be valuable to carry out a more thorough analysis on this update step.

This study attempts to use methods that could be applied at a global scale to eventually improve global flood modelling. The HAND algorithm itself could easily be applied on a DEM with global coverage, but it requires setting a threshold for the accumulated upstream area (as explained in paragraphs 4.4.3 and 5.2, as well as in Appendix A). This threshold is basin-dependent, as larger

basins will require a larger threshold value to keep the model grid relatively small, which is required to keep the coupled model computationally efficient. The same threshold applied at smaller basins could result in such a large value that no streams are identified whatsoever. This implies that the HAND threshold should either be manually set for each individual river basin, or that it should be automatically related to some of the characteristics of the river basin (e.g. basin area, river length), of which the latter is obviously favoured for global applications. It is unknown if this will give good results and it should thus be investigated before this method can be applied at a global scale.

As explained in chapter 6, it was necessary to adjust the source code of PCR-GLOBWB to facilitate the two-way coupling. This goes against one of the principles of model coupling, as it is thought to be of great value if the models can be further developed independently of each other, which is only possible if the source code is kept intact. However, it would have been impossible to create a well-functioning two-way coupled model without the changes made to PCR-GLOBWB. The code has been adjusted in such a way that it can still operate as a stand-alone model, which would make it possible to include the changes made for the two-way coupling and still proceed with the development of the model in general.

8.2 Model results

Some of the above mentioned issues can be substantiated by the model results described in the previous chapter, such as the delay of the flow due to the not properly included channels within the D-Flow FM model grid. The results also revealed some issues that have not been mentioned in this chapter yet. For example, it could be seen from the upstream hydrographs that the models overestimated discharge compared to observed values. This overestimation was still present at Mopti, implying that the used models also overestimate the total amount of water entering the Inner Delta. However, the discharge after the Inner Delta revealed a clear underestimation compared to observed values. This means that the hydrological processes within the Inner Delta are not properly included and that losses are overestimated. This could be related to a number of different factors and it is likely that a combination of these is responsible for the error in model results.

First of all, from the results of the standard two-way coupled model it could be seen that the infiltration flux was extremely high, leading to similarly high values of groundwater recharge and baseflow. These fluxes were a lot higher than those reported in other studies (e.g. Dadson et al., 2010; Mahé et al., 2009). Average yearly groundwater recharge exceeded average yearly baseflow, resulting in a constant increase of the groundwater storage. Adjusting the initial groundwater storage countered this effect for the first simulation year, but it seemed to have little to no effect afterwards. The continuous increase of groundwater storage constitutes an important loss factor of water within the Inner Delta. However, as was already stated in paragraph 7.5.2, many other studies did not include infiltration because surveys indicated that the Niger Inner Delta has a high water table throughout the year which is underlain by an impermeable clay layer (e.g. Dadson et al., 2010; Neal et al., 2012; UNICEF, 2010). If this is indeed the case, it could mean that the properties of the soil are not properly included in PCR-GLOBWB, which causes the model to overestimate infiltration and/or groundwater recharge (the latter removes water from the soil stores and thus creates room for more infiltration). Since it is also stated that baseflow makes up less than one percentage of the annual peak flow (Neal et al., 2012; Pedinotti et al., 2012), and baseflow is very high for the standard two-way coupled model, it is probably related to an overestimation of groundwater recharge. This, in turn, could be related to a capacity of the groundwater reservoir that is not properly included in PCR-

GLOBWB, allowing a continuous increase of the groundwater storage that would not be possible in reality.

While infiltration might be overestimated, it is likely that evapotranspiration is underestimated. In the adjusted two-way coupled model that did not include floodplain infiltration, discharge was relatively equal to the stand-alone D-Flow FM model. The D-Flow FM model did not include additional inputs as a result of precipitation, but many studies on the Niger Inner Delta have stated that the annual evaporation flux exceeds that of precipitation (Dadson et al., 2010; Gourcy et al., 2000; Mahé et al., 2009). The total evapotranspiration flux was also substantially less than that cited by other studies (e.g. Mahé et al., 2009), even though the inflow from the Niger River was a lot higher. This could be related to the overestimation of infiltration and groundwater recharge, which might reduce the amount of water available for evapotranspiration, but this is probably not the only reason. It was already seen in the results that the inclusion of infiltration increased evapotranspiration rates because it is able to draw water from the soil stores as well. It is more likely that it is caused by an underestimation of floodplain evaporation. This is currently using the scheme originally used to calculate the evaporation from the paddy irrigation land cover type, to minimize the changes made to PCR-GLOBWB's source code. However, this might not be a good representation of evaporation when there is a lot of inundation, as the crop factor used in the calculation of potential and actual evapotranspiration leads to an underestimation. During times of large inundation, the scheme for open water evaporation might lead to a more accurate representation of reality. However, it is important to note that the total loss of water within the Inner Delta is severely overestimated regardless of this, which poses a greater problem than the potential underestimation of evaporation and should be investigated first by studies that want to improve upon the work presented here.

One of the issues encountered during this study was the long time that was required to carry out the model simulations (see Table 5 on page 82). While the stand-alone models performed the simulation of the six year time period relatively fast (with a maximum of 30 hours for D-Flow FM), the coupled models all required at least three full days. This is partially caused by the issue with the update step within D-Flow FM, as already discussed earlier in this chapter, but the large differences between simulation times of the coupled models indicate that this is not the only reason. In fact, the one-way coupled model required the longest time of all models (124 hours), with both two-way coupled models being faster. This is probably caused by the amount of water present within D-Flow FM; to increase computational efficiency, the model employs several methods to decrease the required computations per timestep (Deltares, 2015a), which make sure that calculations are only carried out at certain cells. If there is more water within the model, this means that more cells need to be included in the calculations and the model will become slower. Since there are no losses in the one-way coupled model, this model has the largest volume of water within the D-Flow FM grid, leading to the relatively large total simulation time. The adjusted two-way coupled model comes closest to the observed discharge values, which implies that, if the model would be able to accurately replicate observed values, it would require approximately the same time as this model. Since that model still gives a relatively large overestimation of discharge, the total simulation time of an accurate model would probably be slightly less than the 120 hours of the adjusted two-way coupled model. Nonetheless, this is still a relatively long time and if this is extended to a global application it would probably not be possible to run it on a 'normal' computer. This would especially be the case for the coupled model with PCR-GLOBWB at 5 arcmin resolution, as that model was already too

computationally intensive to simulate a time period of more than 3 years for the Niger basin. It should also be noted that the D-Flow FM grid was manually adjusted to improve computational efficiency, by removing all but the most important sections. Without these manual adjustments, which might not be possible in a global application, the total simulation time will be substantially longer. This means that, in order to use the coupled setup presented in this study at the global scale, this would either require a substantial increase in computational power, a revision of the procedures and source code of the coupling functions, or a combination of these.

This study used several different performance indicators to assess overall model performance. While these make a quick and easy comparison between models possible, they should be viewed with care. For example, the NSC and RMSE of the standard two-way coupled at Niamey indicate an improvement over the stand-alone PCR-GLOBWB models, even when there is no discharge there in the coupled model. It could be argued that a relatively constant overestimation that captures the seasonality of the observed flow, as seen in the stand-alone 5 arcmin models, is still better than no discharge whatsoever. Also, a good score on a performance indicator does not necessarily mean that the model is able to accurately replicate reality, as these indicators focus on only one aspect of the model results. For instance, in the comparison of the two-way coupled models with PCR-GLOBWB at 30 and 5 arcmin resolution, it was seen that the 30 arcmin model had better NSC and RMSE values at the station of Dire. But this was caused by the severe overestimation of upstream discharge, followed by the severe overestimation of losses within the Inner Delta, which led to discharge values that came close to the average value of the observed discharge, giving relatively good NSC and RMSE values. The performance indicators downstream of this station, at Niamey, were not as good because the overestimation of losses continued and reduced discharge far below the average value of the observed discharge. This shows that the performance indicators do not reflect the reason behind a potentially good or bad score, and that these should only be used in combination with other analysis tools. It should also be noted that the observed discharge values are assumed to be 'true', even though this is not necessarily the case; the uncertainty in the observed record is expected to be relatively high, because of the uncertainty involved in measuring high flows on a wide floodplain (Dadson et al., 2010).

Given all of the above discussed issues, it could be stated that it would be easier to incorporate a flooding and inundation scheme in the stand-alone PCR-GLOBWB model than to find a solution to all of these issues. However, this would require a new approach to work around the scale-related issue discussed in the introduction (i.e. flood and inundation modelling requires a resolution higher than currently available within PCR-GLOBWB), as the downscaling method first applied under the GLOFRIS framework (e.g. Ward et al., 2013; Winsemius et al., 2013) did not lead to accurate results for the Niger River and other semi-arid regions. This method would need to be incorporated within PCR-GLOBWB to allow for dynamic feedback effects between hydrology and inundation. That is not to say that such an approach would be impossible. For example, Neal et al. (2012) showed the potential of including a sub-grid scheme in a large-scale model, although this model does have the limitations already discussed in the introduction. In the end, future studies on this subject should determine which route has the highest potential to create a well-functioning global flood model.

If we look past the desire to use this model for global flood modelling, it becomes clear that it might have potential in another field, most notably as part of a rapid setup tool (Donchyts et al., 2014; Schellekens et al., 2014). The hydrological model with global coverage and the automated procedure to create a grid for the hydrodynamical model, which also uses data with global coverage, combined

with the general applicability of the coupling scheme, make it possible to set up a coupled model for any location in the world within a relatively short time span. This can be valuable for locations that currently lack accurate modelling tools, especially in data-sparse areas.

9 Conclusions

This study has presented a first attempt at the creation of a two-way coupled model using the global hydrological model PCR-GLOBWB and the high-resolution hydrodynamical model D-Flow FM. The methodology has followed the principle that it should, in theory, be applicable on a global scale and has therefore only used freely available data with global coverage and automated methods. The model has been applied on the Niger River to test its capabilities and evaluate its performance. This allows answering of the research questions described in the introduction, which is done below.

1. *How should the hydrological model be coupled to the hydrodynamical model?*

The model grids have been coupled based on cell centers, to make sure that cells are handled in an identical manner and a D-Flow FM cell is coupled only to a single PCR-GLOBWB cell (and vice versa). The D-Flow FM grid was created using an automated procedure based on the Height Above Nearest Drainage (HAND) algorithm, which refines the grid in a way that creates the highest resolution within areas that are the most relevant for the hydrodynamic calculations. Afterwards, adjustment of properties of both models can be done within the coupled grid only, leaving the original model settings intact outside of this area. For instance, this was used to adjust the LDD of PCR-GLOBWB after its spin-up, by creating pits at the location of all coupled cells, to make sure that the flow of surface water is only calculated in the D-Flow FM model.

PCR-GLOBWB is designed to operate on a daily timestep, while D-Flow FM uses adaptive timestepping and its timestep can range from a millisecond to several hours, depending on user specified values and the flow conditions within the model. The exchange of information between models is done using the Basic Model Interface (BMI), which allows the coupling to take place independently of the models themselves. The daily output of PCR-GLOBWB is converted to smaller timeslices before it is used as input for D-Flow FM, because not doing so would negatively impact model accuracy. Since it does reduce computational efficiency (because it interferes with the adaptive timestepping of D-Flow FM), a balance was found between model accuracy and calculation speed, which resulted in a timeslice of 1800 seconds. Furthermore, accurate modelling of relevant hydrological processes was found to require a distinction between river and floodplain cells within the D-Flow FM grid, which was done based on cell sizes (with the smallest cells representing channels and water bodies as a result of the automated grid creation procedure using the HAND algorithm).

The exchange of information between models depends on several variables. For one-way coupling the output of PCR-GLOBWB that is added to D-Flow FM is discharge for river cells and runoff (plus any water remaining on top of the upper soil layer at the end of the timestep) for floodplain cells. With the two-way coupling, the exchange of information also occurs in the other direction (from D-Flow FM to PCR-GLOBWB); the volume within river cells is added to the channel storage of PCR-GLOBWB and the volume within floodplain cells is added to a newly created variable that handles inundation on the floodplains. The latter is subjected to the same processes as the original variable in PCR-GLOBWB that deals with water on top of the upper soil layer, with a sub-grid scheme to distinguish between the fractions with and without inundation. This fraction also constitutes a new variable within PCR-GLOBWB. These new variables were required to accurately include processes related to inundation; without these, the high-resolution information contained in D-Flow FM would be lost upon exchange with PCR-GLOBWB and the volume would be spread out over the much larger PCR-GLOBWB cell, resulting in an overestimation of the hydrological fluxes related to inundation.

The two-way coupling also meant that potential losses should be accounted for. This was done by calculating the difference between the volumes added from D-Flow FM to PCR-GLOBWB and vice versa (after a timestep of PCR-GLOBWB), separately for the river and floodplain cells. If the calculated difference is negative, it is removed from the current volume within the model by means of a specially designed algorithm. Finally, after testing of the coupled model, it was discovered that there was an issue related to the representation of water bodies within PCR-GLOBWB, which had a negative impact on model simulations. It was decided to remove the water bodies of PCR-GLOBWB within the coupled grid, to fix the issue and make sure that D-Flow FM is responsible for the simulation of all surface water. Due to the time constraints of the study, this issue was only briefly investigated and a better solution, in which water bodies are included, might be possible.

2. *Does the coupled model have the potential to improve the large-scale modelling of river discharge and floods, judging from results obtained by applying the model to the Niger River?*

A number of different criteria, or performance indicators, were used to assess the impact of the coupling and to see whether the coupled model is suitable for the large-scale modelling of river discharge and floods. These include the often used Nash-Sutcliffe model efficiency coefficient (NSC) and root-mean-square-error (RMSE), as well as two criteria related to the simulation of peak flows, being the peak flow error (PFE) and phase error (PE). The total time required to simulate the six year time period is also included, as this gives an indication of the model's potential to be used at a global scale. Hydrographs with daily discharge values were used to allow a visual inspection of modelled discharge. Finally, an analysis of hydrological properties within the Niger Inner Delta was carried out, to allow a better understanding of model results. This also permitted a comparison with other studies that focused on this region.

The results show that the coupled model is indeed able to simulate the inundation patterns that are occurring within the Niger Inner Delta. This inundation influences the hydrological properties in the region, such as evaporation, infiltration and groundwater storage. Two different two-way coupled models were evaluated; a standard model, which uses the coupling as described above, and an adjusted model, which did not include floodplain infiltration and used observed discharge values as input for the upstream sections of the Niger and Bani Rivers instead of PCR-GLOBWB output. The latter was done because tests indicated that infiltration might be overestimated and the stand-alone PCR-GLOBWB models were unable to accurate simulate upstream discharge. Out of all the tested models, this adjusted two-way coupled model had the best results at the most downstream location of the river that was used to assess results (i.e. the gauging station of Niamey). The model scored best on all of the performance indicators, with a NSC of -0.46, a RMSE of 737 m^3/s, a PFE of 58% and a PE of 11 days. However, since this model used observed discharge values as upstream input, it cannot be considered as a model that could potentially be used for a global application, with its results being most valuable to assess the impact of floodplain infiltration and evaporation.

The standard two-way coupled model scored less well on all of the performance indicators, but it still showed a substantial improvement over those of the stand-alone PCR-GLOBWB model. However, this also revealed that such performance indicators should be used with care, as the severe overestimation of hydrological losses in the standard two-way coupled model completely dried up the river before it could reach Niamey. Such results can of course not be seen as an improvement. On the other hand, the adjusted two-way coupled model has shown that the model coupling has a lot of potential, if all hydrological processes are accurately modelled. This probably requires a revision of

the functions used to calculate floodplain infiltration and evaporation. An analysis of the hydrological fluxes within the Inner Delta indeed revealed that infiltration, as well as the related fluxes of groundwater recharge and baseflow, were severely overestimated compared to other studies. This probably implies that the issue is at least partially caused by the overestimation of groundwater recharge, as the soil stores would not be able to accommodate high levels of infiltration without this. Other studies have stated that these fluxes should be very small, because the Niger Inner Delta has a year-round high water table underlain by an impermeable clay layer. This could also mean that these soil properties are not properly included in PCR-GLOBWB.

One other issue that has a large influence on the results is the representation of the river channels and water bodies within the D-Flow FM grid. The 2D grid was assigned elevation values from the online available HydroSHEDS DEM, which requires stream burning to create a more realistic channel geometry. This study has only carried out a brief analysis of the literature and applied a relatively simple stream burning method. It was discovered that this method did not lead to realistic results, although it did substantially improve results compared to a situation without stream burning. With the river channels and water bodies not properly included in the grid, the model underestimates the flow within the channel and overestimates the occurrence of inundation, which in turn is partially responsible for the overestimation of infiltration within the floodplains. At the same time, evapotranspiration is lower than values listed other studies, which probably implies that floodplain evaporation is underestimated by the model. Floodplain evaporation is calculated with the scheme originally used to calculate the evaporation from the paddy irrigation land cover type within PCR-GLOBWB, in order to minimize the changes made to that model's source code. When large volumes of water inundate the floodplain, evaporation is probably better modelled by a scheme for open water evaporation. Nevertheless, the overestimation of infiltration is a more important issue that should be dealt with before any issues with evaporation are considered.

Regardless of the model's ability to accurately simulate discharge and hydrological properties, the total time required to carry out its simulations is an important factor to consider for a potential global application. The model was run on a laptop with 4 GB memory and a 2.5 GHz Intel i5-2520M processor, which resulted in relatively long simulation times. The two-way coupled models required between 82 and 120 hours (3-5 days) to simulate a six year time period. These models were all run with PCR-GLOBWB at 30 arcmin resolution, as the version with 5 arcmin was too computationally intensive. If the computational restraints are ignored, the coupled model with the 5 arcmin resolution version of PCR-GLOBW (which was successfully run for a shorter time period) did show improvements over the 30 arcmin version. This is probably caused by two resolution-related effects; (1) when river channels and water bodies are present within a single PCR-GLOBWB cell, as is the case in the 30 arcmin model, discharge output of PCR-GLOBWB is added to the cells of the water bodies as well as those of the river channels, which reduces the volume of water within the channel and allows evaporation and infiltration to affect the volume within the water bodies, and (2) the soil stores of the cells of the 30 arcmin model are relatively large, allowing for a lot of infiltration, even if the cells are only partially covered by inundation (because the sub-grid scheme only affects the infiltration flux and not the storage in the soil layers), further reducing the amount of surface water. These issues are occurring a lot less in the higher resolution 5 arcmin model. This model does therefore lead to more realistic results, but its applicability is limited by computational restraints.

However, the coupled models with PCR-GLOBWB at 30 arcmin resolution already required several days to simulate a six year time period for the Niger basin, which raises the question whether such a

model can be successfully applied on a global scale. Doing so would substantially increase the computational load of the model. As such, a global version of the current coupled setup would require a relatively large increase in the used computational power, a revision of the procedures and source code of the coupling functions, or a combination of these. It is unknown what the effect of these measures will be on the computational efficiency of the model, and this makes it difficult to issue a final statement. The research objective was formulated as follows: *to determine whether the two-way coupling of a global hydrological model to a high-resolution hydrodynamical model can improve the large-scale modelling of river discharge and floods, by testing and evaluating the coupled model for the Niger River.* Based on what has been stated before, it can be said that the two-way coupled model can indeed improve the large-scale modelling of river discharge and floods, although its applicability on a global scale is uncertain. As was already briefly touched upon at the end of the previous chapter, the coupled setup might also have potential as a rapid setup tool, as it allows a complete model to be created relatively quickly for any location in the world. Regardless of its potential, a solution to the issues described here and in the rest of this work will need be found before the coupled model can be applied successfully in any domain.

In light of what has been stated before, the most important limitations of the coupled setup are:

- The automated methods used to create the D-Flow FM grid and couple this to the grid of PCR-GLOBWB still require some manual adjustments, e.g. the finding of a proper threshold value for the HAND algorithm and the adjustment of the D-Flow FM grid at narrow sections, which poses a challenge for a global application
- The BMI is a powerful tool that makes it possible to easily exchange information between models and adjust model properties for specific model setups, negating the need to adjust the model's source code
- However, the two-way coupling required adjustments to the source code of PCR-GLOBWB to accurately include hydrological processes related to floodplain inundation
- The hydrological processes related to floodplain inundation are not accurately modelled with the coupled setup, with severe overestimations of infiltration and groundwater recharge and a potential underestimation of evaporation
- The geometry of channels and water bodies is not properly included in the D-Flow FM grid and while the applied stream burning does improve results, the final results are still affected by this in a negative way
- The coupled setup poses challenges for computational efficiency, partially related to the adaptive timestepping scheme of D-Flow FM, which hinder its application on a global scale

Which lead to the following recommendations for any studies that want to improve upon the work presented in this thesis:

- Investigate the current scheme of floodplain infiltration, evaporation and groundwater recharge, and see if the functions used to calculate these fluxes can be improved
- Use a 1D network for river channels to create a better representation of river channels
- Investigate potential improvements of the computation efficiency of the coupled model

It is believed that, if these recommendations can be successfully carried out, the coupled model of PCR-GLOBWB and D-Flow FM has the potential to improve large-scale flood modelling as carried out under the GLOFRIS framework. But its application on a global scale heavily depends on the improvement of computational efficiency.

References

Literature:

Alfaya, F. A. V. S., Florenzano, T. G. & Barbosa, C. C. F. (2012). Mapping Amazon River floodplain reach with SRTM-DEM using the HAND descriptor and object based image analysis. In *Proceedings of the 4th GEOBIA* (pp. 137–140).

Akoko, E., Atekwana, E. A., Cruse, A. M., Molwalefhe, L. & Masamba, W. R. L. (2013). River-wetland interaction and carbon cycling in a semi-arid riverine system: the Okavango Delta, Botswana. *Biogeochemistry, 144*(1-3), 359-380. doi: 10.1007/s10533-012-9817-x

Ashton, A. D., Hutton, E. W. H., Kettner, A. J., Xing, F., Kallumadikal, J., Nienhuis, J. & Giosan, L. (2013). Progress in coupling models of coastline and fluvial dynamics. *Computers & Geosciences*, *53*, 21–29. doi:10.1016/j.cageo.2012.04.004

Baugh, C. A., Bates, P. D., Schumann, G. & Trigg, M. A. (2013). SRTM vegetation removal and hydrodynamic modeling accuracy. *Water Resources Research*, *49*(9), 5276–5289. doi:10.1002/wrcr.20412

Beven, K. (2001). *Rainfall-Runoff Modelling: The Primer, Second Edition.* John Wiley & Sons, Ltd. ISBN: 9780470714591. doi: 10.1002/9781119951001

Bierkens, M. F. P. & van Beek, L. P. H. (2009). Seasonal Predictability of European Discharge: NAO and Hydrological Response Time. *Journal of Hydrometeorology*, *10*(4), 953–968. doi:10.1175/2009JHM1034.1

Bourke, P. (1988). *Calculating The Area And Centroid Of A Polygon.* Available online at: http://paulbourke.net/geometry/polygonmesh/

Burston, J., Symonds, A. & Scheel, F. (2014). *Application of D-Flow FM for Storm Surge Modelling.* Poster presentation at the 2014 Ocean Sciences Meeting. Available online at: http://www.griffith.edu.au/__data/assets/pdf_file/0011/589052/Burston_DFlow_OCEANSCIENCES14_poster.pdf

Callow, J. N., Van Niel, K. P. & Boggs, G. S. (2007). How does modifying a DEM to reflect known hydrology affect subsequent terrain analysis? *Journal of Hydrology*, *332*(1-2), 30–39. doi:10.1016/j.jhydrol.2006.06.020

Candogan Yossef, N., van Beek, L. P. H., Kwadijk, J. C. J. & Bierkens, M. F. P. (2012). Assessment of the potential forecasting skill of a global hydrological model in reproducing the occurrence of monthly flow extremes. *Hydrology and Earth System Sciences*, *16*(11), 4233–4246. doi:10.5194/hess-16-4233-2012

Candogan Yossef, N., Winsemius, H., Weerts, A., Van Beek, R. & Bierkens, M. F. P. (2013). Skill of a global seasonal streamflow forecasting system, relative roles of initial conditions and meteorological forcing. *Water Resources Research*, *49*, 1–13. doi:10.1002/wrcr.20350

Casulli, V. & Walters, R. A. (2000). An unstructured, three-dimensional model based on the shallow water equations. *International Journal for Numerical Methods in Fluids, 32*, 331-348.

Casulli, V. & Zanolli, P. (2002). Semi-Implicit Numerical Modelling of Non-Hydrostatic Free-Surface Flows for Environmental Problems. *Mathematical and Computer Modelling, 36*, 1131-1149.

Chen, Y., Wilson, J. P., Zhu, Q. & Zhou, Q. (2012). Comparison of drainage-constrained methods for DEM generalization. *Computers & Geosciences*, *48*, 41–49. doi:10.1016/j.cageo.2012.05.002

Chow, V. T., Maidment, D. R. & Mays, L. W. (1988). *Applied Hydrology.* McGraw-Hill Series in Water Resources and Environmental Engineering. McGraw-Hill: New York. ISBN 0-07-010810-2.

Courant, R., Friedrichs, K. & Lewy, H. (March 1967) [1928]. On the partial difference equations of mathematical physics. *IBM Journal of Research and Development, 11*(2), 215-234. Available online at: http://www.stat.uchicago.edu/~lekheng/courses/302/classics/courant-friedrichs-lewy.pdf

Dadson, S. J., Ashpole, I., Harris, P., Davies, H. N., Clark, D. B., Blyth, E. & Taylor, C. M. (2010). Wetland inundation dynamics in a model of land surface climate: Evaluation in the Niger inland delta region. *Journal of Geophysical Research*, *115*(D23114). doi:10.1029/2010JD014474

Deltares (2015a). D-Flow Flexible Mesh. *Technical Reference Manual, draft version.* Deltares: Delft. Available online at: http://content.oss.deltares.nl/delft3d/manuals/D-Flow_FM_Technical_ Reference.pdf

Deltares (2015b). D-Flow Flexible Mesh. *User Manual, draft version.* Deltares: Delft. Available online at: http://content.oss.deltares.nl/delft3d/manuals/D-Flow_FM_User_Manual.pdf

Dietrich, J. C., Zijlema, M., Westerink, J. J., Holthuijsen, L. T., Dawson, C., Luettich, R. A., Jensen, R. E., Smith, J. M., Stelling, G. S. & Stone, G. W. (2011). Modelling hurricane waves and storm surge using integrally-coupled, scalable computations. *Coastal Engineering, 58*, 45-65.

Donchyts, G., Haag, A., Winsemius, H., Baart, F., Hut, R., Drost, N. & Van De Giesen, N. (2014). *Rapid setup of the high resolution interactive hydrological / hydraulic model for flood forecasting at global scale*. Paper presented at AGU Fall Meeting, San Francisco, USA. Available online at: http://www.researchgate.net/publication/272079997_Rapid_setup_of_the_high_resolution_interactive_hydrological__hydraulic_model_for_flood_forecasting_at_global_scale

Field, C. B., Barros, V., Stocker, T. F., Qin, D., Dokken, D., Ebi, K. L., Mastrandrea, M. D., Mach, K. J., Plattner, G.-K., Allen, S. K., Tignor, M. & Midgley, P. M. (2011). *Summary for policymakers*, in Intergovernmental Panel on Climate Change – Special Report on Managing the Risks of Extreme Events and Disasters to Advance Climate Change Adaptation. Cambridge and New York: Cambridge University Press.

Finaud-Guyot, P., Delenne, C., Guinot, V. & Llovel, C. (2011). 1D–2D coupling for river flow modeling. *Comptes Rendus Mécanique*, *339*(4), 226–234. doi:10.1016/j.crme.2011.02.001

Getirana, A. C. V, Bonnet, M., Filho, O. C. R. & Mansur, W. J. (2009). Improving hydrological information acquisition from DEM processing in floodplains. *Hydrological Processes*, *23*, 502–514. doi:10.1002/hyp.7167

Gichamo, T. Z., Popescu, I., Jonoski, A. & Solomatine, D. (2012). River cross-section extraction from the ASTER global DEM for flood modeling. *Environmental Modelling & Software*, *31*, 37–46. doi:10.1016/j.envsoft.2011.12.003

Gourcy, L., Aranyosy, J.-F., Olivry, J.-C. & Zuppi, G. M. (2000). Space and time variations in the isotopic composition (δ2H- δ18O) of Niger inland delta water (Mali). *Comptes Rendus de l'Académie des Sciences - Series II, 331*, 701-707.

Gregersen, J. B., Gijsbers, P. J. A. & Westen, S. J. P. (2007). OpenMI: Open modelling interface. *Journal of Hydroinformatics*, *9*(3), 175. doi:10.2166/hydro.2007.023

Hagemann, S. & Gates, L. D. (2003). Improving a subgrid runoff parameterization scheme for climate models by the use of high resolution data derived from satellite observations. *Climate Dynamics*, *21*(3-4), 349–359. doi:10.1007/s00382-003-0349-x

Hamon, W.R. (1963). Computation of Direct Runoff Amounts From Storm Rainfall. *Int. Assoc. Sci. Hydrol. Pub. 63*, 52-62.

Hervouet, J.M. (2007). *Hydrodynamics of Free Surface Flows: Modelling with the finite element method.* John Wiley & Sons, Ltd. ISBN: 9780470035580

Hutchinson, M.F. (1989). A new procedure for gridding elevation and stream line data with automatic removal of spurious pits. *Journal of Hydrology, 106*, 211–232.

IPCC (2012). *Managing the risks of extreme events and disasters to advance climate change adaptation: A Special Report of Working Groups I and II of the Intergovernmental Panel on Climate Change*. Cambridge: Cambridge University Press.

Karssenberg, D., Schmitz, O., Salamon, P., de Jong, K. & Bierkens, M. F. P. (2010). A software framework for construction of process-based stochastic spatio-temporal models and data assimilation. *Environmental Modelling & Software, 25*(4), 489-502. doi: 10.1016/j.envsoft.2009.10.004

Kernkamp, H. W. J., Dam, A., Stelling, G. S. & Goede, E. D. (2011). Efficient scheme for the shallow water equations on unstructured grids with application to the Continental Shelf. *Ocean Dynamics*, *61*(8), 1175–1188. doi:10.1007/s10236-011-0423-6

Kim, J., Warnock, A., Ivanov, V. Y. & Katopodes, N. D. (2012). Coupled modeling of hydrologic and hydrodynamic processes including overland and channel flow. *Advances in Water Resources*, *37*, 104–126. doi:10.1016/j.advwatres.2011.11.009

Krekeler, T. (2012). *Discharge Measurements at Niger River and its Tributaries Sota, Tinkisso and Niandan.* Report of the Bundesanstalt für Geowissenschaften und Rohstoffe (BGR), commissioned by the Bundesministerium für wirtschaftliche Zusammenarbeit und Entwicklung (BMZ). BMZ report 2009.2470.4, BGR report 05-2346.

Kuiry, S. N., Sen, D. & Bates, P. D. (2010). Coupled 1D-Quasi-2D Flood Inundation Model with Unstructured Grids. *Journal of Hydraulic Engineering*, *136*, 493–506.

Kuper, M., Mullon, C., Poncet, Y. & Benga, E. (2003). Integrated modelling of the ecosystem of the Niger river inland delta in Mali. *Ecological Modelling, 164*, 83-102.

Lane, S. N. (1998). Hydraulic modelling in hydrology and geomorphology : A review of high resolution approaches. *Hydrological Processes*, *12*, 1131–1150.

Lehner, B., Verdin, K. & Jarvis, A. (2008). New global hydrography derived from spaceborne elevation data. *Eos, Transactions, 89*(10), 93-94. Data is available at www.hydrosheds.org.

Lerat, J., Perrin, C., Andréassian, V., Loumagne, C. & Ribstein, P. (2012). Towards robust methods to couple lumped rainfall–runoff models and hydraulic models: A sensitivity analysis on the Illinois River. *Journal of Hydrology*, *418-419*, 123–135. doi:10.1016/j.jhydrol.2009.09.019

Liersch, S., Cools, J., Kone, B., Koch, H., Diallo, M., Reinhardt, J., Fournet, S., Aich, V. & Hattermann, F. F. (2013). Vulnerability of rice production in the Inner Niger Delta to water resources management under climate variability and change. *Environmental Science & Policy*, *34*, 18–33. doi:10.1016/j.envsci.2012.10.014

Loos, S., Middelkoop, H., van der Perk, M. & Van Beek, R. (2009). Large scale nutrient modelling using globally available datasets: A test for the Rhine basin. *Journal of Hydrology, 369*(3-4), 403-415.

Mahé, G., Bamba, F., Soumaguel, A., Orange, D. & Olivry, J. C. (2009). Water losses in the inner delta of the River Niger: water balance and flooded area. *Hydrological Processes*, *23*, 3157–3160. doi:10.1002/hyp.7389

Mahe, G., Orange, D., Mariko, A. & Bricquet, J. P. (2011). Estimation of the flooded area of the Inner Delta of the River Niger in Mali by hydrological balance and satellite data. In *Hydro-climatology: Variability and Change (Proceedings of symposium J-HO2 held during IUGG2011 in Melbourne, Australia, July 2011)* (pp. 138–143).

Manning, R. (1891). On the flow of water in open channels and pipes. *Transactions of the Institution of Civil Engineers of Ireland, 20*, 161-207.

Mason, D. C., Cobby, D. M., Horrit, M. S. & Bates, P. D. (2003). Floodplain friction parameterization in two-dimesional river flood models using vegetation heights derived from airbone scanning laser altimetry. *Hydrological Processes, 17*(9), 1711-1732.

Maximova, T., Vanlede, J., Plancke, Y., Verwaest, T. & Mostaert, F. (2013). *Testcase D-Flow FM: Model set-up and validation. Version 2_0.* WL Rapporten, 12_146. Flanders Hydraulics Research: Antwerp, Belgium.

Menel Lemos, G. T. (2014). *Next Generation Modelling applied to the Venice Lagoon.* Presentation at Delft Software Days 2014. Available online at http://www.slideshare.net/Delft_Software_Days/ dsdint-2014-symposium-next-generation-hydro-software-nghs-venice-lagoon-3-estuarine-giselle-menel-lemos-technital

Mohamed, Y. A., Savenije, H. H. G., Bastiaanssen, W. G. M. & Van den Hurk, B. J. J. M. (2006). New lessons on the Sudd hydrology learned from remote sensing and climate modeling. *Hydrology and Earth System Sciences, 10*(4), 507-518.

Moore, I. D., Grayson, R. B. & Ladson, A. R. (1992). Digital terrain modeling: a review of hydrological, geomorphological, and biological applications. *Hydrological Processes, 5*(1), 3-30.

Munich Re (2010). *Topics Geo, Natural catastrophes 2009: analyses, assessments, positions.* Munich: Munich Reinsurance Company. Available online at: http://www.preventionweb.net/files/ 13196_ topics2009.pdf

Nash, J. E. & Sutcliffe, J. V. (1970). River flow forecasting through conceptual models part I – a discussion of principles. *Journal of Hydrology, 10*(3), 282–290.

Neal, J., Schumann, G. & Bates, P. (2012). A subgrid channel model for simulating river hydraulics and floodplain inundation over large and data sparse areas. *Water Resources Research*, *48*(11), W11506. doi:10.1029/2012WR012514

Nobre, A. D., Cuartas, L. A., Hodnett, M., Rennó, C. D., Rodrigues, G., Silveira, A., Waterloo, M. & Saleska, S. (2011). Height Above the Nearest Drainage – a hydrologically relevant new terrain model. *Journal of Hydrology*, *404*(1-2), 13–29. doi:10.1016/j.jhydrol.2011.03.051

Nürnberg, R. (2013). *Calculating the area and centroid of a polygon in 2d.* Available online at: http://wwwf.imperial.ac.uk/~rn/centroid.pdf

O'Callaghan, J. F. & Mark, D. M. (1984). The extraction of drainage networks from digital elevation data. *Computer Vision, Graphics, and Image Processing*, *28*(3), 323–344. doi:10.1016/S0734-189X(84)80011-0

OECD (2012). *OECD Environmental Outlook to 2050: The Consequences of Inaction*. Paris: OECD. Available online at: www.oecd.org/environment/indicators-modelling-outlooks/ oecdenvironmentaloutlookto2050theconsequencesofinaction.htm

Ogilvie, A., Mahé, G., Ward, J., Serpantié, G., Lemoalle, J., Morand, P., Barbier, B., Diop, A. T., Caron, A., Namarra, R., Kaczan, D., Lukasiewicz, A., Paturel, J.-E., Liénou, G. & Clanet, J. C. (2010). Water, agriculture and poverty in the Niger River basin. *Water International*, *35*(5), 594–622. doi:10.1080/02508060.2010.515545

Olivry, J. C. (1995). Fonctionnement hydrologique de la Cuvette Lacustre du Niger et essai de modélisation de l'inondation du Delta intérieur. In Grands Bassins Fluviaux Péri-Atlantiques: Congo, Niger, Amazone, 267-280. Boulègue, J. & Olivry, J. C. (eds). INSU/CNRS/ORSTOM: Paris.

Olomoda, I. A. (2002). Impact of climatic change on river Niger. In *Proceedings of the International Workshop, Tripoli, Libya, 2-4 June 2002*.

Pappenberger, F., Beven, K., Horrit, M. & Blazkova, S. (2005). Uncertainty in the calibration of effective roughness parameters in HEC-RAS using inundation and downstream level observations. *Journal of Hydrology, 302*(1-4), 46-69.

Peckham, S. D., Hutton, E. W. H. & Norris, B. (2013). A component-based approach to integrated modeling in the geosciences: The design of CSDMS. *Computers & Geosciences*, *53*, 3–12. doi:10.1016/j.cageo.2012.04.002

Pedinotti, V., Boone, A., Decharme, B., Crétaux, J. F., Mognard, N., Panthou, G., Papa, F. & Tanimoun, B. A. (2012). Evaluation of the ISBA-TRIP continental hydrologic system over the Niger basin using in situ and satellite derived datasets. *Hydrology and Earth System Sciences*, *16*(6), 1745–1773. doi:10.5194/hess-16-1745-2012

Petrescu, A. M. R., Van Beek, L. P. H., Van Huissteden, J., Prigent, C., Sachs, T., Corradi, C. A. R., Parmentier, F. J. W. & Dolman, A. J. (2010). Modeling regional to global CH4 emissions of boreal and arctic wetlands. *Global Biogeochemical Cycles, 24*, GB4009. doi:10.1029/2009GB003610

Peyrard, D., Sauvage, S., Vervier, P., Sanchez-Perez, J. M. & Quintard, M. (2008). A coupled vertically integrated model to describe lateral exchanges between surface and subsurface in large alluvial floodplains with a fully penetrating river. *Hydrological Processes*, *22*, 4257–4273. doi:10.1002/hyp.7035

Ponce, V. M. (1991). Kinematic Wave Controversy. *Journal of Hydraulic Engineering, 117*(4), 511-525. doi: 10.1061/(ASCE)0733-9429(1991)117:4(511)

Postma L. & Hervouet, J. M. (2007). Compatibility between finite volumes and finite elements using solutions of shallow water equations for substance transport. *International Journal for Numerical Methods in Fluids, 53*(9), 1495-1507.

Rebelo, L. M., Senay, G. B. & McCartney, M. P. (2012). Flood Pulsing in the Sudd Wetland: Analysis of Seasonal Variations in Inundation and Evaporation in South Sudan. *Earth Interactions, 16*, article 1. doi: 10.1175/2011EI382.1

Rennó, C. D., Nobre, A. D., Cuartas, L. A., Soares, J. V., Hodnett, M. G., Tomasella, J. & Waterloo, M. J. (2008). HAND, a new terrain descriptor using SRTM-DEM: Mapping terra-firme rainforest environments in Amazonia. *Remote Sensing of Environment*, *112*(9), 3469–3481. doi:10.1016/j.rse.2008.03.018

Sanders, B. F. (2007). Evaluation of on-line DEMs for flood inundation modeling. *Advances in Water Resources*, *30*(8), 1831–1843. doi:10.1016/j.advwatres.2007.02.005

Schär, C. (n.d.). *The Courant-Friedrichs-Levy (CFL) Stability Criterion.* Presentation at the Institut für Atmosphäre und Klima, ETH Zürich. Available online at http://www.iac.ethz.ch/edu/courses/bachelor/vertiefung/numerical_methods_in_environmental_physics/FoI_Ch3_CFL-Criterion.pdf

Schellekens, J., Brolsma, R. J., Damh, R. J., Donchyts, G. V. & Winsemius, H. C. (2014). Rapid setup of hydrological and hydraulic models using OpenStreetMap and the SRTM derived digital elevation model. *Environmental Modelling & Software, 61*, 98-105. doi: 10.1016/j.envsoft.2014.07.006

Schuol, J., Abbaspour, K. C., Srinivasan, R. & Yang, H. (2008). Estimation of freshwater availability in the West African sub-continent using the SWAT hydrologic model. *Journal of Hydrology, 352*, 30-49.

Senay, G. B., Velpuri, N. M., Bohms, S., Demissie, Y. & Gebremichael, M. (2014). Understanding the hydrologic sources and sinks in the Nile Basin using multisource climate and remote sensing data sets. *Water Resources Research, 50*(11), 8625-8650. doi: 10.1002/2013WR015231

Singh, V. P. (1996). *Kinematic Wave Modeling in Water Resources: Surface-Water Hydrology.* John Wiley & Sons, Inc. ISBN: 0-471-10945-2

Sperna Weiland, F. C., Van Beek, L. P. H., Kwadijk, J. C. J. & Bierkens, M. F. P. (2010). The ability of a GCM-forced hydrological model to reproduce global discharge variability. *Hydrology and Earth System Sciences*, *14*(8), 1595–1621. doi:10.5194/hess-14-1595-2010

Sperna Weiland, F. C., Van Beek, L. P. H., Kwadijk, J. C. J. & Bierkens, M. F. P. (2012). Global patterns of change in discharge regimes for 2100. *Hydrology and Earth System Sciences*, *16*(4), 1047–1062. doi:10.5194/hess-16-1047-2012

Sutanudjaja, E. H., Van Beek, L. P. H., Drost, N., de Graaf, I. E. M., De Jong, K., Peßenteiner, S., Straatsma, M. W., Wada, Y., Wanders, N., Wisser, D. & Bierkens, M. F. P. (in prep.) PCR-GLOBWB 2.0: a 5 arc-minute global hydrological and water resources model. *Geoscientific Model Development Discussions*, in prep.

UNISDR (2009). *Global Assessment Report on Disaster Risk Reduction, Risk and Poverty in a Changing Climate*. Geneva: United Nations International Strategy for Disaster Reduction Secretariat. Available online at: http://www.preventionweb.net/english/hyogo/gar/report/ index.php?id=9413

UNISDR (2011). *Global Assessment Report on Disaster Risk Reduction, Revealing Risk, Redefining Development*. Geneva: United Nations International Strategy for Disaster Reduction Secretariat. Available online at: http://www.preventionweb.net/english/hyogo/gar/2011/en/home/ index.html

Vaasen, J.-M., DeVincenzo, P., Charles, H. & Benoit, L. (2010). Strong coupling algorithm to solve fluid-structure-interaction problems with a staggered approach. In *Proceedings of the 11th InternationalWS on Simulation & EGSE Facilities for Space Programmes (SESP '10)* (p. 8).

Van Beek, L. P. H. (2008). *Forcing PCR-GLOBWB with CRU data.* Available online at: http://vanbeek.geo.uu.nl/suppinfo/vanbeek2008.pdf

Van Beek, L. P. H. (2014). *Lecture notes for the course Land Surface Hydrology.* Lectures presented as part of the Master's Programme Earth Surface and Water of Utrecht University. Utrecht, the Netherlands.

Van Beek, L. P. H. & Bierkens, M. F. P. (2008). *The Global Hydrological Model PCR-GLOBWB : Conceptualization, Parameterization and Verification* (p. 53). Available online at: http://vanbeek.geo.uu.nl/suppinfo/ vanbeekbierkens2009.pdf

Van Beek, L. P. H., Wada, Y. & Bierkens, M. F. P. (2011). Global monthly water stress: 1. Water balance and water availability. *Water Resources Research*, *47*(7), W07517. doi:10.1029/2010WR009791

Van der Wegen, M. (2014). *Delft3D Flexible Mesh in the San Francisco Bay Delta system, California*. Presentation at Delft Software Days 2014. Available online at: http://www.slideshare.net/ Delft_Software_Days/dsd-int-2014-symposium-next-generation-hydro-software-nghs-san-francisco-bay-delta-estuarine-mick-van-der-wegen-deltares

Verlaan, M. (2014). *Global tide and storm-surge model with Delft3D Flexible Mesh*. Presentation at Delft Software Days 2014. Available online at: http://www.slideshare.net/Delft_Software_Days/ dsd-int-2014-symposium-next-generation-hydro-software-nghs-global-tide-model-martin-verlaan-deltares

Verwey, A., Kernkamp, H. W. J., Stelling, G. S., Tse, M. L. & Leung, W. C. (2011). Potential And Application Of Hydrodynamic Modelling On Unstructured Grids. In *Proceedings of the Sixth International Conference on Asian and Pacific Coasts (APAC 2011)* (pp. 1–8).

Visser, H., Bouwman, A., Petersen, A. & Ligtvoet, W. (2012). *Weather-Related Disasters: Past, Present and Future*. Bilthoven: PBL Netherlands Environmental Assessment Agency. Available online at: www.pbl.nl/en/publications/2012/weather-related-disasters-past-present-and-future

Wada, Y., Van Beek, L. P. H., van Kempen, C. M., Reckman, J. W. T. M., Vasak, S. & Bierkens, M. F. P. (2010). Global depletion of groundwater resources. *Geophysical Research Letters, 37*, L20402. doi:10.1029/2010GL044571

Wada, Y., Van Beek, L. P. H. & Bierkens, M. F. P. (2012). Nonsustainable groundwater sustaining irrigation: A global assessment. *Water Resources Research*, *48*, W00L06. doi:10.1029/2011WR010562

Ward, P. J., Jongman, B., Weiland, F. S., Bouwman, A., Van Beek, R., Bierkens, M. F. P., Ligtvoet, W. & Winsemius, H. C. (2013). Assessing flood risk at the global scale: model setup, results, and sensitivity. *Environmental Research Letters*, *8*(4), 044019. doi:10.1088/1748-9326/8/4/044019

Wesseling, C. G., Karssenberg, D., Burrough, P. A. & van Deursen, W. P. A. (1996). Integrating dynamic environmental models in GIS: The development of a Dynamic Modelling language. *Transactions in GIS, 1*(1), 40-48.

Westerink, J. J., Luettich, R. A., Feyen, J. C., Atkinson, J. H., Dawson, C., Powell, M. D., Dunion, J. P., Roberts, H. J., Kubatko, E. J. & Pourtaheri, H. (2008). A Basin to Channel Scale Unstructured Grid Hurricane Storm Surge Model as Implemented for Southern Louisiana. *Monthly Weather Review, 136*, 833-864.

Winsemius, H. C., Van Beek, L. P. H., Jongman, B., Ward, P. J. & Bouwman, A. (2013). A framework for global river flood risk assessments. *Hydrology and Earth System Sciences*, *17*(5), 1871–1892. doi:10.5194/hess-17-1871-2013

Yamazaki, D., Baugh, C. A., Bates, P. D., Kanae, S., Alsdorf, D. E. & Oki, T. (2012). Adjustment of a spaceborne DEM for use in floodplain hydrodynamic modeling. *Journal of Hydrology*, *436-437*, 81–91. doi:10.1016/j.jhydrol.2012.02.045

Yamazaki, D., O'Loughlin, F., Trigg, M. A., Miller, Z. F., Pavelsky, T. M. & Bates, P. D. (2014). Development of the Global Width Database for Large Rivers. *Water Resources Research*, *50*, 1–14. doi:10.1002/2013WR014664

Zhou, Q. & Liu, X. (2002). Error assessment of grid-based ow routing algorithms used in hydrological models, *16*(8), 819–842.

Zwarts, L., Beukering, P. Van, Koné, B., Wymenga, E. & Taylor, D. (2006). The Economic and Ecological Effects of Water Management Choices in the Upper Niger River: Development of Decision Support Methods. *International Journal of Water Resources Development*, *22*(1), 135–156. doi:10.1080/07900620500405874

Websites, sorted by footnote number (accessed between 01-05-2014 and 28-02-2015):

1. http://floods.wri.org/
2. http://www.wri.org/resources/maps/aqueduct-global-flood-analyzer
3. http://www.fao.org/docrep/w4347e/w4347e0i.htm
4. http://www.hydrosheds.org/
5. http://www.naturalearthdata.com/
6. http://www.bafg.de/GRDC/EN/Home/homepage_node.html
7. http://rsis.ramsar.org/ris/1365
8. http://www.wetlands.org/Portals/0/publications/Other%20publication/floodplains%20of%20IND.jpg
9. http://www.globalhydrology.nl/
10. http://pcraster.geo.uu.nl/projects/applications/pcrglobwb/
11. http://stream2.cma.gov.cn/pub/comet/HydrologyFlooding/StreamflowRoutingInternationalEdition/comet/hydro/basic_int/routing/media/graphics/flood_wave_prop.jpg
12. http://pcraster.geo.uu.nl/pcraster/4.0.2/doc/manual/_images/accu_Ldd.png
13. http://pcraster.geo.uu.nl/pcraster/4.0.2/doc/manual/op_accutraveltime.html
14. http://oss.deltares.nl/web/delft3d/d-flow-flexible-mesh
15. http://publicwiki.deltares.nl/display/nghs/Projects-Flexible+Mesh

Appendices

A HAND procedure

This appendix gives a brief description of the HAND procedure. The main report refers to this appendix in paragraph 4.4.3 on page 36.

A.1 Steps to derive a HAND map

From a hydrologically sound local drainage direction map (LDD) the accumulated area is calculated, which is in indication of how much cells are located upstream of each cell. A threshold is then used to identify stream heads, i.e. the beginning of a channel. This is visualized in Figure 47 below.

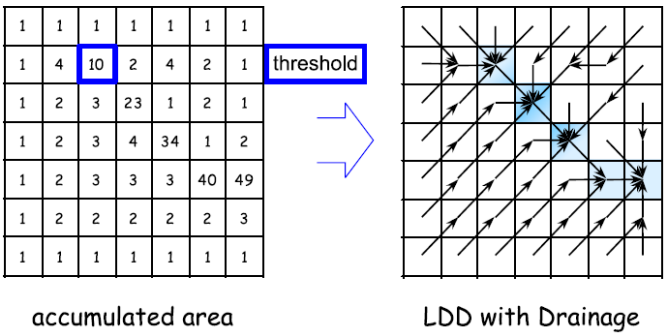

Figure 47: Accumulated area grid, generated by computing the total upslope area accumulated in each cell, and the threshold corresponding to channel initiation (Nobre et al., 2011)

The LDD and the chosen threshold together form the drainage network, indicating the location of streams and which cells are hydrologically connected to the streams, from which a flow path map can be derived. The flow path map assigns each stream cell a value, starting at zero at the most downstream cell, and assigns the same value to all non-stream cells connected to it. This is combined with the original DEM as input for the HAND algorithm, which checks the elevation differences between all cells with the same value in the flow path map. This procedure is shown in Figure 48.

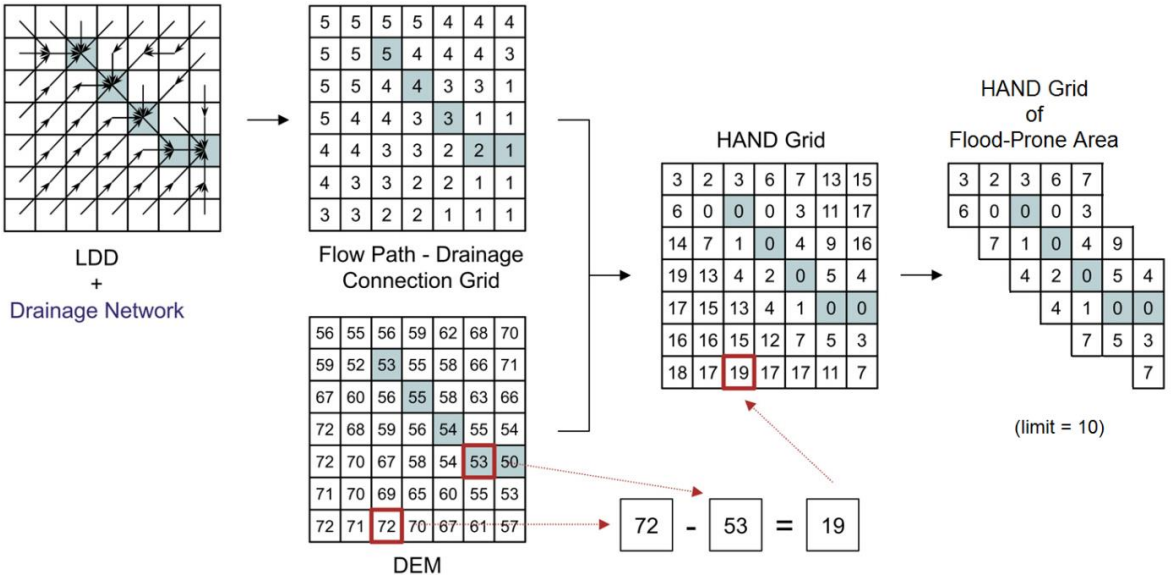

Figure 48: Procedure to calculate HAND grid [adapted from Rennó et al. (2008)]

When the HAND grid is calculated a certain limit can be imposed, removing all values above it to decrease the total size of the grid. This limits represents the water level that is thought to be never exceeded during model runs, making the cells with higher values unnecessary. This reduces file sizes and creates a more computationally efficient grid. The final grid is the HAND grid of the flood-prone area and represents channels and low-lying floodplains.

A.2 Influence of chosen threshold

The chosen threshold of the accumulated area will have a strong impact on the final HAND grid. Depending on the chosen value, large sections will either be identified as streams or not. When these are not identified as such they are considered to be a hillslope connected to another stream that was identified with the used threshold. This will give these cells a relatively high HAND value and that will result in streams not being accurately represented in the HAND grid. The threshold has therefore be determined with great care, as it should not include too much small tributaries (since one of the purposes of HAND in this study is to limit the extent of the grid of D-Flow FM), but it should include all the relevant floodplains along the major streams.

To illustrate the effect that this threshold has on the generation of the HAND grid, the HAND grid of the flood-prone area as shown in Figure 48 has been calculated again using three different threshold values. The results are shown in Figure 49 below, with the original threshold of 10 (A) and threshold values of 4, 35 and 45 (B, C and D respectively). While the flood-prone area itself does not change a lot, although it does slightly decrease in size when the threshold is increased (and vice-versa), it can be seen that the flow paths and the values of the HAND grid do change. It should be noted that this example constitutes an extremely small area when compared to the high-resolution maps of large river basins. The differences shown here will only increase when the area gets larger and the range of elevation values increases.

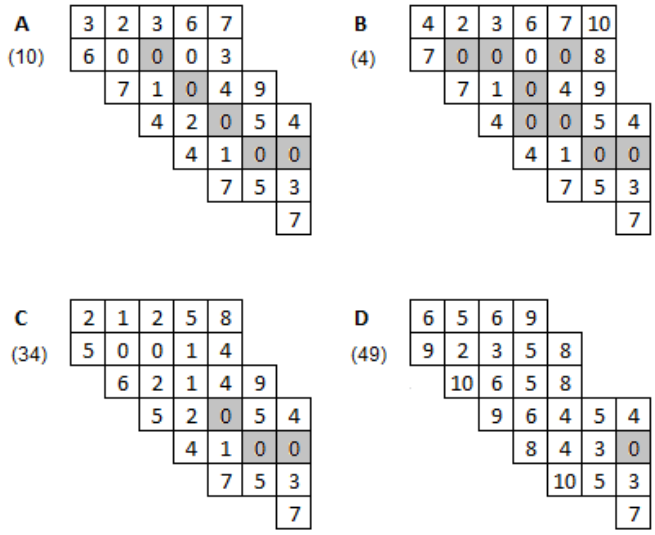

Figure 49: HAND grid with different threshold values

B Generation of D-Flow FM grid

This appendix describes the steps that were carried out to create the D-Flow FM grid used in this study. The main report refers to this appendix in paragraph 5.3 on page 42. These steps require a HAND raster file that can be loaded into D-Flow FM (which requires an .asc or .xyz format) and a shapefile of the extent of the HAND grid (.pol format to load in D-Flow FM).

Step 1: Uniform curvilinear grid

The first step is the creation of a uniform curvilinear grid that encompasses the entire study area. This can be done in the D-Flow FM GUI menu under 'operations – create uniform curvilinear grid', which requires the specification of a number of parameters. To make sure that the grid covers the study area, these were calculated from the extent of the study area. The Niger basin is located within the rectangle between the following points (using the WSG84 or EPSG4326 projection, i.e. spherical coordinates): between x-coordinates (latitudes) -11.8 and 16, and between y-coordinates (longitudes) 4.2 and 24. By dividing the total distance by the widths of the cells in the opposite direction, this gives the number of cells in their respective direction. To get a grid with square cells, the widths in both directions are assumed to be equal. The full set of parameter values used in this study is shown below, which resulted in the uniform curvilinear grid shown in Figure 50 below.

Maze type (0 for square):	0
nr of mazes x:	99
nr of mazes y:	139
maze angle:	90
maze size:	50
line thickness:	8
origin x:	-11.8
origin y:	4.2
origin z:	0
dx (for type 0 only):	0.2
dy (for type 0 only):	-0.2

Figure 50: Uniform curvilinear grid created in D-Flow FM

Step 2: load HAND file

The second step involves loading in a HAND file of the study area. This is straightforward and can be done in the menu under 'file – load samples'. The result is shown in Figure 51 below.

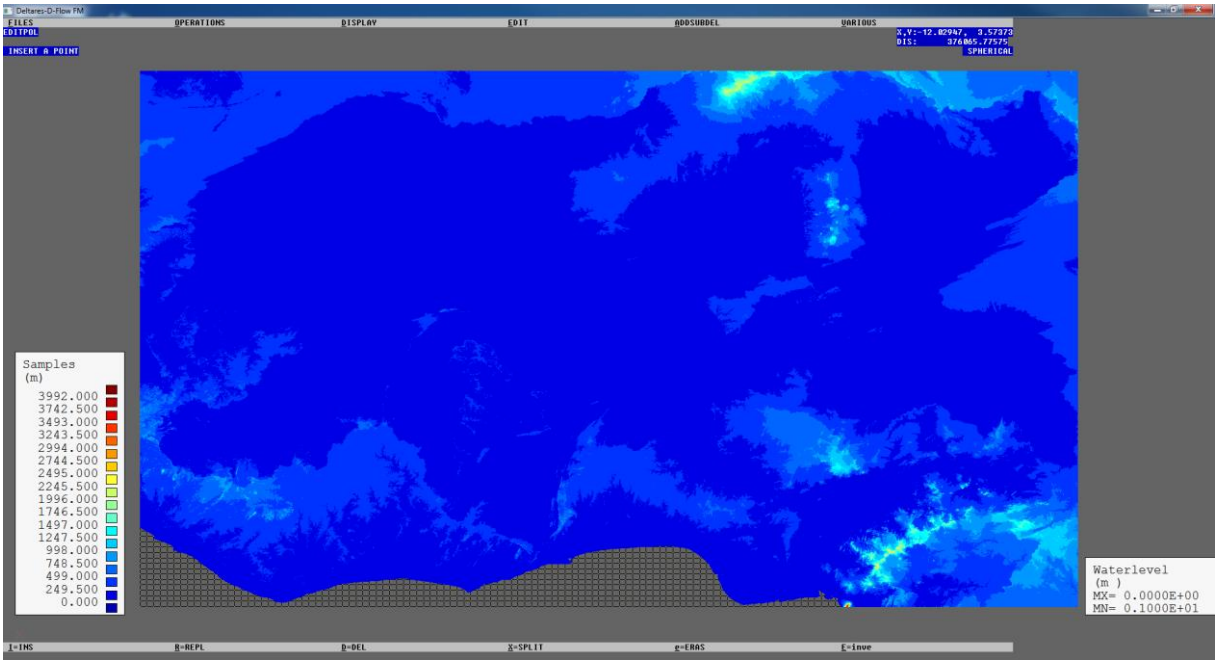

Figure 51: HAND data in D-Flow FM

Step 3: Courant-based grid refinement

This step involves the automatic refinement of the grid based on the loaded HAND data. This requires the curvilinear grid to be converted to a 'network' ('operations – convert grid to net'). The refinement process is activated in D-Flow FM's menu under 'operations – refine cells and faces factor 2', which requires the specification of a few parameters. There are two possible options; (1) ridge detection and (2) wave courant number, of which the latter is chosen. The maximum timestep is set at 600 seconds, as this is the same maximum timestep specified in the D-Flow FM configuration file. The minimum cell length, which limits the refinement to this value, is set at 450 meters, since this is the resolution of the HAND data and smaller cells would result in a grid of too many cells for efficient computations. The other two parameters are both turned off (using a value of zero), but turning them on did not seem to influence the final grid in any way. This will start the grid refinement, which will perform one iteration that refines all eligible cells by a factor two before asking the user whether to continue this process or stop. In this case, the process is continued until the specified minimum cell length is reached. This process is shown in Figure 52 on the next page.

Step 4: Obtaining the relevant area

In this step a polygon file based on the extent of the HAND grid using a certain limit (20 meters for this study, see also Figure 17 on page 39) is loaded into D-Flow FM, which is then used to remove the areas that are assumed to be irrelevant. This is done to increase computational efficiency, reduce file sizes and to make it easier to inspect results. After the polygon file has been loaded ('file – load polygon'), the network parameters have to be adjusted because otherwise it will delete the area within the polygon instead of the area outside of it. This can be done in the menu under 'various – change network parameters – select inside polygon (0/1)' and changing the value from 1 to 0. This will only affect one action before it reverts back to its default value. Now the irrelevant area can be deleted by using 'addsubdel – delete network'. The result is shown in Figure 53 on the next page.

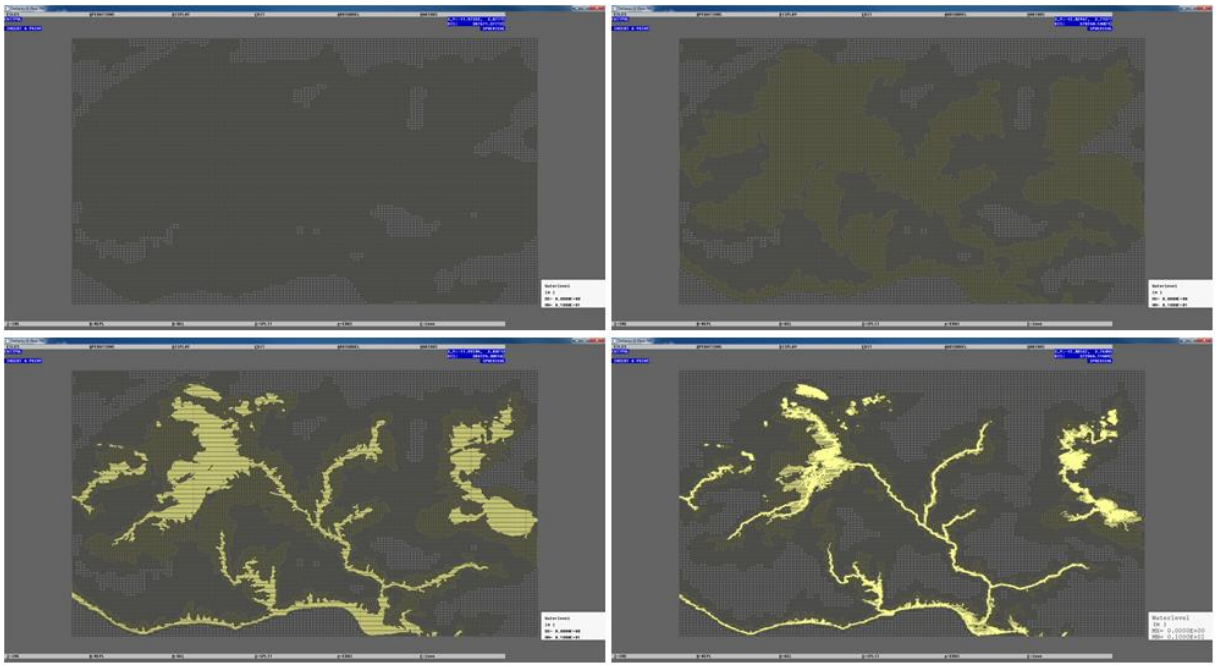

Figure 52: Courant-based grid refinement

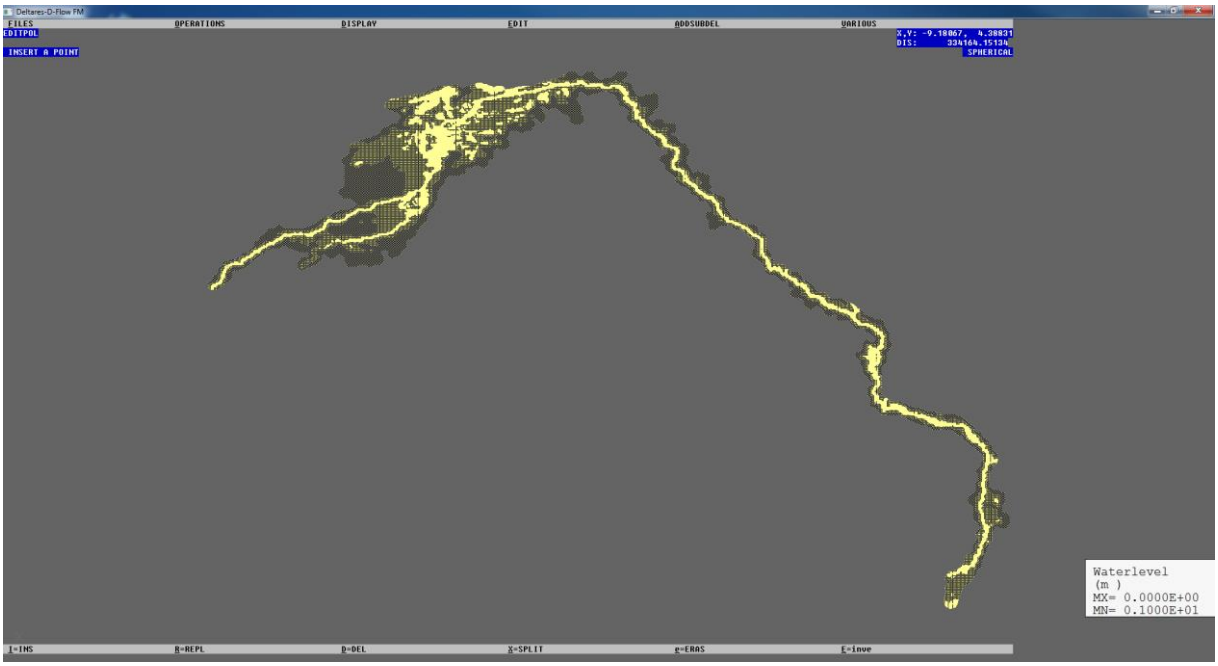

Figure 53: D-Flow FM grid of relevant area only

From the grid shown in Figure 53 above it can be seen that all tributaries of the Niger River that were present in the last step of the refinement shown in Figure 52 have been removed (with the exception of the upstream Bani River). As also explained in the main report, this was done to increase computational efficiency, as the inclusion of the tributaries was slowing down the calculation speed of the model while their effect on the results at the specified gauging stations was negligible.

Step 5: Finalizing the grid

At this stage, the grid should be inspected for any errors (e.g. unconnected cells, see also the next paragraph) and, when desired, manual corrections could be carried out. Afterwards, elevation values can be assigned and any missing elevation values should be corrected, as described in the D-Flow FM User Manual (Deltares, 2015b). When these steps are completed, the grid is ready to be used.

Side note: polygon buffer

After a first attempt to create a grid using the above described steps, it was found that this had two serious issues; (1) at some sections the polygon derived from the extent of HAND was very narrow, which would remove too many cells and (2) the irregular shape of the polygon, with a lot of small extensions from the main branch, would result in patches of cells that are no longer connected to the rest of the grid. An example of these issues is shown in Figure 54 below.

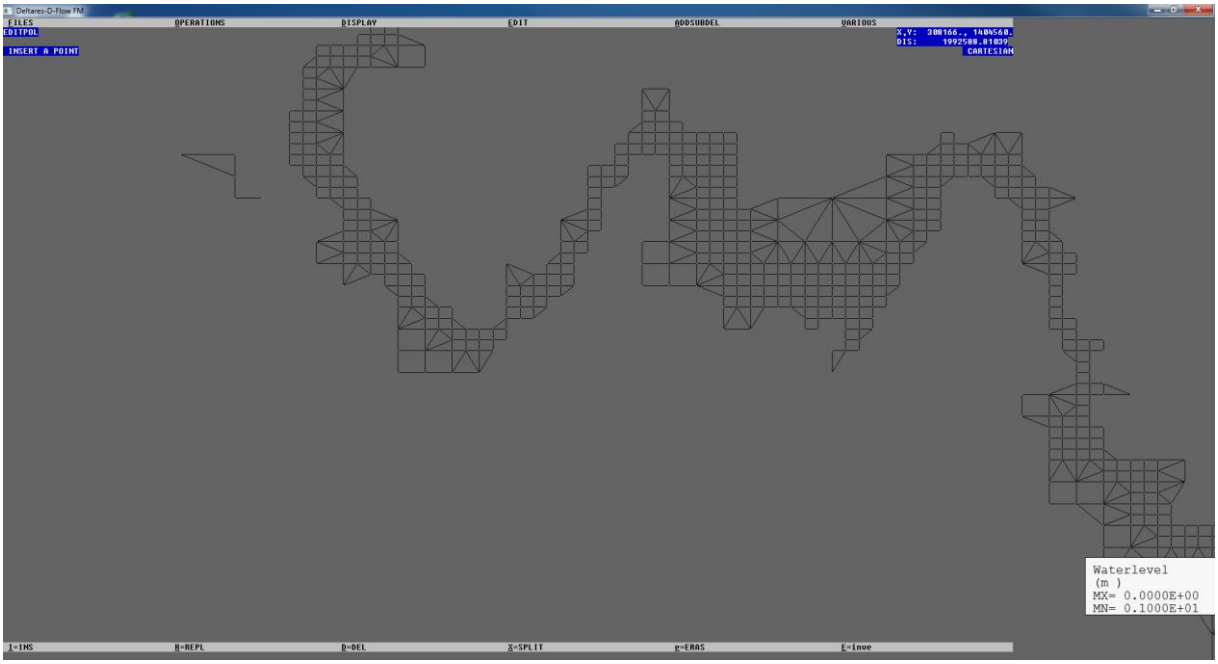

Figure 54: Section of the grid with unconnected cells and an otherwise very narrow flowpath

The first issue is probably caused by the fact that the river is very narrow at these sections in reality, with a width less than that of the used grid resolution. This could be solved by further increasing the resolution of the grid, but, as stated before, this would lead to a decrease in simulation speed. Another option would be to use a limit of the HAND grid larger than the currently used 20 meters. However, this did not solve the issue until such large values were used that the model grid had become very large, again decreasing computational efficiency. Therefore, another approach was taken to fix both of these issues; the application of a 'buffer' on the original polygon. This is visualized in Figure 55 below, with the area represented in the grid of Figure 54 highlighted by a red circle.

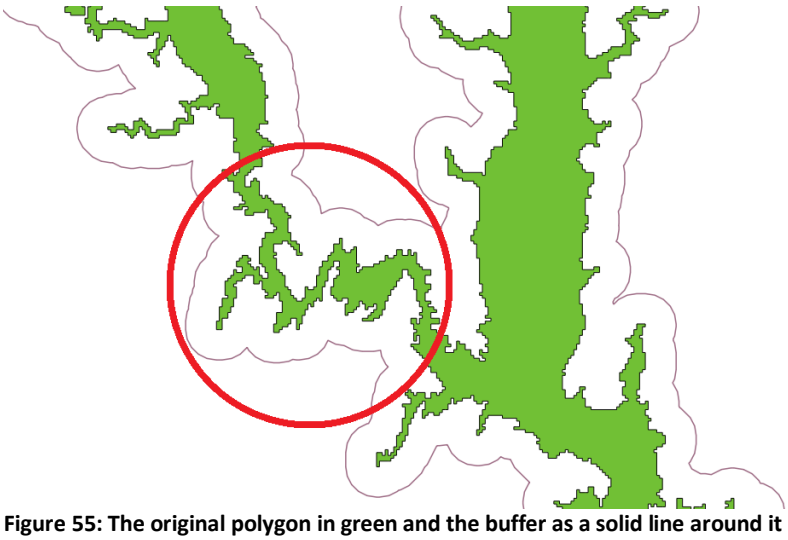

Figure 55: The original polygon in green and the buffer as a solid line around it

From Figure 55 it can be seen that the buffer not only fixes the problem of too narrow flowpaths, it also smooths out the polygon, essentially removing the small, narrow extensions. The new grid, using this buffered polygon, is shown in Figure 56 on the next page. This shows that there are no longer any loose patches of cells and the flowpath is represented in a much better way. This obviously increases the size of the total grid, but not nearly as much as a larger HAND limit would do.

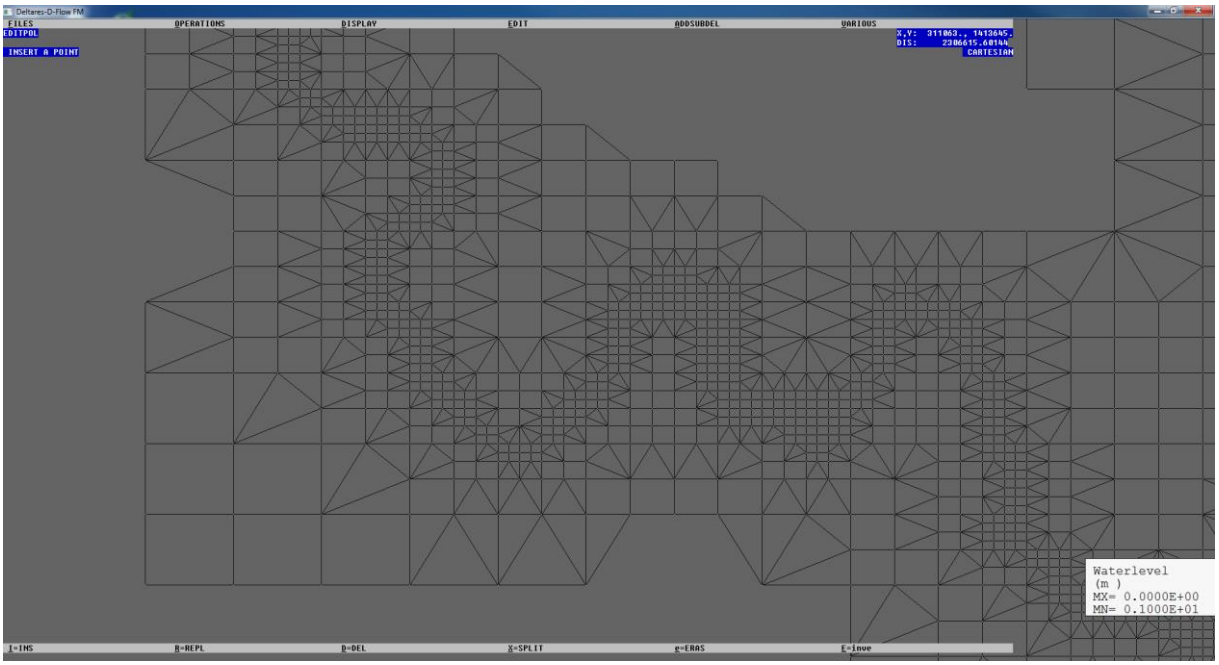

Figure 56: The same section of the grid as shown in Figure 54, after application of the buffer

C Extra information on model data and setups

This appendix includes: (1) an analysis of HydroSHEDS DEMs, (2) a test of model results without stream burning, (3) a test of the adjusted LDD of PCR-GLOBWB, (4) the method used to identify river and floodplain cells within the D-Flow FM grid, (5) the area of the Niger Inner Delta for coupled models with PCR-GLOBWB at 5 arcmin resolution and (6) the hydrograph for the station of Douna with corrected missing values. These topics are addressed at different sections of the main report, but are combined in this appendix to reduce the total number of appendices.

C.1 HydroSHEDS stream burning

This appendix briefly describes the choice for the DEM used in this study and explains why the conditioned DEM of HydroSHEDS, on which stream burning was already applied, was not used. This is done by comparing elevation profiles of three cases (a lake, a stream and floodplains) for three different DEMs; the original SRTM data at 30 arcsec resolution, the HydroSHEDS 15s non-conditioned DEM and the HydroSHEDS 3s conditioned DEM (with stream burning). The main report refers to this appendix in paragraph 5.4 on page 43.

Figure 57 below shows one of the largest lakes within the Niger basin; the Kainji Reservoir. The red line on the map represents the cross-section of which the elevation profile is shown underneath. It can be seen that the SRTM and normal, non-conditioned HydroSHEDS DEMs do have the lowest elevation within the lake, but it is relatively shallow with a depth of only 5-10 meter. The burning is clearly visible in the conditioned HydroSHEDS DEM, which gives the lake a much larger depth of approximately 20 meter. This is probably a more realistic representation.

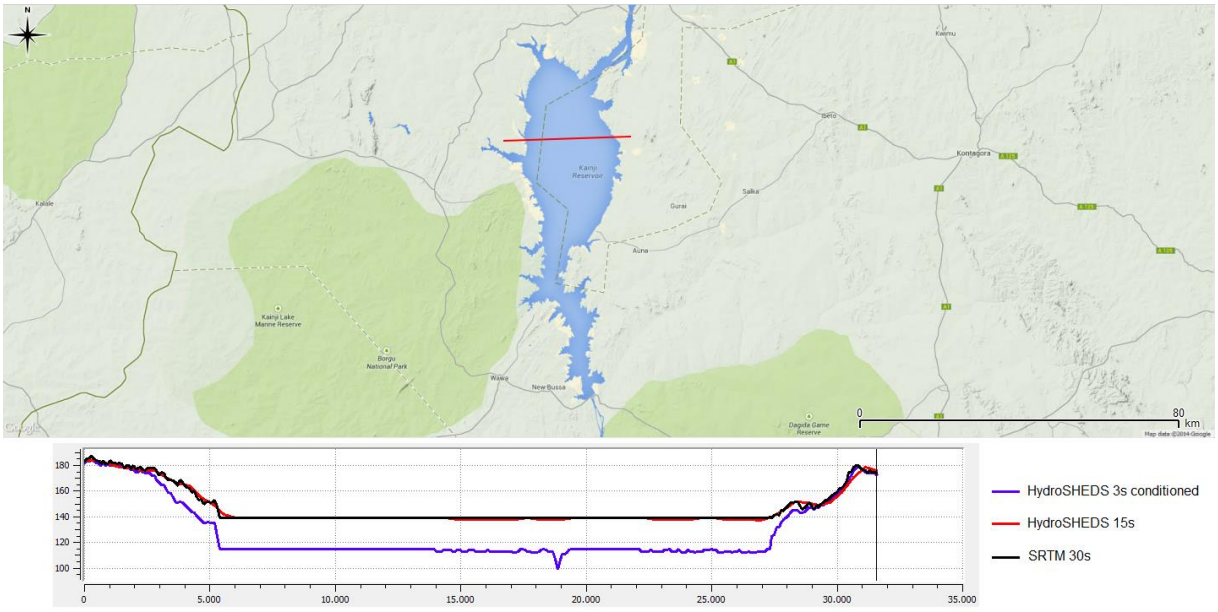

Figure 57: Elevation profile of a cross-section at the Kainji Reservoir using SRTM and HydroSHEDS DEMs

The burning of the conditioned DEM can also be seen in Figure 58 on the next page, which shows the northern section of the Niger Inner Delta between Lac Debo and Lac Fati. However, the burning carried out here resulted in a channel with a depth of roughly 40 meter. This is the main reason why this DEM was not used for this study. Channels of such depth are thought to be unrealistic and would not allow any flooding to take place. It can also be seen that the original SRTM DEM and the normal HydroSHEDS DEM have a relatively similar elevation profile, just as in the previous figure.

Figure 59 shows a section of the floodplains just north of Lac Debo in the Inner Delta. As expected, no strong burning has been carried out here. What can be seen is the strong variability of elevation values of the original SRTM DEM, with the HydroSHEDS DEM giving a more smoothed profile. This smoothed profile is the result of averaging carried out for this DEM, which is thought to decrease potential errors (Neal et al., 2012). This, combined with the factors already mentioned in the main report, led to the decision to use the non-conditioned HydroSHEDS DEM at 15 arcsec resolution for the creation of the D-Flow FM grid in this study.

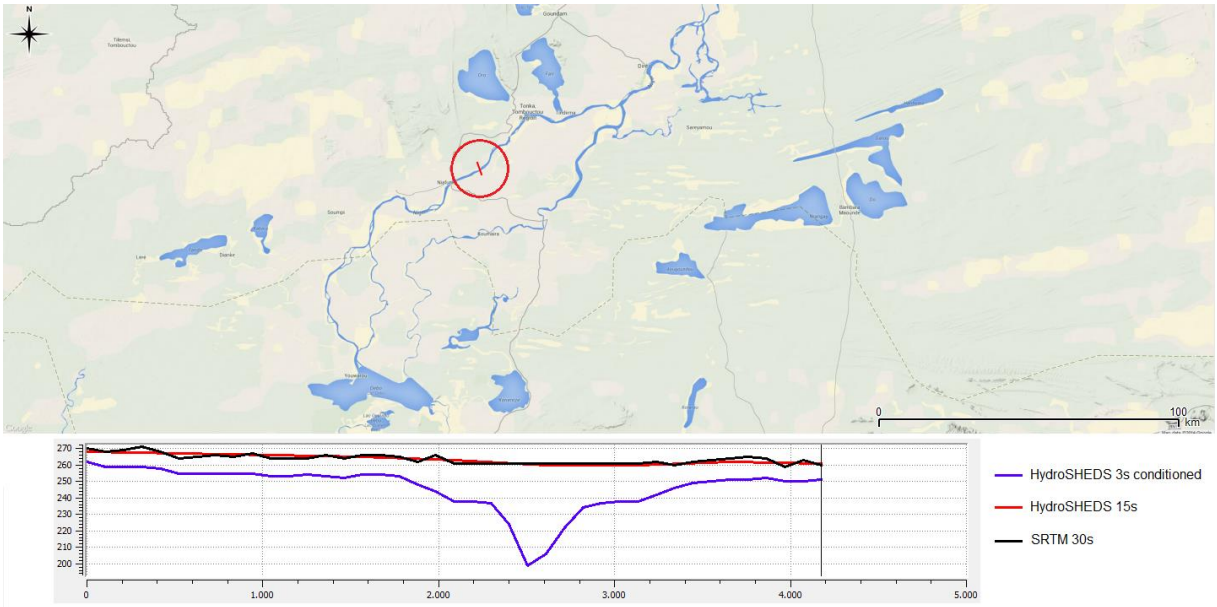

Figure 58: Elevation profile of a cross-section of a channel in the Niger Inner Delta using SRTM and HydroSHEDS DEMs

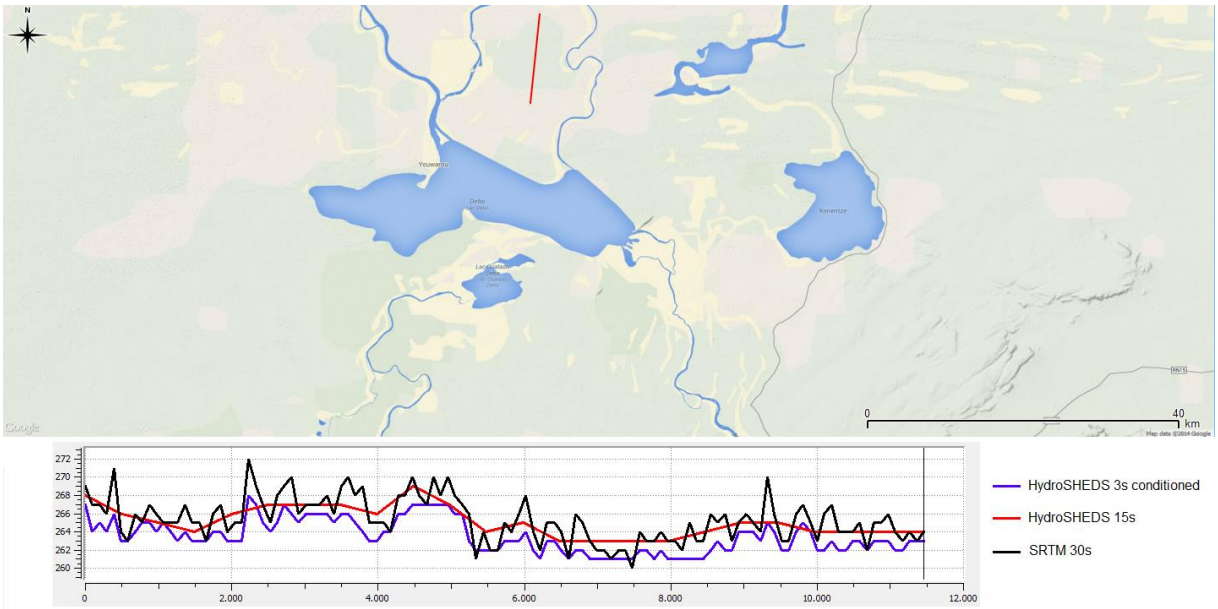

Figure 59: Elevation profile of a cross-section of floodplains in the Niger Inner Delta using SRTM and HydroSHEDS DEMs

C.2 Model results without stream burning

This appendix briefly describes the influence of using a DEM without stream burning (or any other procedure to improve the representation of channels). This is done by means of two figures showing modelled water depths at a certain date several years apart. The main report refers to this appendix in paragraph 5.4 on page 43.

Figure 60 below shows the modelled water depths in the Niger Inner Delta for the 12th of September in the years 1980 (top) and 1982 (bottom), which were obtained during tests using the time period 1979-1982. The model started without any water in the D-Flow FM model, to be able to assess how the incoming water travels through the grid. During the wet season of 1980, floods resulted in the inundation pattern shown in the image below. What can also be seen is that there is no water north of a latitude of 15.5. And this is still the case two years later, in 1982. While the water depths in some of the lakes have increased, the flow of water seems to be blocked towards the north. This resulted in a larger inundated area, as the water is forced beyond the banks of the (shallow) channel.

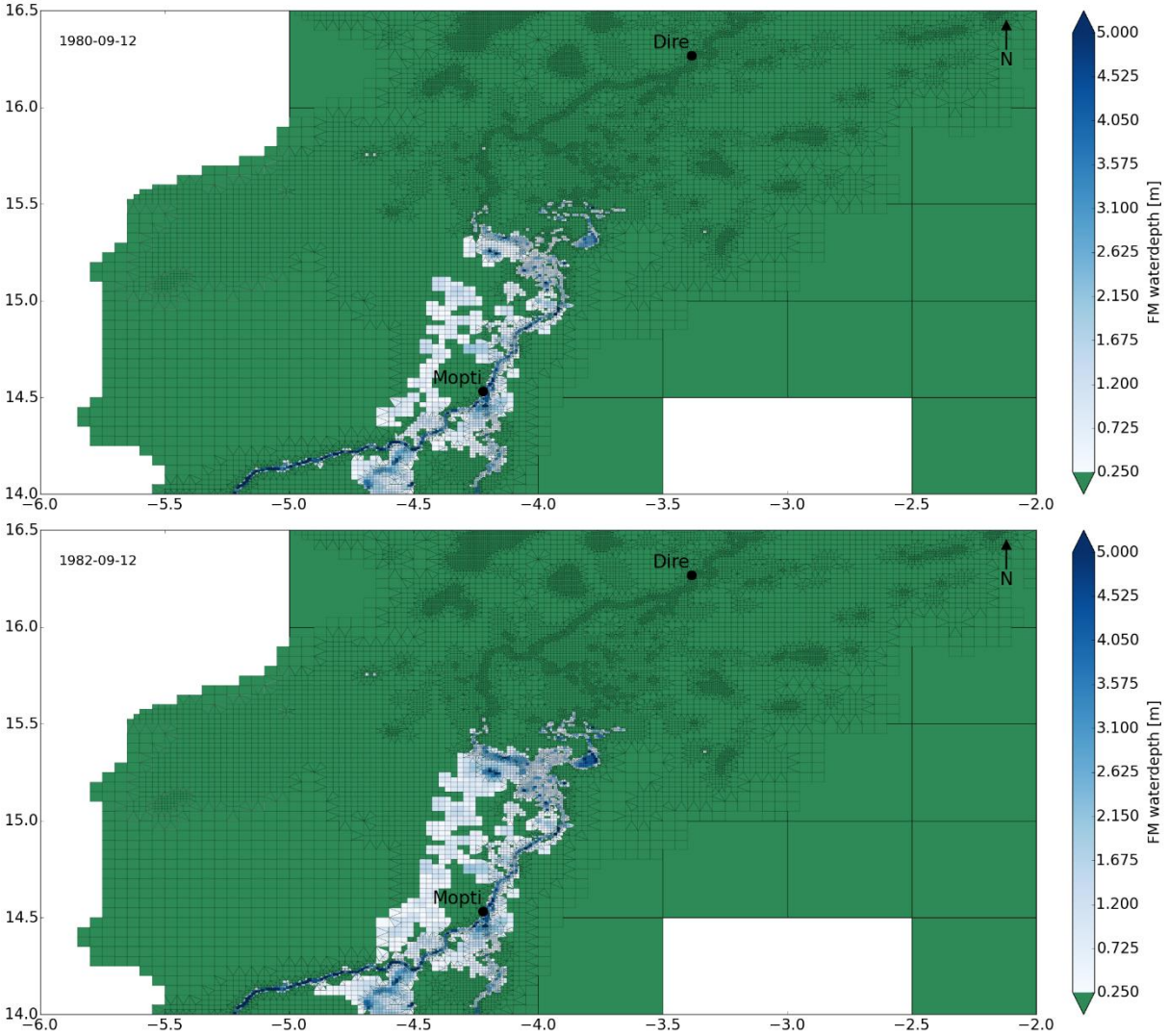

Figure 60: Water depths in the Niger Inner Delta during the wet season, modelled during a test of the two-way coupled model, for the second simulated year (top) and two years later (bottom)

This did not give major problems in the one-way coupled model, as there was no infiltration and evaporation, so when the water levels increased the flow resumed towards the north. However, in the two-way coupled model, infiltration and evaporation remove the water from the floodplains, which creates room for more water to spill over from the channel. This, in turn, will be subjected to infiltration and evaporation again, and these fluxes are apparently able to remove enough water to prevent the water from reaching the levels required to flow further towards the north. This shows the importance of having elevation values that accurately represent channels, lakes and floodplains. When stream burning is applied to the DEM, the depth of the channel increases, allowing larger water depths without flooding and thus making sure that the flow can be modelled more accurately.

C.3 Testing adjusted LDD

This appendix briefly discusses the tests carried out to make sure that the adjusted LDD functions properly. The main report refers to this appendix in paragraph 6.3.1 on page 51. Tests were carried out on the total discharge, total runoff and total amount of water within the model without any issues being discovered. The runoff itself was not changed, as can be seen from the right image of Figure 61 below (the graphs are exactly the same). The adjusted LDD did change the timing of the discharge (see left image of Figure 61), as all water in the channels now immediately flows out of the cell (since it was changed to represent a pit in the LDD). As such, the discharge now follows the pattern of the runoff. This is exactly as intended, as all surface water should be handled by the hydrodynamical model for the coupled cells, because it can simulate the flow of water more accurately.

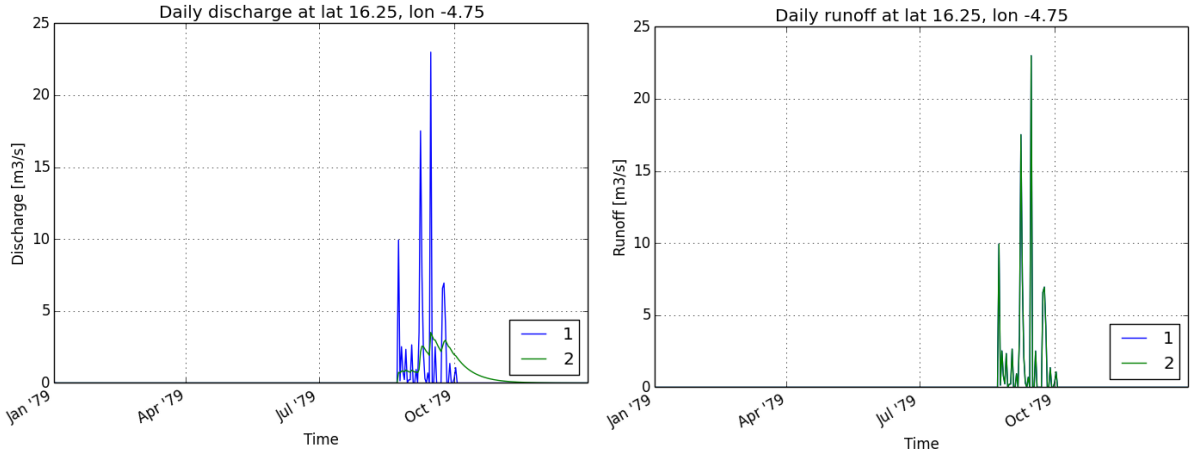

Figure 61: Modelled discharge (left) and runoff (right) using a stand-alone PCR-GLOBWB model with its LDD adjusted as described in paragraph 6.3.1 (with 1 being the adjusted LDD and 2 being the normal LDD)

C.4 Identifying river and floodplain cells

This appendix briefly describes the process of identifying river and floodplain cells within the D-Flow FM grid, as mentioned in the main report at paragraph 6.3.3 on page 53. To illustrate the process, an example cell is shown in the top image of Figure 62 on the next page.

While it might seem like the smallest cells all have the same area, this is in fact not the case. Because a spherical coordinate system is used, the cells will have a different area based on their latitude/longitude location. This means that a threshold has to be chosen that is sufficiently large to include all small cells regardless of their latitude/longitude location. However, the triangle-shaped cells will have a smaller area than some of the square-shaped cells, which results in a lot of the triangle-shaped cells to be identified as river cells, as illustrated in the bottom left image of Figure 62 on the next page. These might not necessarily represent part of the river channel or water body. To solve this issue, two separate threshold values are used; one for all square-shaped cells and another one, with a lower value, for all triangle-shaped cells. This results in the bottom right image of Figure 62, which is thought to give a better representation of channels and water bodies.

Since this reduces the total amount of river cells compared to that of the left image, this also means that there will be more floodplain cells. This will have an influence on model results, since river cells and floodplain cells are subjected to different hydrological processes in the coupled model. No tests were carried out to see if different threshold values or the removal of the cell-shape based threshold improved results.

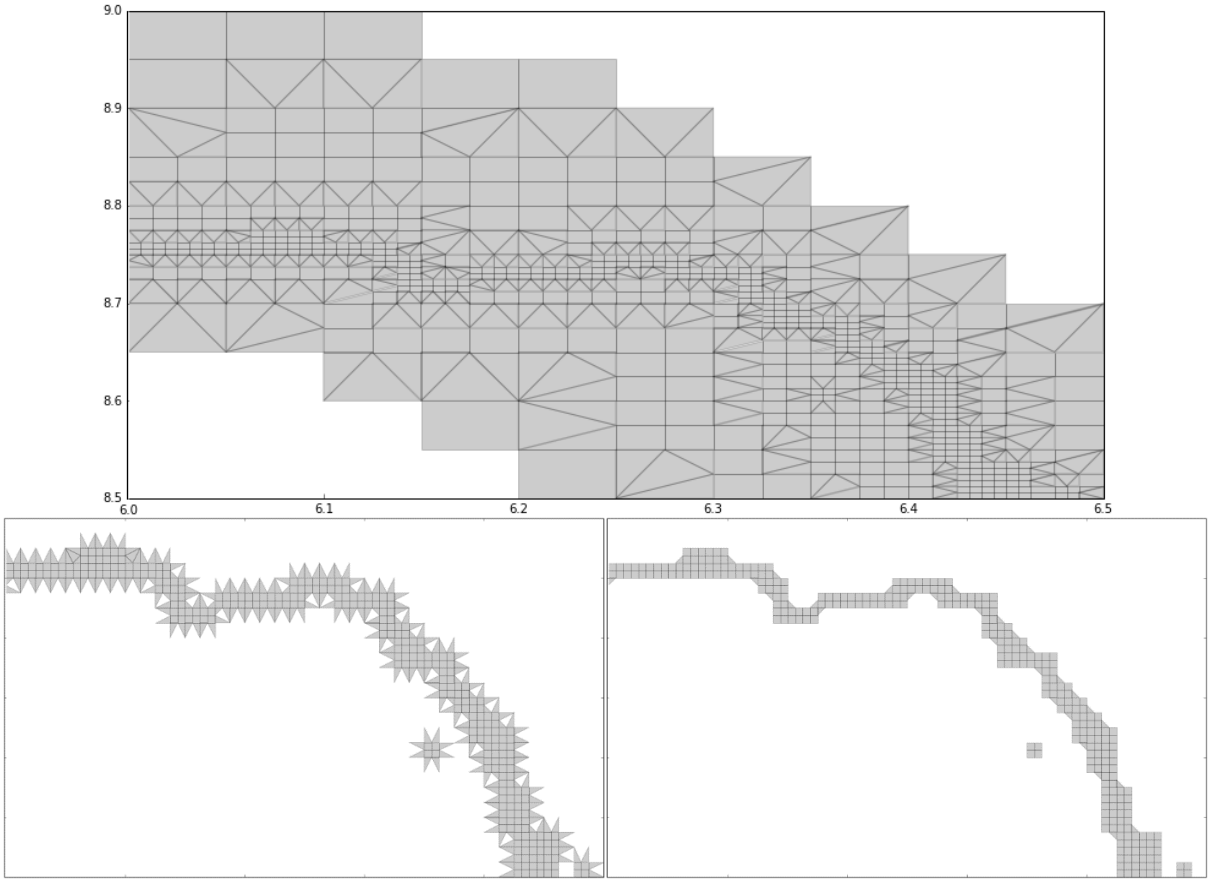

Figure 62: (top) Example PCR-GLOBWB cell with its coupled D-Flow FM cells, (bottom left) identified river cells using a single threshold and (bottom right) identified river cells using two separate thresholds based on cell shape

C.5 Niger Inner Delta area for hydrological analysis

This appendix shows the area representing the Niger Inner Delta for hydrological analysis of coupled models with PCR-GLOBWB used at 5 arcmin resolution (see Figure 63 below). The main report refers to this appendix in paragraph 7.2.2 on page 70.

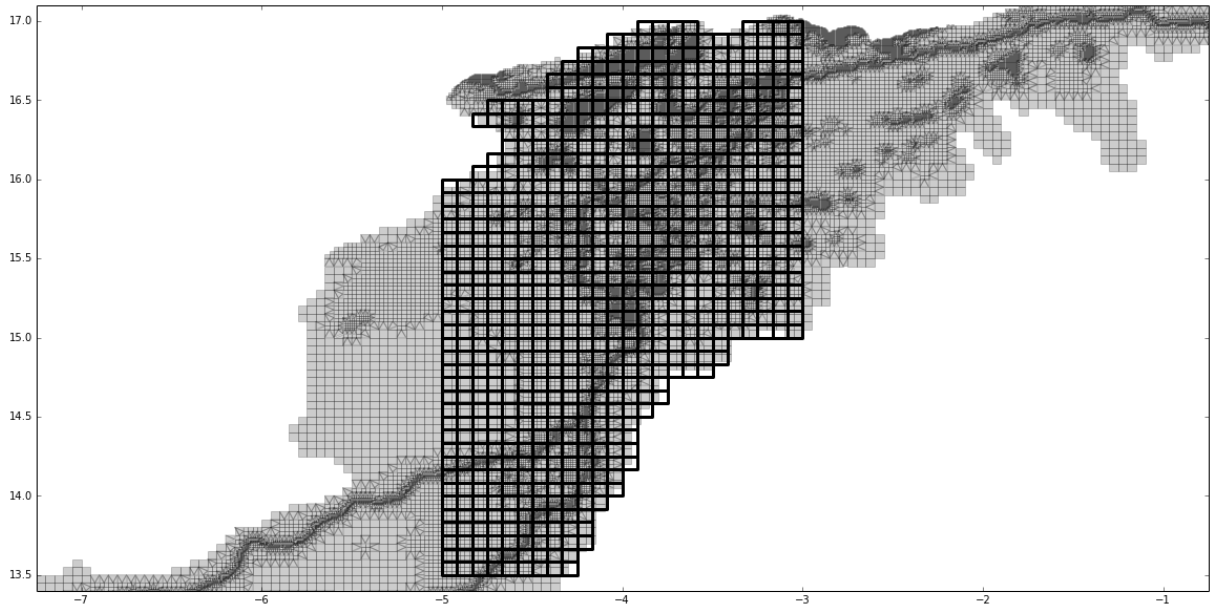

Figure 63: The area of the Niger Inner Delta, visualized by coupled cells of PCR-GLOBWB (at 5 arcmin resolution) overlaid on the D-Flow FM grid.

This area differs from the 30 arcmin resolution because the shape of the Niger basin is different at both resolutions and the border of the basin is located close to the boundaries of the Inner Delta. The total area covered by the 30 arcmin version is roughly 69,000 km^2, while that of the 5 arcmin version is roughly 60,000 km^2.

C.6 Handling of missing discharge data at Douna

This appendix briefly describes how missing data at the gauging station of Douna is corrected for the model runs using upstream discharge boundary conditions (i.e. the stand-alone D-Flow FM model and the two-way coupled model that uses GRDC data instead of PCR-GLOBWB output as upstream discharge values). The main report refers to this appendix in paragraph 7.4 on page 74.

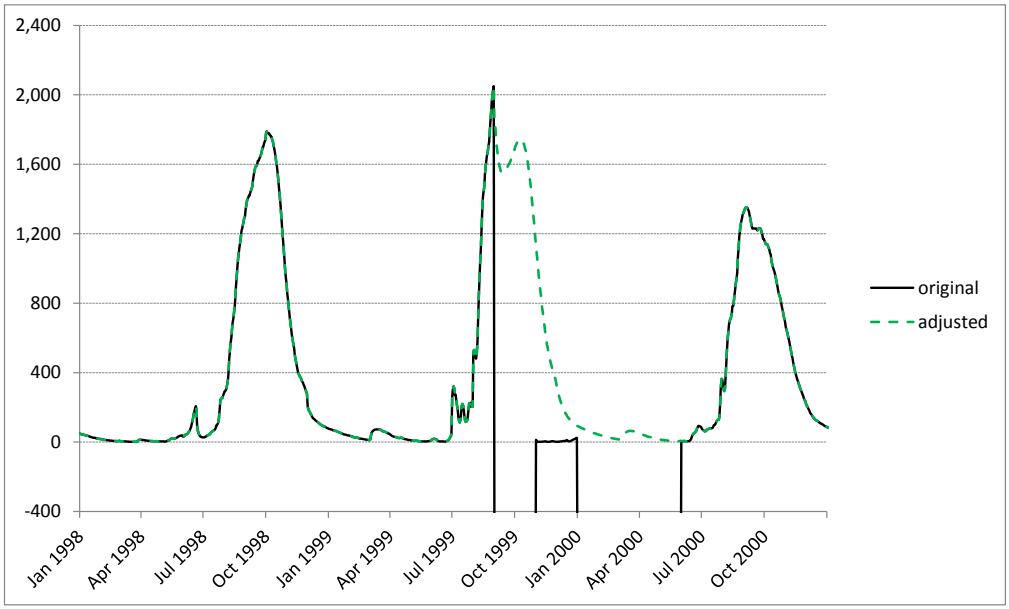

Figure 64: Discharge data at Douna, showing original values as received from the GRDC and adjusted values used in the stand-alone D-Flow FM model

The missing data are corrected by taking the average of the last three values and that of the same day one year earlier, which is thought to be better than simply setting the values to zero, as that would probably introduce a larger error than the scheme used now. This method ensures that the discharge follows a relatively similar pattern as observed in other years, while also taking into account the conditions of the year itself. It should be noted that this method was otherwise mostly used for its simplicity and no effort has been put into finding common methods to deal with missing values as it was not deemed to be of critical importance for this study and the discharge values resulting from the described method seemed to be good. The original and adjusted discharge data for the period that includes missing data are shown in Figure 64 above.